JUSTUS-LIEBIG-
UNIVERSITÄT
GIESSEN

Characterizations of protein *S*-nitrosylation and the 26S proteasome network in the malaria parasite *Plasmodium falciparum*

A thesis submitted to the
Faculty of Biology and Chemistry (FB 08)
in fulfilment of the requirements of the
Doctor of Science Degree of Justus Liebig University
Giessen, Germany

by

Lihui Wang

From

Beijing, China

February 2014

The present work was carried out at the Department of Biochemistry and Molecular Biology (Faculty 09), Justus Liebig University of Giessen between February 2010 and February 2014 under the supervision of Prof. Dr. Katja Becker and Prof. Dr. Annegret Wilde.

First supervisor: Prof. Dr. Katja Becker

Biochemie und Molekularbiologie

Interdisziplinäres Forschungszentrum

Justus-Liebig Universität Giessen

Heinrich-Buff-Ring 26-32,

35392 Giessen, Deutschland

Second supervisor: Prof. Dr. Annegret Wilde

Institut für Biologie III

Molekulare Genetik

Albert Ludwigs Universität Freiburg

Schänzlestr. 1,

79104 Freiburg i. Breisgau, Deutschland

DECLARATION

I declare that this thesis is my original work and other sources of information have been properly quoted. This work has not been previously presented to obtain any other degree from any other university.

Ich erkläre: Ich habe die vorgelegte Dissertation selbständig und ohne unerlaubte fremde Hilfe und nur mit den Hilfen angefertigt, die ich in der Dissertation angegeben habe. Alle Textstellen, die wörtlich oder sinngemäß aus veröffentlichten Schriften entnommen sind, und alle Angaben, die auf mündlichen Auskünften beruhen, sind als solche kenntlich gemacht. Bei den von mir durchgeführten und in der Dissertation erwähnten Untersuchungen habe ich die Grundsätze guter wissenschaftlicher Praxis, wie sie in der „Satzung der Justus-Liebig-Universität Gießen zur Sicherung guter wissenschaftlicher Praxis“ niedergelegt sind, eingehalten.

Giessen, February 14th, 2014

_____

Lihui Wang

DEDICATION

To my family

ACKNOWLEDGEMENTS

First of all, I wish to sincerely thank Prof. Katja Becker for supervising my Ph.D study. I am greatly indebted to Prof. Kajta Becker for not only hosting me in her research group but also leading me into the fields of redox biology and parasitology. Her profound knowledge, continuous encouragement and guidance strongly supported me throughout my Ph.D study. I also wish to thank Prof. Annegret Wilde for being my second supervisor and giving me valuable advice.

I would like to express my sincere gratitude to Dr. Stefan Rahlfs for his professional assistance and instructive suggestions during my entire Ph.D study. Dr. Esther Jortzik, Dr. Sebastian Kehr, Dr. Janina Preuss and Christina Brandstädter, I wish to thank for their valuable suggestions and very helpful discussions with me on my Ph.D projects and I really appreciate the wonderful time that we spent together in our office. Special thanks should go to Elisabeth Fisher, Siegrid Franke and Franziska Mohring for their excellent work in the cell culture of *P. falciparum*. Many thanks go to Michaela Stumpf for her great technical support in protein purification. I would like to thank Timothy D. Bostick for his efficient corrections of my papers and thesis. Besides, I would like to thank all other group members, including Beate Hecker, Rimma Iozef, Marina Fischer, Jipeng Ma, Tao Zhang, Dennis Matovu Kasozi, Jette Pretzel, Jochen Bathke, Kathleen Zocher, Mahsa Rahbari, Karin Fritz-Wolf, Ulrike Burkhard-Zahrt, Sina Ludwig, Melissa Schmidt and Doris Heinke for all the help I have received from you.

Specially, I wish to thank Prof. John Yates III and Dr. Claire Delahunty at the Scripps Research Institute for their excellent work in mass spectrometry which has been intensively used in my projects. I also would like to thank the China Scholarship Council for the financial support throughout my Ph.D study.

Finally, I would like to give my deepest gratitude to my beloved family for their continuous support. I feel grateful to my mother for her sacrifices of being separated from me through these years. To my father, who has profoundly inspired me with his courage and persistence, I dedicate to you this thesis to express my appreciation and deepest longing. At last but not least, I wish to give my heartfelt gratitude to my fiancée Shan Su, who is always supporting and encouraging me to pursue my dream.

PUBLICATIONS

Peer-reviewed journal articles

1. **Wang L.**, Yang Z., Fu J., Yin H., Xiong K., Tan Q., Jin H., Li J., Wang T., Tang W., Yin J., Cai G., Liu M., Kehr S., Becker K. and Zeng H. (**2012**) Ethaselen: a potent mammalian thioredoxin reductase 1 inhibitor and novel organoselenium anticancer agent. *Free Radic Biol Med.* 52:898-908.

2. **Wang L**, Delahunty C., Helena J.P., Rahlfs S., Jortzik E., Yates III J.R. and Becker K. (**2013**) Protein *S*-nitrosylation in *Plasmodium falciparum*, *Antioxid Redox Signal.* In press.

3. **Wang L**, Delahunty C. Rahlfs S. Yates III J.R. and Becker K. (**2014**) Characterizations of the *Plasmodium falciparum* 26S proteasome reveal novel antimalarial strategy. In preparation.

Peer-reviewed reviews and book chapters

1. Jortzik E., **Wang L.** and Becker K. (**2012**) Thiol-based posttranslational modifications in parasites. *Antioxid Redox Signal.* 17:657-673. (Review)

2. Jortzik E., **Wang L.**, Ma J., Becker K. (**2014**) Flavins and Flavoproteins – Applications in medicine. In: E. Schleicher (editor): Methods in Molecular Biology: Flavins and Flavoproteins. Humana Press USA, in press. (Book chapter)

CONTRIBUTIONS TO CONFERENCES

1. **Wang L.**, Delahunty C., Helena J.P., Rahlfs S., Jortzik E., Yates III J.R. and Becker K. Protein *S*-nitrosylation in *Plasmodium falciparum.* The 11th Malaria Meeting, Aachen, Germany, 11/08-09/2013. (Oral presentation)

2. **Wang L.**, Delahunty C., Rahlfs S., Jortzik E., Yates III J.R. and Becker K. Structural and functional analyses of the 26S proteasome of *Plasmodium falciparum.* The 6th Annual Conference of the International Giessen Graduate School for the Life Sciences (GGL), Giessen, Germany, 09/11-12/2013. (Poster)

3. **Wang L.**, Delahunty C., Helena J.P., Rahlfs S., Jortzik E., Yates III J.R. and Becker K. Protein *S*-nitrosylation in *Plasmodium falciparum.* The 5th Annual Conference of the International Giessen Graduate School for the Life Sciences (GGL), Giessen, Germany, 09/18-19/2012. (Poster)

4. **Wang L.**, Delahunty C., Helena J.P., Rahlfs S., Jortzik E., Yates III J.R. and Becker K. Protein *S*-nitrosylation in *Plasmodium falciparum.* The 4th Annual Conference of the International Giessen Graduate School for the Life Sciences (GGL), Giessen, Germany, 09/21-22/2011. (Poster)

SUMMARY

Malaria remains a detrimental tropical disease caused by the protozoan parasites known as *Plasmodium* and is threatening almost half the world's population. Nitric oxide (NO) and NO-derived reactive nitrogen species are well-known *in vivo* effector molecules for controlling the malaria parasites in both mosquito transmitting vectors and humans. However, NO targets and the profound mechanism of NO actions in the malaria parasites remain largely unexplored. Protein *S*-nitrosylation (SNO), a protein posttranslational modification induced by NO and RNS, has been recognized to substantially mediate diverse biological effects of NO *in vivo*. In this thesis, we describe a comprehensive analysis of protein *S*-nitrosylation in the most deadly malaria parasite *Plasmodium falciparum*. By using a biotin-switch assay coupled with mass spectrometry, we have identified, for the first time, 319 potential *S*-nitrosylation targets in *Plasmodium falciparum* that are widespread in various cellular pathways. Interestingly, some metabolic pathways such as glycolysis show an accumulation of *S*-nitrosylated proteins, indicating a high susceptibility to NO-mediated regulation. A major redox protein, *P. falciparum* thioredoxin 1 (PfTrx1) was found to be able to transfer or remove NO to or from other proteins, thus possibly mediating the transnitrosylation and denitrosylation in the parasites. We thus propose a redox status-based model of the role of PfTrx1 in the regulation of SNO in *P. falciparum*. The model suggests that PfTrx1 may protect the parasite from nitrosative stress via protein denitrosylation, whereas upon intensive nitrosative stress PfTrx1 may switch its role to transduce nitrosative stress via protein transnitrosylation. We believe that this study contributes to our understanding of how central metabolic processes in malaria parasites are regulated by NO and suggests that *P. falciparum* employs the thioredoxin system to deal with the nitrosative challenge.

The protein turnover via the ubiquitin-proteasome system (UPS) is well-acknowledged as an essential mechanism profoundly involved in many cellular events in eukaryotes. The classical UPS pathway in eukaryotes typically consists of polyubiquitination of protein substrates, polyubiquitinylated substrates transportation, and substrate recognition by the eukaryotic 26S proteasome, and substrate degradation by the proteasome. Although compelling data have indicated the presence of a functional 26S proteasome network in *P. falciparum*, the componential integrity and the functionality of the plasmodial 26S proteasome has not been systematically studied so far. In this thesis, we aimed to characterize the mechanism of substrate recognition by the 26S proteasome of *P. falciparum*. By using *in silico* analysis and biochemical investigations, we have identified three ubiquitin receptor domains inherited by two plasmodial proteasome subunits, the Rpn10 and Rpn13 subunits. These newly identified plasmodial ubiquitin receptor domains include two putative ubiquitin-interacting motif (UIM) domains and a putative Pleckstrin-like receptor for ubiquitin (Pru) domain. The *P. falciparum* UIM domains (PfUIMs) and Pru domain (PfPru) were demonstrated to bind ubiquitin-like domains (UBLs) from the plasmodial homologues of Rad23 and Dsk2, which are important UBL-containing proteins involved in the transportation of proteasomal substrates to the 26S proteasome. Strikingly, only PfUIM2 domain was found to be able to directly bind polyubiquitin chains, indicating that PfUIM2 is the site for the direct recognition of polyubiquitinylated substrates for proteasomal degradation. Based on the affinity of PfUIM2 domain to the UBL domain of the plasmodial Rad23, we successfully established a simple and efficient affinity purification method

to isolate the *P. falciparum* 26S proteasome complex together with a number of putative proteasome-interacting proteins (PIPs) directly from the parasite extracts. With this method, we provide the first insight into the componential composition of the plasmodial 26S proteasome. More importantly, the co-purification of putative PIPs in *P. falciparum* has allowed us to take a first view of the protein metabolism network orchestrated by the plasmodial UPS, and may provide new targets for developing novel antimalarial agents targeting the plasmodial UPS or related pathways.

ZUSAMMENFASSUNG

Die verheerende tropische Erkrankung Malaria wird durch Protozoen, bekannt als *Plasmodien*, hervorgerufen und bedroht fast die Hälfte der Weltbevölkerung. Stickstoffmonoxid (NO) und die von ihm abgeleiteten reaktiven Stickstoffspezies (RNS) sind bekannte *in vivo* Effektormoleküle, welche den Malariaparasiten sowohl im transmittierenden Vektor als auch im Menschen kontrollieren. Jedoch gilt der profunde Mechanismus des NO-Einflusses und seine Zielmoleküle im Malariaerreger als weitgehend unerforscht. Die *S*-Nitrosylierung von Proteinen (SNO), eine posttranslationale Modifikation induziert durch NO und RNS, stellt einen substantiellen Mediator diverser biologischer Effekte von NO *in vivo* dar. Mit dieser Arbeit stellen wir eine umfassende Analyse der *S*-Nitrosylierung von Proteinen in dem tödlichsten der Malariaparasiten, *Plasmodium falciparum*, dar. Durch die Anwendung des Biotin Switch Assays gekoppelt mit Massenspektrometrie gelang es uns zum ersten Mal 319 potentielle Ziele der *S*-Nitrosylierung in *Plasmodium falciparum* darzustellen, die in einer Vielzahl von zellulären Abläufen zu finden sind. Interessanterweise zeigen einige Stoffwechselwege, wie die Glykolyse, eine Akkumulation von *S*-nitrosylierten Proteinen, welches eine hohe Empfänglichkeit für NO-vermittelte Regulationen vermuten lässt. Das wichtige Redoxprotein Thioredoxin 1 aus *P. falciparum* (PfTrx1) konnte als möglicher Vermittler von Transnitrosylierung oder Denitrosylierung im Parasiten identifiziert werden, indem es in der Lage ist, NO zu anderen Proteinen zu transportieren oder diese von ihnen zu entfernen. Wir vermuten folglich ein Redoxstatus-basiertes Modell der Rolle von PfTrx1 in der Regulation von SNO in *P. falciparum*. Das Modell weist darauf hin, dass PfTrx1 den Parasiten vor Stickstoffstress durch Denitrosylierung von Proteinen schützen kann, wohingegen PfTrx1 bei hohem NO bedingtem Stress seine Funktion zur Transnitrosylierung von Proteinen ändert. Wir sind der Meinung, dass diese Arbeit zum Verständnis beiträgt, wie zentrale metabolische Prozesse im Malariaparasiten durch NO reguliert werden können und vermuten, dass *P. falciparum* das Thioredoxsystem nutzt, um Stickstoffstress entgegenzuwirken.

Der Proteinumsatz durch das Ubiquitin-Proteasom-System (UPS) ist als essentieller Mechanismus, der tiefgreifend in viele zelluläre Ereignisse in Eukaryoten eingreift, bekannt. Der klassische UPS-Weg in Eukaryoten besteht typischerweise aus einer Polyubiquitinylierung von Proteinsubstraten, deren Transport und Substraterkennung durch das eukaryotische 26S Proteasom sowie der Degradation dieser Substrate durch das Proteasom. Obwohl eindeutige Daten die Präsenz eines funktionellen 26S-Proteasom-Netzwerkes in *P. falciparum* vermuten lassen, wurde die Integrität und Funktionalität des plasmodialen 26S Proteasoms bisher nicht systematisch erforscht. Mit der vorliegenden Arbeit adressieren wir eine Charakterisierung des Mechanismus der Substraterkennung des 26S Proteasoms von *P. falciparum*. Durch die Verwendung von *in silico* Analysen und biochemischen Untersuchungen konnten wir drei Ubiquitin-Rezeptoreinheiten auf zwei plasmodialen Proteasom-Untereinheiten, Rpn10 und Rpn13, bestimmen. Diese neu identifizierten plasmodialen Ubiquitin-Rezeptoreinheiten beinhalten zwei potentielle Ubiquitin-Interaktionsmotive (UIM) und eine potentielle Pleckstrin-like Rezeptordomäne für Ubiquitin (Pru). Die *P. falciparum* UIM-Domänen (PfUIMs) und Pru-Domäne (PfPru) können an Ubiquitin-like-Domänen (UBLs) der plasmodialen Homologe von Rad23 und Dsk2 binden, welche wichtige UBL-beinhaltende Proteine darstellen, die im Transport zum 26S Proteasom

involviert sind. Erstaunlicherweise war nur PfUIM2 in der Lage direkt Ubiquitinketten zu binden, was darauf hinweist, dass PfUIM2 zur direkten Erkennung von polyubiquitinylierten Substraten zur proteasomalen Degradation dient. Basierend auf der Affinität der PfUIM2-Domäne zur UBL-Domäne der plasmodialen Rad23, konnten wir eine einfache und effektive Methode der Affinitätsreinigung zur direkten Isolierung des *P. falciparum* 26S Proteasomskomplexes zusammen mit einer Reihe potentieller Proteasom-interagierender Proteine (PIPs) aus dem Parasitenextrakt entwickeln. Mit dieser Methode konnten wir erste Einblicke in die Zusammenstellung der Komponenten des plasmodialen 26S Proteasoms liefern. Zudem erlaubte uns die Co-Reinigung der potentiellen PIPs aus *P. falciparum* einen ersten Blick auf das metabolische Proteinnetzwerk instrumentalisiert durch das plasmodiale UPS und bietet neue Ziele zur Entwicklung neuartiger Antimalariawirkstoffe, welche auf die plasmodiale UPS oder verwandte Stoffwechselwege abzielt.

TABLE OF CONTENTS

LIST OF FIGURES

LIST OF TABLES

LIST OF ABBREVIATIONS

ACTs	Artemisinin-based combination therapies
APS	Ammoniumpersulfate
ATP	Adenosine triphosphate
BSA	Bovine serum albumin
DMSO	Dimethyl sulfoxide
DNA	Deoxyribonucleic acid
DNase	Deoxyribonuclease
dNTP	Deoxynucleotide triphosphate
DTT	1, 4-Dithiothreitol
E. coli	*Escherichia coli*
EDTA	Ethylenediaminetetraacetic acid
FPLC	Fast protein liquid chromatography
HK	Hexokinase
IPTG	Isopropyl-β-D-thiogalactopyranoside
kDa	Kilodalton
kDa	Kilodalton
LB	Lysogeny Broth Medium
Ni-NTA	Nickel nitrilotriacetic acid
OD	Optical density
PBS	Phosphate buffered saline
PCR	Polymerase chain reaction
Pf	*Plasmodium falciparum*
PMSF	Phenylmethylsulfonylfluoride
PVDF	Polyvinyl difluoride
SDS	Sodium dodecyl sulphate
SDS-PAGE	Sodium dodecyl sulphate-polyacrylamide gel electrophoresis
TB	Terrific Broth medium
TEMED	N,N,N',N'-Tetramethylethylenediamine
WHO	World Health Organisation
µg	Microgram
µL	Microliter
µM	Micromolar
AMC	7-amino-4-methylcoumarin
BLAST	Basic Local Alignment Search Tool
Da	Dalton
DUB	Deubiquitinase
ERAD	Endoplasmic reticulum-associated degradation
FAD	Flavin adenine dinucleotide
FMN	Flavin mononucleotide
FP IX	Ferri/ferroprotoporphyrin IX
GR	Glutathione reductase
Grx1	Glutaredoxin 1
GSH/GSSG	Glutathione (reduced /oxidized)

GSNO	*S*-nitrosoglutathione
GSNOR	*S*-nitrosoglutathione reductase
H_2O_2	Hydrogen peroxide
HEPES	4-(2-hydroxyethyl)-1-piperazineethanesulfonic acid
HPLC	high-performance liquid chromatography
IAA	Iodoacetamide
mg	Milligram
mL	Milliliter
mM	Millimolar
MMTS	Methyl methanethiosulfonate
MS	Mass spectrometry
MS/MS	Tandem mass spectrometry
NaAsc	Sodium ascorbate
NAD^+	Nicotinamide adenine dinucleotide
NADPH	Nicotinamide adenine dinucleotide phosphate, reduced
NO	Nitric oxide
NOS	Nitric oxide synthase
PfGAPDH	*P. falciparum* glyceraldehyde-3-phosphate dehydrogenase
PfGrx1	*P. falciparum* glutaredoxin 1
PfGST	*P. falciparum* glutathione *S*-transferase
PfHK	*P. falciparum* hexokinase
PfLDH	*P. falciparum* lactate dehydrogenase
PfPGM	*P. falciparum* phosphoglycerate mutase
PfPK	*P. falciparum* pyruvate kinase
PfPrx1a	*P. falciparum* peroxiredoxin 1a
PfPrx6	*P. falciparum* peroxiredoxin 6
PfSAMS	*P. falciparum S*-adenosylmethionine synthetase
PfTrx1	*P. falciparum* thioredoxin 1
PfTrxR	*P. falciparum* thioredoxin reductase
PIPs	Putative proteasome-interacting proteins
PPP	Pentose phosphate pathway
Pru	Pleckstrin-like receptor for ubiquitin
PSMs	Peptide/spectrum matches
RNS	Reactive nitrogen species
ROS	Reactive oxygen species
RT	Room temperature
sGC	Soluble guanylate cyclase
SNO	Protein *S*-nitrosylation
Ub	Ubiquitin
UBA	Ubiquitin-associated (domain)
UBL	Ubiquitin-like (domain)
UIM	Ubiquitin-interacting motif
Xcorr	Cross-correlation score

1. INTRODUCTION

1.1 Malaria

1.1.1 Malaria

Malaria is the most serious tropical disease caused by protozoan parasites of the genus *Plasmodium*, which are transmitted to human hosts by the infected *Anopheles* mosquito. Patients with malaria often experience chills, fever, headache, and flu-like illness. Left untreated, they may develop severe complications and die (CDC website 2013).

Historically, the term "Malaria" originates from Medieval Italian "mal' aria" meaning "bad air" (Tuteja 2007). Between 1880 and 1890, the causative agents of malaria – the *Plasmodium* parasites – were identified, and the transmission of the parasites between humans and mosquitoes were also discovered (Chernin 1988; Guillemin 2002). In 1900, more than 77% of the world's population in 140 countries was at risk of malaria (Hay *et al.,* 2004). Malaria used to be widespread in temperate regions until the middle of the 20th century but was wiped out after the "Global Malaria Eradication Program" between 1955 and 1969 (Hay *et al.,* 2004). This campaign against malaria was successful by relying on malaria treatment with chloroquine-based chemotherapy and prevention with DDT-based vector control. In the 1970s, malaria was successfully eradicated from most parts of Europe and North America. However, the program was abandoned in 1972 due to the emergence of chloroquine-resistant *Plasmodium* parasites and DDT-resistant *Anopheles* mosquitoes (Enayati *et al.,* 2010). Nowadays, malaria is still endemic in tropical and subtropical regions in Africa, South East Asia, Eastern Mediterranean Regions, and parts of Central and South America. It threatens about 40% of the world's population and remains a scourge of poorer countries **(Figure 1)**. The WHO estimates that in 2010 there were 219 million cases of malaria resulting in 660,000 deaths. About 90% of malaria deaths are in Africa, and most of the death cases happen to children under the age of five (WHO 2010).

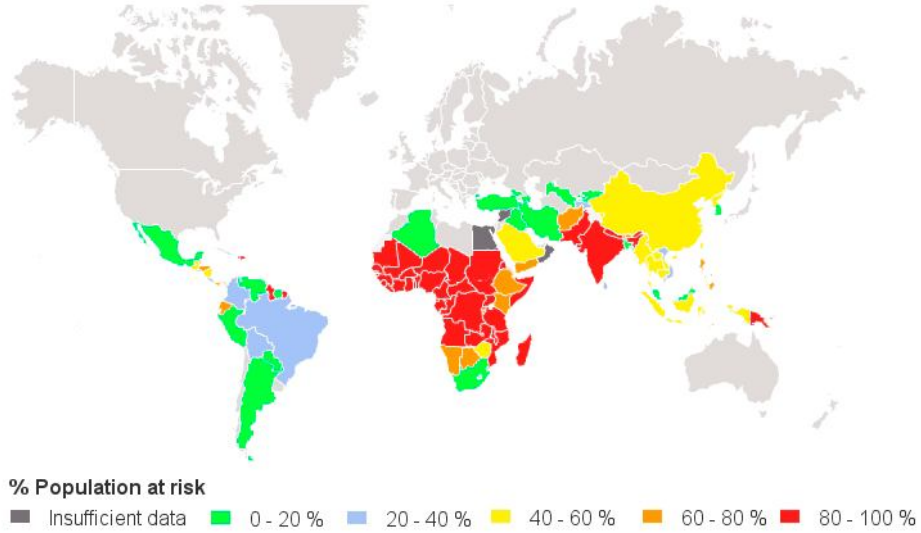

Figure 1. Percentage of national population at risk of malaria. Taken from http://www.worldmalariareport.org/node/57.

In response to this dreadful situation, several programs have been launched to concertedly control malaria, for example the Roll Back Malaria, the Malaria Vaccine Initiative and the Medicines for Malaria Venture. The artemisinin-based combination therapies (ACTs) are largely involved in the treatment of malaria to overcome the chloroquine resistance in malaria parasites (WHO 2010). However, the emergence of multiple drug resistant parasites, including suspected artemisinin-resistant *Plasmodium* parasites in some areas (Phyo *et al.,* 2012), is threatening our last line of defense against malaria. New antimalarial agents, effective vaccines and anti-vector strategies are urgently required.

1.1.2 Malaria parasites

1.1.2.1 Life cycle

The causative agents of malaria are eukaryotic, unicellular organisms of the genus *Plasmodium*, which belong to the phylum *Apicomplexa* (Tuteja 2007; Kappe *et al.,* 2010). Generally, five species of *Plasmodium* infect humans, including *P. falciparum*, *P. vivax*, *P. knowlesi*, *P. ovale* and *P. malariae* (Kappe *et al.,* 2010; Hafalla *et al.,* 2011). Among them, *P. falciparum* and *P. vivax* are responsible for the most malaria infections worldwide. *P. vivax* is mainly distributed in Asia, America, some parts of Africa and usually causes uncomplicated malaria, whereas *P. falciparum*, the most deadly species of human malaria parasites, is predominant in Africa and accounts for most malaria deaths (WHO 2010).

Human malaria parasites undergo a complex life cycle within the mosquito vector and human hosts (Kappe *et al.,* 2010). The life cycle of *P. falciparum* with several developmental transitions is given in **Figure 2.** Infection with malaria begins following the bite of an infected female mosquito, which transmits the parasite sporozoites into the blood stream of human hosts. The sporozoites circulate and invade liver cells, where they undergo asexual developments (the pre-erythrocytic stage) and divide into thousands of merozoites within several days. Once the hepatocytes rupture, the invading merozoites are released to the blood stream and invade erythrocytes, initiating the asexual blood stage development (intraerythrocytic stage). Within about 48 hours of rapid multiplication and development, *P. falciparum* undergoes ring, trophozoite, and schizont stages and finally form around 20 merozoites, which further rupture the erythrocyte and invade new erythrocytes. A small portion of parasites undergo sexual development and differentiate into male and female forms of gametocytes, the only form of the parasite taken up by the mosquito in a blood meal. In the mosquito midgut, the gametocytes develop into micro- and macrogametes and further form ookinetes, which invade the mosquito midgut. Within the midgut epithelium, the parasites develop into mature oocysts. Sporogony in the oocyst results in the production of sporozoites, which further migrate to the salivary gland of the mosquito. When the mosquito bites a new individual, the sporozoites are transferred to a new host, and the life cycle of the parasite starts again.

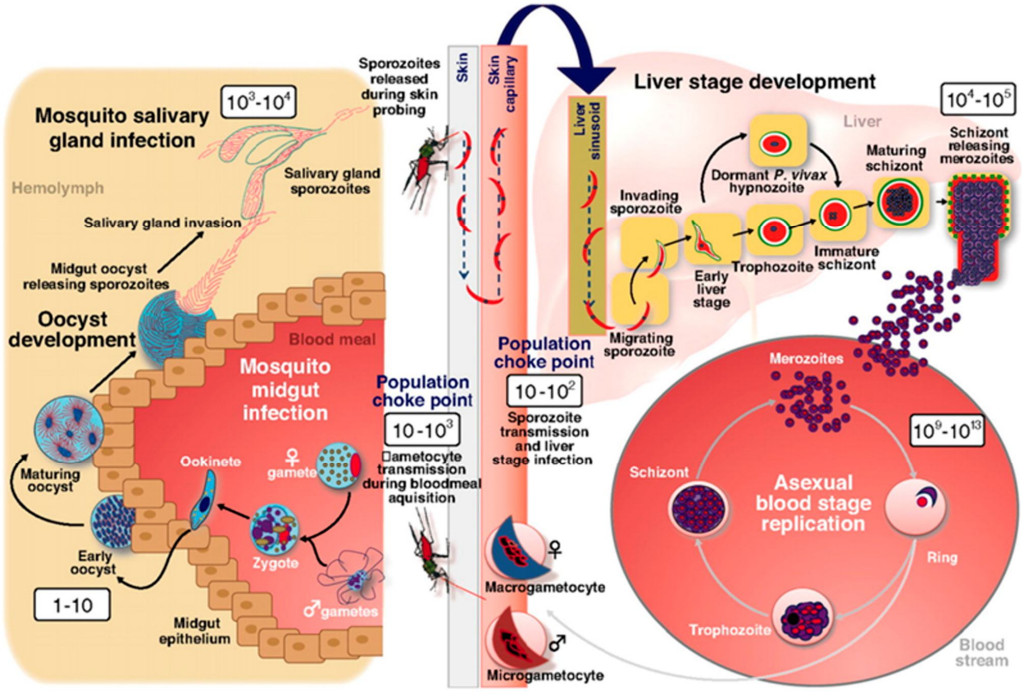

Figure 2. Life cycles of human malaria parasites in humans and mosquito vectors. The numbers indicate the size of the parasite population during life cycle progression. Taken from Kappe *et al.,* 2010.

1.1.2.2 Redox metabolism of malaria parasites

During its life cycle, the malaria parasites are exposed to oxidative and nitrosative stresses due to either a high metabolic rate of the rapidly growing and multiplying parasites or the host immune responses to *Plasmodium* infection (Becker *et al.,* 2004). Furthermore, the intraerythrocytic *Plasmodium* constantly digests hemoglobin of infected erythrocytes as the major source of amino acids. The digestion of hemoglobin in the parasitic food vacuole leads to the formation of toxic free heme (ferri/ferroprotoporphyrin IX; FP IX), which needs to be detoxified by sequestration into crystalline hemozoin (Atamna *et al.,* 1993). However, residual heme that escapes the detoxification process will lead to a significant induction of oxidative stress, causing protein and membrane damages in the parasites (Atamna *et al.,* 1993). Apart from the metabolically derived oxidative stress, reactive oxygen and nitrogen species (RONS) generated from the host immune system increase the oxidative/nitrosative burden of the parasitized cell (Lim *et al.,* 2005; Molina-Cruz *et al.,* 2008).

To cope with the deleterious effects of oxidative/nitrosative stresses, malaria parasites are equipped with a sophisticated antioxidant network (Muller 2004; Jortzik *et al.,* 2012). Two central components of the antioxidant network in *Plasmodium* are the NADPH-dependent thioredoxin (Trx) and glutathione (GSH) systems (**Figure 3**).

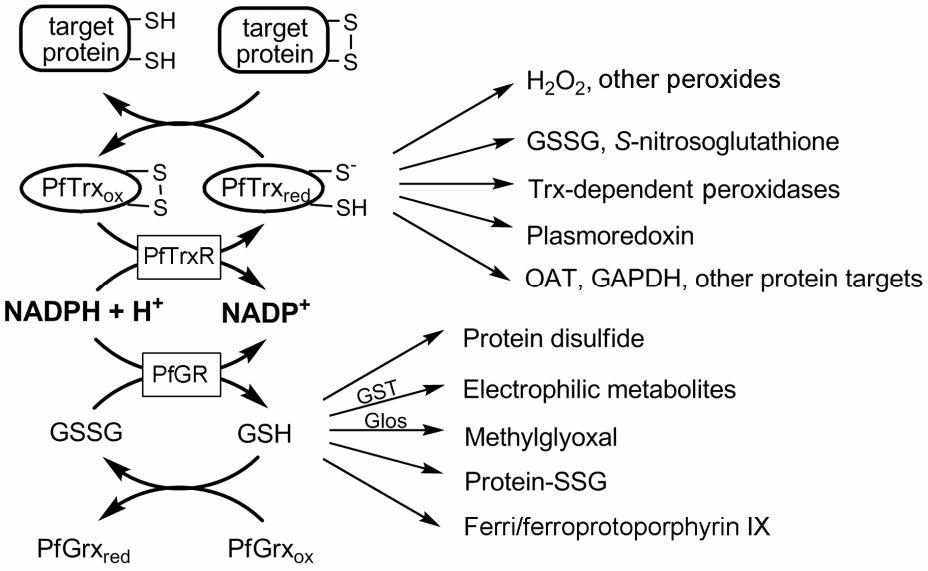

Figure 3. The NADPH-dependent thioredoxin system and GSH system in the antioxidant defense of *P. falciparum*. TrxR, thioredoxin reductase; GR, glutathione reductase; Grx, glutaredoxin; GST, glutathione *S*-transferase; Glos, glyoxalase; GAPDH, glyceraldehyde 3-phosphate dehydrogenase; FP IX,; OAT, ornithine δ-aminotransferase.

1.1.2.2.1 The thioredoxin system of *P. falciparum*

The thioredoxin system, composed of thioredoxin (Trx), thioredoxin reductase (TrxR) and NADPH, plays a central role in the redox homeostasis of cells (Muller 2004). *P. falciparum* possesses three classic Trxs that can be reduced by *P. falciparum* TrxR (PfTrxR) and two Trx-like proteins that cannot be reduced by PfTrxR (Jortzik *et al.,* 2012). The cytosolic *P. falciparum* thioredoxin 1 (PfTrx1) is the best studied Trx in *P. falciparum* and has been shown to be a central player in the antioxidant system of the parasites (Krnajski *et al.,* 2001; Kanzok *et al.,* 2002). PfTrx1 has an active site motif WCGPC, where the two catalytic cysteine residues are located. PfTrx1 directly counteracts oxidative stress by reducing oxidized glutathione (GSSG), hydrogen peroxide (H_2O_2), *tert*-butylhydroperoxide (tBuOOH), and *S*-nitrosoglutathione (GSNO) (Kanzok *et al.,* 2000; Krnajski *et al.,* 2001). Besides, PfTrx1 also maintains the reduced status of thioredoxin-dependent peroxidases and plasmoredoxin, a *Plasmodium*-specific oxidoreductase (Becker *et al.,* 2003). Furthermore, PfTrx1 has been shown to interact with several plasmodial proteins involved in protein folding, glycolysis, polyamine metabolism and redox homeostasis (Sturm *et al.,* 2009).

PfTrxR is a dimeric flavoenzyme catalyzing the NADPH-dependent reduction of the active site disulfide of PfTrx1. The C-terminal redox center of PfTrxR employs two non-adjacent cysteine residues (Cys535 and Cys540) to interact with the active site dithiols of PfTrx1, in contrast to the consecutive Cys-Sec pair at the C-terminus of mammalian TrxRs (Jortzik *et al.,* 2012). The most striking structural differences between PfTrxR and human TrxR are the insertion of a *Plasmodium*-specific loop at the C-terminus of PfTrxR and the architecture of the flexible C-terminal arm. The loop seems to be important for the intermolecular interaction between PfTrxR and PfTrx1, as a depletion of parts of the loop leads to a decreased efficiency of PfTrxR in the reduction of PfTrx1 (Fritz-Wolf *et al.,* 2013). PfTrxR was demonstrated to be crucial for the erythrocytic stages

of *P. falciparum* (Krnajski *et al.,* 2002). However, a recent knockout study reported that TrxR of the rodent malaria parasite *P. berghei* is not essential for the parasites in the mammalian host and the mosquito vector (Buchholz *et al.,* 2010). The dispensable role of TrxR might be explained by compensation for the loss of functions by the parasitic glutathione system.

1.1.2.2.2 The glutathione system of *P. falciparum*

The tripeptide GSH is the major low-molecular-weight antioxidant in almost all aerobic cells (Sies 1999). GSH generally exists at milimolar intracellular concentrations (Monostori *et al.,* 2009). It plays a pivotal role in cellular antioxidant defense by counteracting deleterious free radicals and peroxides and maintaining the redox status of protein thiols (Frey 1997; Sies 1999). *Plasmodium* possesses the GSH biosynthesis pathway and a functional GSH-dependent antioxidant system, consisting of GSH, glutathione reductase (GR), glutaredoxins (Grxs), glyoxalase (Glos), and glutathione *S*-transferase (GST) (Becker *et al.,* 2003; Muller 2004). GSH biosynthesis was demonstrated to be particularly important in the mosquito stages, since genetic disruption of *P. berghei* gamma-glutamylcysteine synthetase (γ-GCS), a critical enzyme in the GSH biosynthesis pathway, dramatically inhibits plasmodial sporogony in the mosquito (Buchholz *et al.,* 2010).

In *P. falciparum*, the reduced form of GSH is mainly recycled by the *P. falciparum* glutathione reductase (PfGR), which reduces GSSG back to GSH in the presence of NADPH (Becker *et al.,* 2003). The redox potential of 2GSH/GSSG (E_{GSH}), determined by the intracellular molar ratio of GSH to GSSG, reflects the cellular redox status. Probed by a GSH biosensor comprising the human Grx1 linked to a redox-sensitive green fluorescent protein, the basal cytosolic E_{GSH} of *P. falciparum* (3D7 strain) has been recently determined to be -314.2±3.1 mV, indicating a highly reducing cytosol of the parasites (Kasozi *et al.,* 2014).

Apart from its role in direct detoxification of oxidizing agents, GSH serves as a cofactor for glutathione *S*-transferase to detoxify electrophilic metabolites (Harwaldt *et al.,* 2002), for glyoxalase to detoxify methylglyoxal (Iozef *et al.,* 2003), and for glutaredoxin to regulate the redox status of various proteins (Rahlfs *et al.,* 2001). Additionally, GSH/GSSG functions as the major thiol redox buffer in cells. Particularly, protein thiols can be reversibly modified by GSSG via *S*-glutathionylation**,** which can be further de-glutathionylated by reduced GSH and other enzymatic factors (Dalle-Donne *et al.,* 2007). Through this mechanism, GSH protects protein thiols from irreversible overoxidations under oxidative stress (Giustarini *et al.,* 2004). Recently, a systematic approach identified nearly five hundred endogenously *S*-glutathionylated proteins in *P. falciparum* (Kehr et al., 2011). PfGrx1, PfTrx1, and plasmoredoxin have been shown to be capable of catalyzing the de-glutathionylation process *in vitro* (Kehr et al., 2011). Besides, a particular role of GSH in *Plasmodium* is the detoxification of free FP IX, which escapes its sequestration in the food vacuole. It has been shown that free FP IX is degraded non-enzymatically by GSH, and this mechanism can be inhibited by chloroquine (Atamna *et al.,* 1995; Zhang *et al.,* 1999). Therefore, a high level of reduced GSH is usually considered to be relevant to the chloroquine resistance of malaria parasites (Zhang *et al.,* 1999; Deharo *et al.,* 2003).

1.2 Nitric oxide and *Plasmodium*

1.2.1 Nitric oxide in biology

Nitric oxide (NO) is a gaseous signaling molecule involved in various physiological and pathological processes (Moncada *et al.,* 1991). The important bioactivity of NO was not recognized *per se* until the late 1980s when researchers identified NO as the endothelium-derived relaxing factor (EDRF), which regulates vasodilation of blood vessels (Marsh *et al.,* 2000; Loscalzo 2013). The discovery of the regulatory role of NO in the cardiovascular system has led to an explosion in research focusing on signaling functions of NO. To date, NO has been shown to participate in a wide range of physiological events such as platelet aggregation and adhesion (Kalinowski *et al.,* 2002), smooth muscle cell proliferation (Tsihlis *et al.,* 2011), neurotransmission (Vincent 2010), and innate immune response to pathogen infections (Wink *et al.,* 2011). Besides, NO is also involved in the pathogenesis of a number of diseases, including cancer, arthritis, atherosclerosis, diabetes, and several neuronal degenerative diseases (Gross *et al.,* 1995).

As an uncharged and almost nonpolar molecule, NO is more soluble in hydrophobic solvents than in water (Toledo *et al.,* 2012). Therefore NO readily diffuses the hydrophobic double layer of biological membranes (Toledo *et al.,* 2012). Despite its molecular simplicity, NO possesses diverse chemical reactivity and reacts with a wide range of biological targets, including DNA, protein, metal, low-molecular weight thiols, and reactive oxygen intermediates (**Figure 4**). A striking feature of NO in an aerobic environment is that it undergoes autoxidation to form dinitrogen trioxide (N_2O_3), which strongly reacts with amines and thiols to form nitrosamines and *S*-nitrosothiols, respectively (Gardner *et al.,* 2004; Toledo *et al.,* 2012). The second-order autoxidation rate for NO indicates that the half life of NO in the reaction is dependent on the concentration of NO (Wink *et al.,* 1998). This further indicates a concentration-dependent atmospheric fate for NO: in low concentrations (*e.g.* under physiological conditions), NO has a relatively long lifetime that allows NO to access and interact with biological targets, whereas in high concentrations (*e.g.* under inflammatory conditions), NO may undergo rapid oxidation to form reactive nitrogen species (RNS, *e.g.* N_2O_3), thus elevating local nitrosative stress. Under oxidative stress, NO reacts with superoxide (O_2^-), leading to the generation of peroxynitrite ($ONOO^-$), which is a powerful oxidant and nitrating agent that can damage a wide array of biomolecules (Toledo *et al.,* 2012). Moreover, NO directly reacts with ferrous to form ferrous-nitrosyl complexes, which are of particular importance in the modulation of hemeproteins by NO. For example, NO binds to the heme iron in soluble guanylate cyclase (sGC) and releases the heme-bound histidine, resulting in a subsequent conformational change of the protein and activation of the enzyme (Stone *et al.,* 1994). Besides sGC, the heme proteins hemoglobin and cytochrome *c* oxidase are important NO targets in cells (Sarti *et al.,* 2012; Helms *et al.,* 2013).

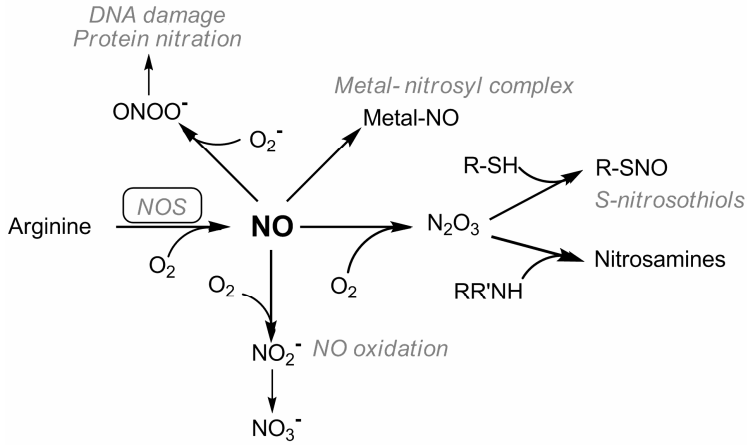

Figure 4. Schematic representation of the biological production and reactivity of nitric oxide. NOS, nitric oxide synthase.

The physiological and pathophysiological levels of NO vary significantly depending on the rates of NO production and metabolism. A widely accepted range of physiological concentrations of NO is 1 nM to 100 nM, although several studies have even observed NO concentrations in the picomolar range (Toledo *et al.,* 2012). However under infectious and inflammatory conditions, NO levels can dramatically increase by several orders of magnitude. This is mainly due to the elevated expression and activity of inducible NO synthase that produces an inflammatory level of NO (see below).

In mammals, biological NO is mainly produced from the oxidation of the amino acid L-arginine catalyzed by specialized nitric oxide synthases (NOSs) (Griffith *et al.,* 1995). NOS typically functions by forming homodimers (**Figure 5**). In eukaryotes, each NOS monomer consists of an N-terminal oxygenase and a C-terminal reductase domain. The oxygenase domain is the site for binding arginine, a heme prosthetic group, and the cofactor tetrahydrobiopterin (BH_4), whereas the reductase domain has binding sites for flavin mononucleotide (FMN), flavin adenine dinucleotide (FAD), and NADPH. The interdomain linking the oxygenase and reductase domain contains a calmodulin (CaM)-binding motif. Binding calmodulin enables electron flow from flavin prosthetic groups in the reductase domain to heme, facilitating the turnover of O_2 and L-arginine to NO and L-citrulline (Alderton *et al.,* 2001).

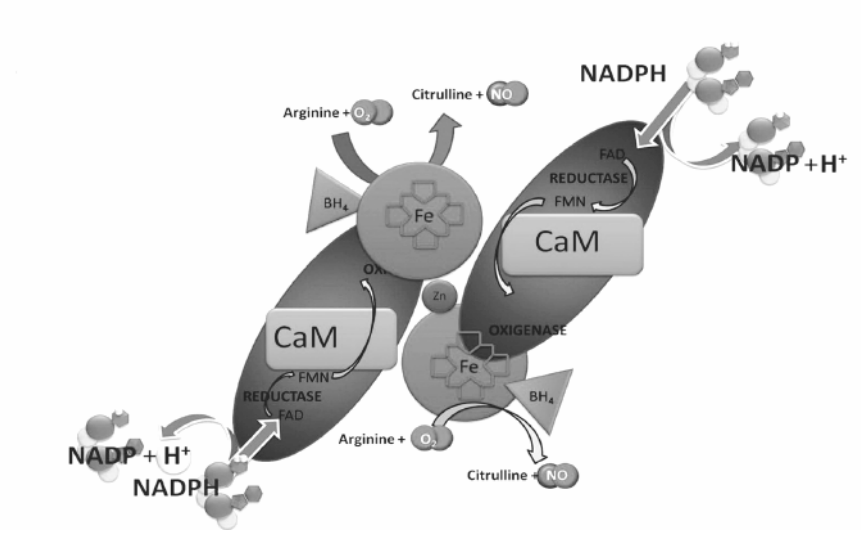

Figure 5. A model for the generation of NO by the NOS homodimers. BH_4, tetrahydrobiopterin; CaM, calmodulin; FAD, flavin adenine dinucleotide; FMN, flavin mononucleotide. Modified from (Maron *et al.,* 2012)

There are two classes of NOS that have been found (Knowles *et al.,* 1994). The constitutive NOS (NOS I) includes the endothelial NOS (eNOS) and neuronal (nNOS), each of which produces low amounts of NO under physiological conditions in a calcium-dependent manner. By contrast, the inducible NOS (iNOS, NOS II) can be stimulated to produce large amounts of NO under infectious and inflammatory conditions (Menshikova *et al.,* 2000). High-output of transcription and expression of iNOS can be induced by several pro-inflammatory cytokines, such as interleukin-1, tumor necrosis factor alpha (TNF-α) and interferon-γ (IFN-γ) (Green *et al.,* 1994). High levels of NO generated by iNOS have been shown to have anti-microbial and anti-cancer activities *in vivo*, thereby pinpointing the important role of iNOS in the host immune system (Fang 2004).

1.2.2 *Plasmodium* encounters nitrosative stress

1.2.2.1 NO in *Plasmodium* infections

Nitric oxide has long been recognized as a potent antiparasitic effector molecule *in vivo* (**Figure 6**) (Bogdan 2001). Compelling evidence has shown that NO derived from NOS is an important component of innate immune response against *Plasmodium* parasites in both mammalian hosts and *Anopheles* mosquito vectors (Nahrevanian 2006; Rivero 2006). In mammals, iNOS is ubiquitously present in epithelial cells, hepatocytes, and various immune cells, including macrophages, NK cells, and dendritic cells (Bogdan 2001). The expression of iNOS can be induced in response to several pro-inflammatory cytokines during *Plasmodium* infection. It is generally accepted that NO derived from host iNOS partially mediates the killing of malaria parasites (Nahrevanian 2006). Supporting this concept, it has been found that NO generated by human monocytes can kill *P. falciparum in vitro* (Gyan *et al.,* 1994). Besides, upon the invasion of live cells by sporozoites, induction of NO in mammalian hepatocytes has also been reported to have antiplasmodial activity against sporozoites (Klotz *et al.,* 1995). Notably, the mechanism of the stimulation of NO production in macrophages by *Plasmodium* has been intensively studied. Malarial antigens, including glycosylphosphatidylinositol (GPI) and hemozoin as well as

several pro-inflammatory cytokines (*e.g.* IFN-γ and TNF-α) can induce iNOS expression in macrophages and lead to the synthesis of inflammatory levels of NO that damage the erythrocytic *Plasmodium* (Tachado *et al.,* 1996; Carney *et al.,* 2006).

Similarly, the role of NO in the control of *Plasmodium* is also preserved in mosquito vectors. The *Anopheles* mosquito possesses an invertebrate NOS that is homologous to the characterized mammalian NOSs (Luckhart *et al.,* 1998; Akman-Anderson *et al.,* 2007). In response to several parasite-induced pro-inflammatory cytokines and parasitic antigens, expression of mosquito NOS is significantly elevated in the midgut lumen by the invasion of *Plasmodium*. Later increases of mosquito NOS expression and enzyme activity have also been observed at the beginning of sporozoite release (Luckhart *et al.,* 1998). The induction of mosquito NOS leads to the synthesis of inflammatory levels of NO in the blood-filled midgut, adversely impacting *Plasmodium* development in the mosquito (Luckhart *et al.,* 1998; Rivero 2006). Consistently, it was found that the hemolymph level of NO is markedly higher in the *Plasmodium*-infected mosquitoes compared to uninfected mosquitoes (Herrera-Ortiz *et al.,* 2011). The mosquito-produced NO has been shown to induce apoptosis of a large fraction of invading ookinetes and mediate the killing of young oocysts. Pharmaceutically, inactivation of mosquito NOS results in a decreased proportion of apoptotic ookinetes and an increased number of developed oocysts in mosquitoes (Ali *et al.,* 2010). More recently, mosquito-produced NO has been shown to impair gametogenesis of male *Plasmodium* parasites and reduce the fertility of both male and female gametes (Ramiro *et al.,* 2011). These important observations highlight the important participation of NO in the mosquito's immune system against *Plasmodium*.

In accordance, several *in vitro* studies have confirmed that a number of NO donors have both cytostatic and cytotoxic effects on *Plasmodium* parasites (Rockett *et al.,* 1991; Taylor-Robinson 1997; Balmer *et al.,* 2000; Venturini *et al.,* 2000). Notably, the NO donors are much more potent in inhibiting the *Plasmodium* parasite than NO itself, suggesting that NO impacts the parasites in an indirect way, presumably dependent upon NO-derived RNS (Sobolewski *et al.,* 2005). Several parasitic targets have been suggested to be NO targets. Falcipain-1, a key plasmodial hemoglobinase, has been suggested to be an NO target. NO donors have been shown to inhibit falcipain-1 activity, presumably by targeting its active site cysteine (Venturini *et al.,* 2000).

Although the generation of NO from host immune defense combats *Plasmodium*, the parasites facilitate its survival by developing strategies to alleviate the insult of NO. Particularly, the erythrocytic *Plasmodium* is surrounded by a large amount of hemoglobin, which is a strong scavenger for NO (Liu *et al.,* 1998; Sobolewski *et al.,* 2005). The presence of intraparasitic hemoglobin may thereby reduce the NO burden to which the parasites are exposed. Importantly, *Plasmodium* parasites possess arginase, which catalyzes the conversion of L-arginine into L-ornithine and urea. Due to the fact that arginase and NOS share the same substrate (L-arginine), the parasite-encoded arginase attenuates the production of parasiticidal NO from host iNOS via arginine depletion (Vincendeau *et al.,* 2003). Moreover, the *P. falciparum* peroxiredoxin 1a (PfPrx1a) has been shown to degrade the most harmful reactive nitrogen intermediate, peroxynitrite, thus protecting the parasites from severe nitrosative stress (Nickel *et al.,* 2005).

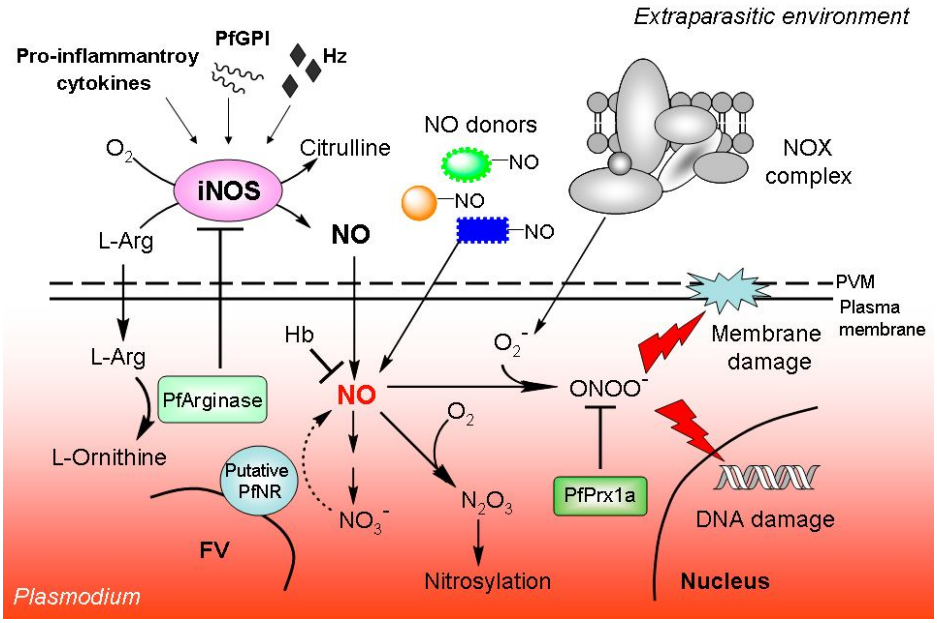

Figure 6. NO sources in *Plasmodium* parasites and the defense mechanism of *Plasmodium* against nitrosative stress. FV, food vacuole; Hb, hemoglobin; Hz, hemozoin; L-Arg, L-arginine; PfGPI, *P. falciparum* glycosylphosphatidylinositol; PfPrx1a, *P. falciparum* thioredoxin-dependent peroxiredoxin 1a; PfNR, *P. falciparum* nitrate reductase; PVM, parasitophorous vacuole membrane; NOX, NADPH oxidase.

1.2.2.2 NO production in *Plasmodium*

Although plasmodial homologs of NOS cannot yet be identified, the endogenous NO and RNS have been clearly detected in the erythrocytic stages of *Plasmodium* as well as in *Plasmodium* gametocytes (Ostera *et al.,* 2008). A strong intraparasitic NO signal was detected around the parasitic food vacuole (FV), where a putative plasmodial homolog of plant nitrate reductases (NRs) is localized (Ostera *et al.,* 2008; Ostera *et al.,* 2011). This indicates the endogenous NO in *Plasmodium* might be also derived from the reduction of nitrate/nitrite. The endogenous produced NO has been recently suggested to play a role in heme speciation inside the FV (Ostera *et al.,* 2011).

1.3 Protein *S*-nitrosylation

Protein thiols are major intracellular targets of NO. Particularly, protein *S*-nitrosylation (SNO) is an important protein posttranslational modification (PTM) induced by NO (Hess *et al.,* 2005). SNO refers to the reversible, covalent attachment of a nitroso group (-NO) to a reactive cysteine thiol of a protein to form *S*-nitrosothiol, which modulates conformation, stability, activity, localization, and functions of the respective protein (Hess *et al.,* 2005). In the past decade, accumulating evidence indicates that SNO has emerged as the principal mechanism in either NO signaling or NO-related toxicity, depending on the targeted pathway. So far, SNO has been studied in mammals, plants, and *E. coli* (Anand *et al.,* 2012; Astier *et al.,* 2012; Seth *et al.,* 2012), and over 3,000 proteins have been identified as potential targets of SNO (dbSNO website: dbsno.mbc.nctu.edu.tw/). In recent years, a growing body of research indicates that SNO is a tightly controlled process subjected to

spatiotemporal regulations by SNO-promoting and SNO-metabolizing factors **(Figure 7)**.

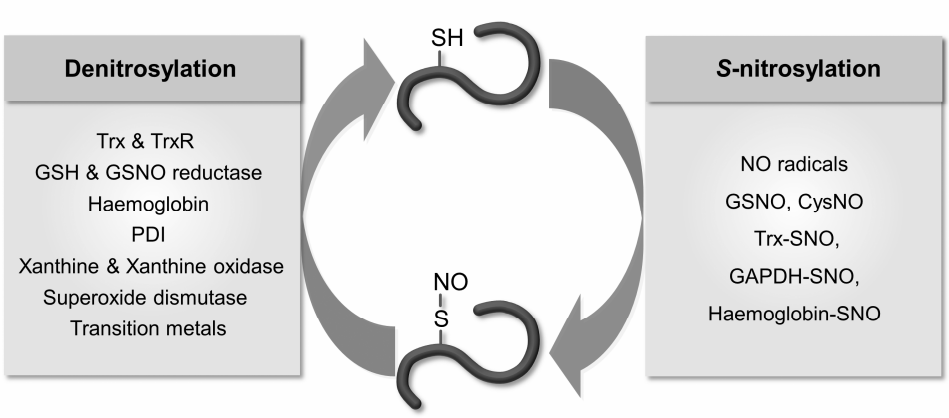

Figure 7. Catalysis of protein *S*-nitrosylation and denitrosylation. The figure is taken from (Jortzik *et al.,* 2012). Trx, thioredoxin; TrxR, thioredoxin reductase; GSH, reduced glutathione; GSNO, *S*-nitrosoglutathione; GSNOR, *S*-nitrosoglutathione reductase; PDI, protein disulfide-isomerase; NO, nitric oxide; Cys-NO, *S*-nitrosocysteine; Trx-SNO, *S*-nitrosylated thioredoxin; GAPDH-SNO, *S*-nitrosylated glyceraldehyde 3-phosphate dehydrogenase; haemoglobin-SNO, *S*-nitrosylated haemoglobin.

1.3.1 Formation of SNO

Protein *S*-nitrosylation can be formed in a direct reaction of protein thiols with higher NO oxides (*e.g.* N_2O_3) or metal-NO complexes (Hogg 2002). The reaction of thiols with nitrosylating equivalents is particularly relevant to SNO formation in the vicinity of a NO-generating source, for example, NOS. More importantly, SNO can be formed via transnitrosylation, in which the nitroso group is transferred from an *S*-nitrosothiol to a protein thiol (Hogg 2002; Hess *et al.,* 2005). Both low-molecular-weight *S*-nitrosothiols and protein *S*-nitrosothiols can transnitrosylate proteins. Notably, *S*-nitrosoglutathione (GSNO), which is derived from the interaction of glutathione with NO derivatives or protein *S*-nitrosothiols, is the major low-molecular-weight *S*-nitrosothiol in cells (Broniowska *et al.,* 2013). Given a higher cellular concentration of GSNO compared to free NO radicals, GSNO is considered an endogenous NO carrier and donor (Broniowska *et al.,* 2013). GSNO can efficiently induce SNO by transferring its nitroso group to protein thiols, thus playing an important role in mediating NO signaling (Hess *et al.,* 2005). Furthermore, protein-protein transnitrosylation represents another important pathway leading to the formation of SNO in cells (Nakamura *et al.,* 2013). Protein transnitrosylation generally requires a direct interaction of the two proteins and a spatial closeness of the *S*-nitrosothiol and the acceptor thiol to facilitate NO transfer (Hess *et al.,* 2005; Nakamura *et al.,* 2013). Specifically, the redox potential of the respective cysteine is a determinant for transnitrosylation: the *S*-nitrosylated thiol with a higher redox potential tends to lose the nitroso group and transfer it to a free thiol nearby with lower redox potential (Nakamura *et al.,* 2013). Because of these restrictive parameters, protein-protein transnitrosylation is expected to occur in a specific subset of proteins and therefore has a particular role in modulating specific signaling pathways.

1.3.2 Removal of SNO-denitrosylation

SNO is reversible. The reverse process of SNO is termed denitrosylation, which regulates the homeostasis of SNO (Benhar *et al.,* 2009). SNO decomposition can be catalyzed by a number of enzymes and transition metals. Importantly, recent research has revealed that the biologically relevant denitrosylation is an enzymatically controlled process. Particularly, the GSH/GSNO reductase system and thioredoxin system are two major denitrosylase systems in mammals and plant **(Figure 8)**.

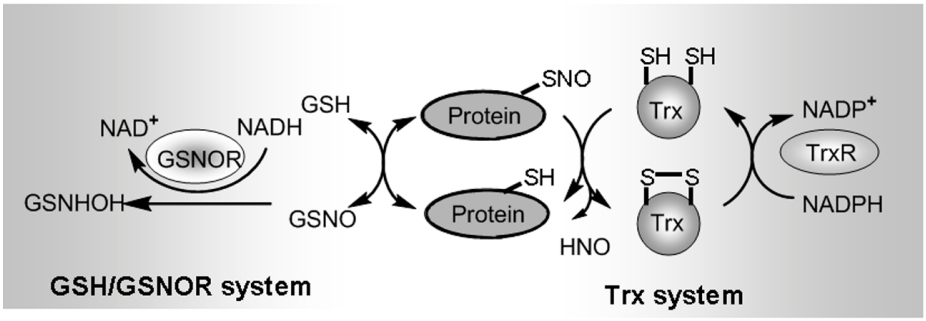

Figure 8. The schematic diagram of protein denitrosylation catalyzed by the thioredoxin system and GSH/GSNOR system. GSNOR, *S*-nitrosoglutathione reductase; Trx, thioredoxin; TrxR, thioredoxin reductase. Modified from (Benhar *et al.,* 2009)

S-nitrosothiols can be reduced to thiols by GSH, leading to the formation of GSNO (Broniowska *et al.,* 2013). The enzymatic metabolism of GSNO was not clear until a specialized GSNO-metabolizing enzyme was identified as class III alcohol dehydrogenase (ADH3), which has thus been renamed GSNO reductase (GSNOR) (Liu *et al.,* 2001). GSNOR plays a key role in decomposing SNO by acting on GSNO but not directly on protein *S*-nitrosothiols (Jensen *et al.,* 1998; Benhar *et al.,* 2009). GSNOR catalyzes the NADH-dependent reduction of GSNO to form glutathione sulfonamide, which can be further derived to oxidized glutathione (Benhar *et al.,* 2009). Through this mechanism, GSNOR governs protein *S*-nitrosothiols and controls SNO-based NO signaling by regulating cellular levels of GSNO. Depletion of GSNOR from yeast or mouse has been shown to result in increased cellular levels of GSNO and *S*-nitrosylated proteins as well as an increased susceptibility of cells to nitrosative stress, thus highlighting the important role of GSNOR in regulating the homeostasis of SNO in cells (Liu *et al.,* 2001; Liu *et al.,* 2004).

Another important denitrosylase system is the Trx system, which is composed of Trx, TrxR, and NADPH (Wu *et al.,* 2011). Trx is a ubiquitous protein disulfide reductase and a central player in cellular redox metabolism. The denitrosylating activity of Trx has been intensively studied in recent years. It has been found that Trx is able to denitrosylate a broad spectrum of *S*-nitrosylated proteins and many low-molecular-weight *S*-nitrosothiols, including GSNO, *S*-nitrosocysteine (CysNO), and *S*-nitroso-*N*-acetylpenicillamine (SNAP) (Stoyanovsky *et al.,* 2005; Sengupta *et al.,* 2007). The denitrosylating activity of Trx is attributed to the catalytic cysteine residues located in the conserved active-site Cys-Gly-Pro-Cys motif (Sengupta *et al.,* 2013). Trx-mediated denitrosylation may involve two possible transition states, either by forming an intermolecular disulfide intermediate between

Trx and the substrate or by a transnitrosylation of Trx at one active-site cysteine thiol to form a transient *S*-nitroso-monothiol. The denitrosylation reaction leads to the release of HNO and the formation of an active-site disulfide in Trx (*i.e.* the oxidized Trx). Subsequently, TrxR reduces the disulfide of Trx to recycle the reduced Trx (Benhar *et al.,* 2009; Sengupta *et al.,* 2013).

The key role of TrxR/Trx in cellular denitrosylation is highlighted by the fact that the Trx system regulates the denitrosylation of caspase-3. It has been shown that in resting human lymphocytes, Trx1 actively denitrosylates cytosolic caspase-3 and thereby maintains a low steady-state amount of *S*-nitrosylated caspase-3. Upon apoptotic stimulus, the mitochondrial form of Trx (Trx2) mediates the denitrosylation of mitochondria-associated caspase-3, thereby activating caspase-3 and promoting apoptosis (Benhar *et al.,* 2008).

Besides caspase-3, a wide range of proteins appear to be denitrosylation substrates of the Trx system such as albumin, metallothionenin, caspase-8, and caspase-9 (Sengupta *et al.,* 2007; Benhar *et al.,* 2009; Sengupta *et al.,* 2010). Indeed, it was observed that Trx-catalyzed denitrosylation accounts for a 72% reduction of protein *S*-nitrosothiol levels in isolated liver homogenates (Doulias *et al.,* 2010). Furthermore, an impaired Trx system with mutated TrxR in Hela cells has led to a dramatically decreased denitrosylation efficiency and a marked accumulation of *S*-nitrosothiols in cells (Stoyanovsky *et al.,* 2005). Taken together, these studies point out an indispensable role of the Trx system in the reversible regulation of SNO.

1.3.3 Biological significance of SNO

Protein *S*-nitrosylation serves as a major mode of redox signaling in cells (Nakamura et al., 2013). An early study by Jia *et al.* first reported a physiological transnitrosylation between hemoglobin (Hb) and the anion exchanger 1 (AE1), an erythrocyte membrane-bound protein (Jia et al., 1996). Hemoglobin auto-catalyzes *S*-nitrosylation of its β-chain at Cys93 by using the heme-bound NO group. The *S*-nitrosylated Hb then undergoes conformational change, allowing the binding to the cytoplasmic tail of AE1 and the subsequent transnitrosylation of AE1. The *S*-nitrosylated AE1 further releases NO out of the erythrocyte, thus mediating the vascular relaxing activity of NO **(Figure 9A)**.

More recently, transnitrosylation by Trx has been shown to regulate cell death. In addition to the active-site cysteine, human Trx possesses three additional cysteine residues (Cys62, Cys69, and Cys73). In contrast to the active-site cysteine that mediates denitrosylaion, Cys73 of Trx can be *S*-nitrosylated to form *S*-nitrosylated Trx (Trx-Cys73-NO) and mediate transnitrosylation activity of Trx. The nitrosylation of Cys73 appears to occur when the active-site cysteines are oxidized to a disulfide, therefore indicating that Trx may transduce NO stress upon oxidative/nitrosative stress via transnitrosylation (Wu et al., 2010). Interestingly, an exemplary transnitrosylation substrate of Trx is caspase-3, which is also a denitrosylation substrate of Trx (Mitchell et al., 2005). The *S*-nitrosylated caspase-3 can transnitrosylate the X-linked inhibitor of apoptosis (XIAP), which is an E3 ubiquitin ligase that prevents apoptosis by binding to caspase-3 and promoting the proteasomal degradation of caspase-3 (Nakamura *et al.,* 2010; Nakamura *et al.,* 2013). Nitrsosylation of XIAP inhibits its E3 ubiquitin ligase activity, thereby blocking its ability to inhibit apoptosis (Tsang *et al.,* 2009). As such, transnitrosylation of XIAP by *S*-nitrosylated caspase-3 contributes to the preservation of active caspase-3, thereby mediating cell

apoptosis under nitrosative stress (Nakamura *et al.,* 2013) **(Figure 9B)**.

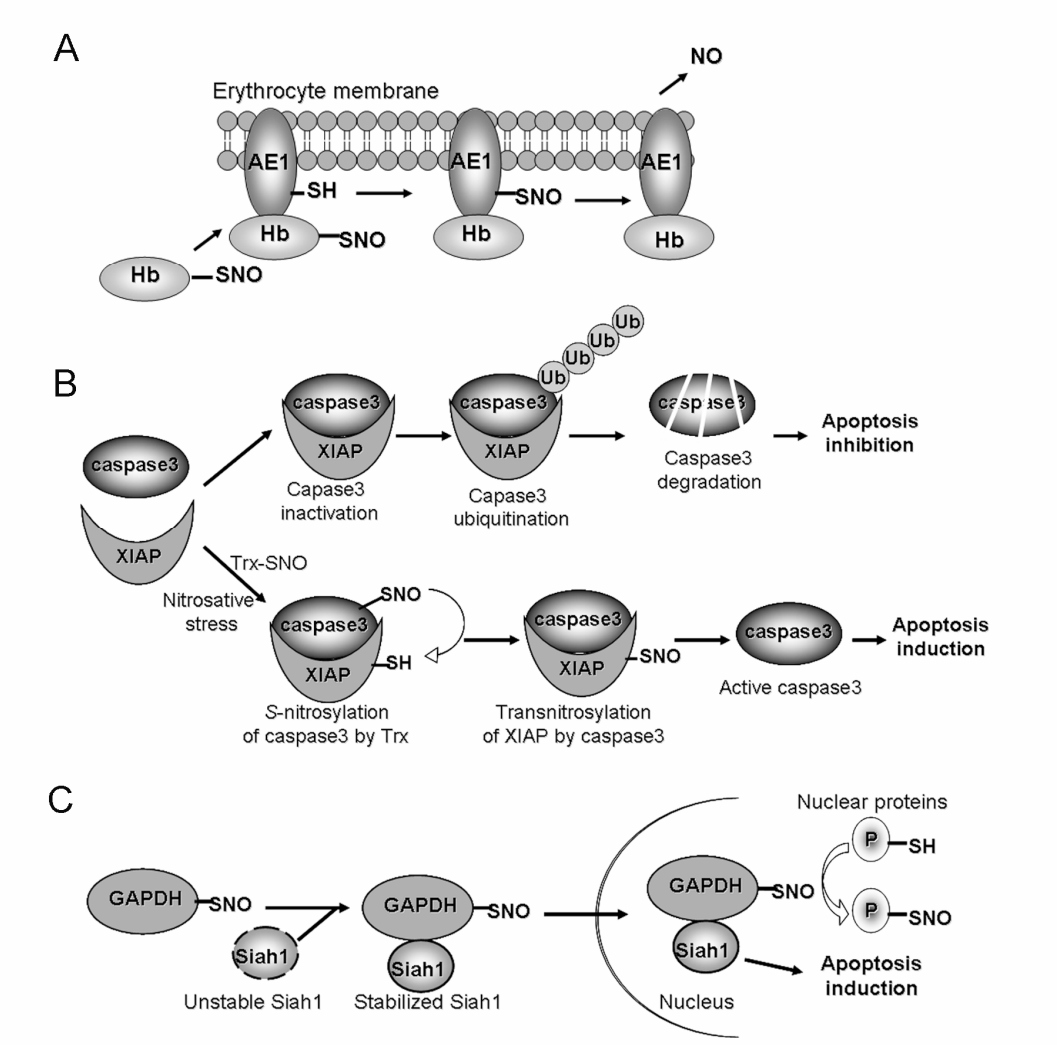

Figure 9. Schematic illustration of different cellular pathways regulated by SNO. A) The pathway exporting NO from erythrocytes requires transnitrosylation of AE1 by the *S*-nitrosylated Hb. AE1, anion exchanger 1; Hb, hemoglobin. B) Transnitrosylation in Trx-caspase3-XIAP pathway mediates apoptotic cell death. Trx, thioredoxin; XIAP, X-linked inhibitor of apoptosis. Ub, ubiquitin C) *S*-nitrosylation of GAPDH mediates the binding of Siah1, nuclear translocation of the GAPDH-Siah1 complex and cell apoptosis. Siah1 is an E3 ubiquitin ligase encoded in humans by the *SIAH1* gene. Modified from (Nakamura *et al.,* 2013)

Furthermore, *S*-nitrosylation of GAPDH has been shown to mediate its nuclear translocation and induce apoptotic cascades. Hara *et al.* have found that *S*-nitrosylation of the catalytic cysteine of GAPDH promotes the binding of Siah1, an E3 ubiquitin ligase possessing a nuclear localization signal. Then, the GAPDH/Siah1 complex is translocated to the nucleus, where GAPDH stabilizes Siah1, promoting the Siah1-mediated degradation of nuclear proteins and causing apoptotic cell death (Hara *et al.,* 2005). More recently, Kornberg *et al.* found that nucleus-localized *S*-nitrosylated GAPDH physiologically transnitrosylates nuclear proteins, including the deacetylating enzyme sirtuin-1 (SIRT1), histone deacetylase-2 (HDAC2), and DNA-activated

protein kinase (DNA-PK) (Kornberg *et al.,* 2010). They further demonstrated that transnitrosylation of SIRT1 inhibits the activity of SIRT1 and decreases the transcriptional activity of PGC1α, a downstream effector of STRT1 (Kornberg *et al.,* 2010). As such, the GAPDH-mediated transnitrosylation in GAPDH-SIRIT1 pathway has been suggested to have pathophysiological relevance in neurodegeneration and metabolic dysfunctions (Nakamura *et al.,* 2013) **(Figure 9C)**.

1.4 The ubiquitin-proteasome system

Intracellular protein degradation is an intricately regulated process that governs protein homeostasis by removing damaged or misfolded proteins. In eukaryotic cells, the majority of intracellular proteins are degraded by the ubiquitin-proteasome system (UPS) (Glickman *et al.,* 2002).

1.4.1 The ubiquitin system

Degradation of proteins by the UPS typically involves a covalent attachment of the small protein ubiquitin (Ub) to the protein destined to be degraded, the so-called ubiquitination process, a major type of protein posttranslational modification (Goldstein *et al.,* 1975; Pickart 2001). The modification process most commonly attaches the last amino acid (Gly76) of ubiquitin to a lysine residue on the substrate. Ubiquitination consists of three main steps, which are concertedly catalyzed by a cascade of three enzymes, namely ubiquitin-activating enzyme (E1), ubiquitin-conjugating enzyme (E2), and ubiquitin ligase (E3) (Glickman *et al.,* 2002). The human genome encodes two ubiquitin-specific E1s, about fifty E2s, and hundreds of E3s (Pickart *et al.,* 2004). It is generally believed that the specificity of ubiquitination largely depends on the respective E3 that specifically catalyzes a certain group of proteins (Glickman *et al.,* 2002).

Ubiquitination begins with the ATP-dependent activation of Ub catalyzed by an E1, resulting in a thioester linkage formed between the C-terminal carboxyl group of Ub and the cysteine sulfhydryl group in the active site of E1. Then, an E2 enzyme further catalyzes the transfer of Ub from E1 to the active site cysteine of E2. In the final step, by directly binding to both E2 and the specific target protein, an E3 enzyme creates an isopeptide bond between the C-terminal glycine of Ub and a lysine of the target protein, thereby adding the Ub molecule to the target protein **(Figure 10)**.

Ubiquitination can be generally divided into two classes: the monoubiquitination and polyubiquitination (Komander 2009). Monoubiquitination refers to the addition of one Ub molecule to one site or to multiple sites (multi-monoubiquitination) on the substrate protein. Monoubiquitination has been shown to be involved in several non-proteolytic events, such as membrane trafficking, endocytosis, and viral budding (Miranda *et al.,* 2007; Ikeda *et al.,* 2008). In contrast, polyubiquitination is the formation of a polyubiquitin (polyUb) chain on a single site on the substrate protein. After the attachment of the first Ub to a target protein, further Ub molecules can be added stepwise by linking the glycine residue of a Ub molecule to a lysine residue of another ubiquitin, thus forming the polyUb chain on the targeted protein. The Ub molecule possesses seven lysine residues (K6, K11, K27, K29, K33, K48, and K63) available for polyUb linkage (Komander 2009). Particularly, the K48-linked polyubiquitination, the best characterized type of polyubiquitination, targets proteins for

proteasomal degradation (Komander 2009). Notably, at least four Ub molecules must be built up during polyubiquitination in order to facilitate recognition of the protein for proteasomal degradation (Hicke 2001). After the protein is tagged with the polyUb chain, the protein can either be transported by substrate shuttle proteins to the proteasome or directly binds to the proteasome for degradation (Glickman *et al.,* 2002).

Protein ubiquitination is reversed by the deubiquitination process. Deubiquitination is catalyzed by deubiquitylating enzymes (DUBs), which cleave ubiquitin from its target proteins (Wilkinson 1997). DUBs represent a large group of proteases that fall into two major classes, cysteine proteases and metalloproteases. Most DUBs are cytsteine proteases, which can be subdivided into four classes, the ubiquitin-specific proteases (USPs), ubiquitin C-terminal hydrolases (UCHs), ovarian tumor proteases (OTU), and Machado-Josephin domain proteases (MJDs). The metalloprotease group contains only the Jab1/Mov34/MPN+ (JAMM) domain-containing proteases (Glickman *et al.,* 2002; Reyes-Turcu *et al.,* 2009). Nearly a hundred DUBs are encoded in the human genome, whereas twenty DUBs have been found in yeast, implying the importance of deubiquitination and the diverse substrate specificity of DUBs in cells (Amerik *et al.,* 2000; Reyes-Turcu *et al.,* 2009). While most DUBs are free enzymes, three DUBs have been found to be physiologically associated with the 26S proteasome, indicating the importance of deubiquitination for proteasomal functions (Finley *et al.,* 2012).

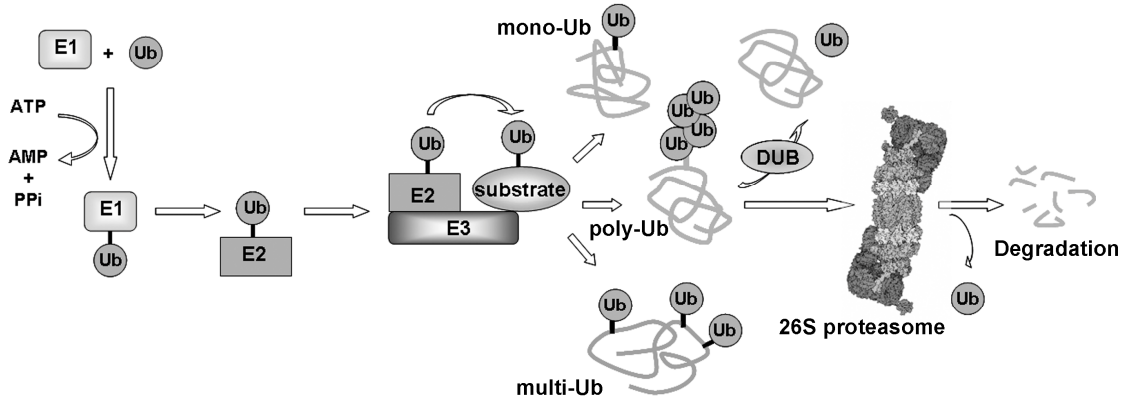

Figure 10. A schematic overview of protein degradation by the UPS system. E1, ubiquitin-activating enzyme; E2, ubiquitin-conjugating enzyme; E3, ubiquitin ligase. DUB, deubiquitinase. Ub, ubiquitin.

1.4.2 The 26S proteasome

1.4.2.1 The structure of the 26S proteasome

The proteasome holoenzyme (known as the 26S proteasome) is a ~2.5 MD ATP-dependent chambered protease present in the nucleus and cytoplasm of eukaryotes (Tomko *et al.,* 2013). The main function of the proteasome is to degrade damaged or misfolded proteins via proteolysis (Tomko *et al.,* 2013). The 26S proteasome is a barrel-shaped complex composed of a 20S core particle (CP) and two 19S regulatory particles (RP) that stack to both ends of the 20S CP (Peters *et al.,* 1994) (**Figure 11**). Purified proteasomes usually contain a mixture of free 20S CP (i.e. the 20S proteasome), single or double 19S RP-capped 20S CP. The structure of 20S CP is built

up with four stacked heptameric rings (Tanahashi *et al.,* 2000; Tomko *et al.,* 2013). In mammals, each of the two identical outer rings consists of seven different alpha-subunits (α_1-α_7) and each of the two identical inner rings contains seven different beta-subunits (β_1-β_7). The proteolytic activity of the proteasome is found in three 20 CP beta-subunits: β_1, β_2, and β_5, which possess peptidylglutamyl-peptide hydrolytic (PGPH) activity, trypsin-like activity, and chymotrypsin-like activity, respectively (Tomko *et al.,* 2013). Free 20S CP found in cells usually has a low proteolytic activity by itself, at least against folded proteins (Coux *et al.,* 1996). This is due to the fact that entry into the inner proteolytic chamber is generally occluded by the outer alpha-subunits, of which N-termini form a closed "gate" that blocks protein entry (Rabl *et al.,* 2008). However, the binding of 19S RP or the proteasome activator PA28 to the 20S CP can mediate the "gate" opening, thus inducing the peptidase activity of the 20S CP (Lehmann *et al.,* 2008; Rabl *et al.,* 2008).

In mammals, alternative forms of β_1, β_2, and β_5 (β_1i, β_2i, and β_5i) can be expressed in response to pro-inflammatory cytokines, especially in hematopoietic cells (Haorah *et al.,* 2004). They can be incorporated into the 20S CP by replacing the corresponding beta-subunits, thereby altering the proteolytic specificity of the 20S CP. The proteasome assembled with these alternative subunits is known as the immunoproteasome, which has important functions in antigen presentation and the defense of pathogens (Angeles *et al.,* 2012).

The 19S RP functions as a highly regulated keeper that responsible for the binding, deubiquitylation, unfolding, and translocation of substrates into the 20S CP as well as regulating the gating of the 20S CP (Tomko *et al.,* 2013). The 19S complex is an asymmetric particle composed of at least 19 different subunits. It can be divided into two subassemblies, the base and lid. The base contains six regulatory particle triple-A ATPases (Rpts) and four regulatory particle non-ATPases (Rpns). The ATPase subunits form a heterohexameric ring in the order of Rpt1/Rpt2/Rpt6/Rpt3/Rpt4/Rpt5 and directly contact with the 20S alpha-ring (Beckwith *et al.,* 2013). Importantly, these ATPase subunits function in unfolding and translocation of the substrates as well as mediating the gate opening of 20S CP, thereby facilitating the entry of substrate proteins into the 20S catalytic chamber (Beckwith *et al.,* 2013). The Rpn1 and 2 are the two largest subunits in the proteasome. They form scaffolds for the docking of substrates and other proteasome-interacting partners (Tomko *et al.,* 2013). Particularly, Rpn10 and 13 function as intrinsic ubiquitin receptors of the proteasome, thereby mediating the recognition of ubiquitinated substrate by the proteasome (Sakata *et al.,* 2012). The lid is composed of nine non-ATPase subunits covering the base (Sharon *et al.,* 2006). One best known function of the lid is the substrate deubiquitination, which is attributed to the Rpn11 subunit (Verma *et al.,* 2002). The Rpn11 subunit contains a highly conserved Jab1/MPN domain-associated metalloisopeptidase (JAMM) motif as a zinc-binding site serving for the hydrolysis of ubiquitin from a ubiquitinated protein. This deubiquitination process plays important roles in recycling ubiquitin and facilitating the substrate degradation by the proteasome.

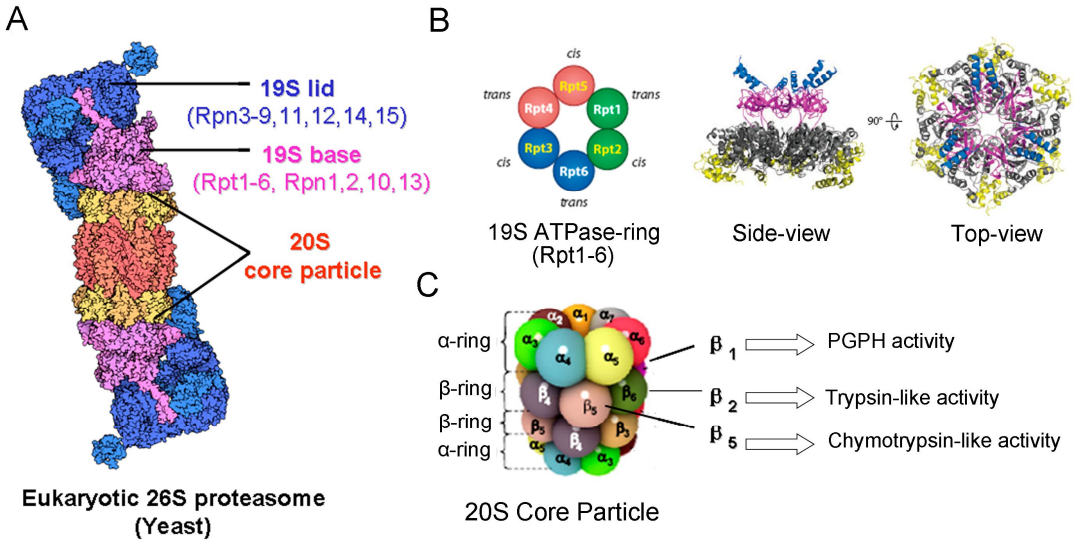

Figure 11. The structure of the eukaryotic 26S proteasome. A) The 26S proteasome is composed of a 20S core particle capped with two 19S regulatory particles, which can be divided into the 19S lid and the 19S base. B) The arrangement (top-view) of ATPase subunits in forming the 19S ATPase-ring (left) and the complex structure of the ATPase-ring in side- and top-view. C) The 20S CP consists of two heptameric alpha-rings and two heptameric beta-rings, in which three beta-subunits with different proteolytic activities are located. Modified from (Jung *et al.,* 2013; Tomko *et al.,* 2013). The 26S proteasome image was downloaded from http://www.rcsb.org (October 2013 Molecule of the Month by David Goodsell).

1.4.2.2 The mechanism of action of the 26S proteasome

Protein degradation by the 26S proteasome is a highly controlled process that involves substrate recognition and processing, unfolding, translocation and proteolysis, which will be described in the following paragraphs (Glickman *et al.,* 2002).

1.4.2.2.1 Substrate recognition

Over the past decades, structural and mechanistic studies of the 19S RP have provided significant insights into the specialized roles of 19S RP components in regulating proteasomal function. Of particular importance, two 19S RP subunits, Rpn10 and Rpn13, have been identified as intrinsic ubiquitin receptors of the proteasome for substrate recognition (Mueller *et al.,* 2003; Fujiwara *et al.,* 2004; Husnjak *et al.,* 2008). Rpn10 (in human termed S5a) was the first identified ubiquitin receptor in the 19S RP. It has a von Willebrand factor A (vWA) domain at the N-terminal region, and one or more ubiquitin-interacting motifs (UIMs) in the carboxyl-terminal half of the protein, depending on the species (Tomko *et al.,* 2013). For example, human S5a contains two UIMs: UIM1 and UIM2, whereas the *Saccharomyces cerevisiae* homolog of human S5a (Rpn10) contains only UIM1 (Young *et al.,* 1998). In human S5a, the two UIMs are approximately 30-amino acids long and are separated by 50 intervening residues. The UIMs form an α-helical structure and possess a special amino acid sequence containing 5 hydrophobic residues Leu-Ala-Leu-Ala-Leu (LALAL), which has been demonstrated to be essential for

binding the K-48-linked polyubiquitin chain. Each UIM has been shown to have greater affinity to bind the longer polyubiquitin chain, and UIM2 appears to have a higher affinity than UIM1. The selectivity of binding the polyubiquitin chain most likely arises from the hydrophobic interaction between the UIM helix with the hydrophobic patch of ubiquitin and the association of the helix with the opposing ubiquitin present at an interface among two ubiquitins (Fisher *et al.,* 2003) **(Figure 12)**. Indeed, the human S5a accordingly has much stronger binding affinity for polyubiquitinated protein than for mono- and di-ubiquitinated proteins, which may be responsible for the preferential recognition of polyubiquitinated proteins as proteasome substrate (Young *et al.,* 1998).

A recent study screening additional ubiquitin receptors identified Rpn13 as another important intrinsic ubiquitin receptor in the proteasome (Husnjak *et al.,* 2008; Schreiner *et al.,* 2008). Rpn13 docks at the 19S RP by binding to Rpn2 and has a C-terminal region that binds a deubiquitinase Uch37/UCHL5. Importantly, it was found that Rpn13 binds ubiquitin and a subset of ubiquitin-like proteins via a conserved N-terminal region termed the Pleckstrin-like receptor for ubiquitin (Pru) domain, which has been shown to bind K48-linked diubiquitin with an affinity of approximately 90 nM (Schreiner *et al.,* 2008). The Pru domain contains two β-sheets orthogonally packed against each other and a C-terminal α-helix, which is located in the crevice of a β-sandwich. The ubiquitin binding entities of Rpn13 are distributed into three non-contiguous loops within the Pru domain, significantly differing from those of Rpn10 **(Figure 12)**. Sequence analysis reveals that the Pru domain is highly conserved in eukaryotic organisms from yeast to mammals, indicating that the Pru domain of Rpn13 is indeed an inhered ubiquitin receptor of the 26S proteasome (Husnjak *et al.,* 2008).

Besides the intrinsic ubiquitin receptors in the 26S proteasome, several UBL-UBA proteins appear to be extrinsic ubiquitin receptors involved in the recognition of proteasome substrates and the delivery of the substrates to the proteasome (Winget *et al.,* 2010). These proteins typically have a ubiquitin-like (UBL) domain and one or two ubiquitin-associated (UBA) domain(s) (Elsasser *et al.,* 2005). The N-terminal UBL domain serves as a docking site for the 19S RP of the proteasome, whereas the UBA domain binds ubiquitin (Elsasser *et al.,* 2005). The 19S RP-localized Rpn10 and Rpn1 have been shown to be possible binding sites for the UBL domain of the UBL-UBA proteins (Hiyama *et al.,* 1999; Elsasser *et al.,* 2002). The UBA domain forms a large hydrophobic surface patch that interacts with the hydrophobic surface on the five-stranded β-sheet of ubiquitin (Mueller *et al.,* 2002). As such, the UBL-UBA proteins function as shuttle factors that deliver the ubiquitinated substrates to the proteasome for degradation (Elsasser *et al.,* 2005). Three UBL-UBA proteins have been identified in yeast, namely Rad23, Dsk2, and Ddi1, which have multiple orthologs in higher eukaryotes (Elsasser *et al.,* 2005). The UBL-UBA proteins may have different ubiquitin chain specificities. The UBA domain of hRad23A (human Rad23 isoform A) prefers K48-linked chains, whereas the UBA domain in human Dsk2 has no notable preference for K48- compared to K63-linked ubiquitin chains (Zhang *et al.,* 2008).

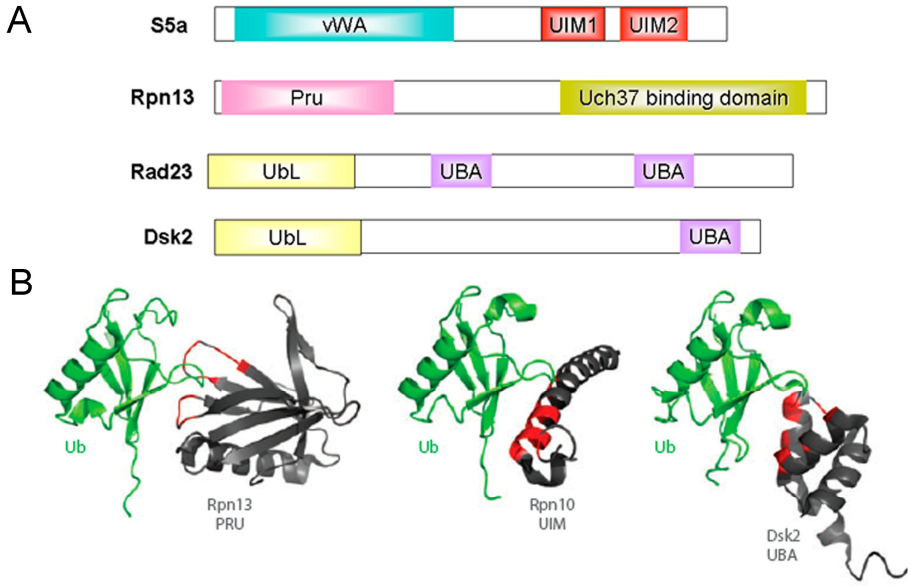

Figure 12. Ubiquitin receptors. A) Domain organization of the intrinsic Ub receptors S5a (human) and Rpn13 and the extrinsic receptors Rad23 and Dsk2. B) Distinct modes of interaction with Ub are used by different ubiquitin receptors. Amino acids of each ubiquitin-interacting domain are highlighted in red. vWA, von Willebrand factor A domain; UIM, ubiquitin-interacting motif; Pru, Pleckstrin-like receptor for ubiquitin domain; UBL, ubiquitin-like domain; UBA, ubiquitin-associated domain. Modified from (Tomko *et al.,* 2013)

1.4.2.2.2 Deubiquitination at the proteasome

After binding to the proteasome, the polyubiquitinated substrates undergo deubiquitination at the proteasome either prior to or potentially concomitant with substrate unfolding (Tomko *et al.,* 2013). As aforementioned, a lid metalloprotease Rpn11 is responsible for the cleavage of the ubiquitin chain off the substrate (Yao *et al.,* 2002). Although Rpn11 is unlikely an ATPase, the deubiquitinating activity of Rpn11 appears to be ATP-dependent, most likely due to the fact that protein unfolding by the ATPase(Rpt)-ring facilitates the action of Rpn11 (Lee *et al.,* 2011). A recent study using electron microscopy reported that the active site of Rpn11 is positioned 10-20 Å over the pore of the ATPase-ring. During the protein unfolding process, a conformational change in the protein positions the polyubiquitin chain near the pore of the ATPase-ring, bringing it into the position that allows Rpn11 to act (Lander *et al.,* 2012). In agreement, Rpn11 preferentially cleaves the ubiquitin proximal to the substrate protein's end, thereby cutting the polyubiquitin chain as a whole. The deubiquitination catalyzed by Rpn11 may further promote protein unfolding and threading through the ATPase-ring (Verma *et al.,* 2002).

In addition to Rpn11, the 26S proteasome harbors two extrinsic DUBs associated with the 19S RP, the ubiquitin carboxy-terminal hydrolase-37 (Uch37) and the ubiquitin-specific protease-6 (Ubp6, in human USP14) (Lee *et al.,* 2011). Both of them are cysteine proteases, which are different from the Zn^{2+}-dependent metalloprotease Rpn11. Uch37 binds the 19S RP by docking to the C-terminal domain of Rpn13, whereas Ubp6 principally binds to Rpn1 via its N-terminal ubiquitin-like domain. Interestingly, both enzymes must be activated via incorporation into the 19S complex, indicating that their ubiquitin chaining-trimming role is important and

restricted at the proteasome (Leggett *et al.,* 2002; Hu *et al.,* 2005). In contrast to Rpn11, Uch37 and Ubp6 trim ubiquitin chains from the distal end, thereby editing the length of the polyubiquitin chain of substrate proteins (Kim *et al.,* 2011). More strikingly, the removal of ubiquitin catalyzed by the two DUBs appears to antagonize the protein degradation by the proteasome (Hanna *et al.,* 2006). A commonly accepted view is that trimming the ubiquitin chain with the two DUBs provides a quality control mechanism, allowing poorly ubiquitinated or unproductively bound substrates to escape the proteasomal degradation (Ehlinger *et al.,* 2013). Therefore, the deubiquitination concertedly operated by Rpn11, Uch37 and Ubp6 at the proteasome plays important decisive roles in initiating the proteasomal degradation.

1.4.2.2.3 Substrate unfolding and translocation

In order to be degraded, the substrate protein must enter the 20S CP and come in contact with the proteolytic beta-subunits. Unfolding of protein substrates is therefore necessary in order for the protein to enter into the narrow channel of the 20S CP (Finley *et al.,* 2012). Substrate unfolding has been demonstrated to be a strictly ATP-dependent process, which is catalyzed by the heterohexameric ATPase-ring in the 19S base (Rabl *et al.,* 2008). The studies on the archaeal ATPase complex PAN (Proteasome-Activating Nucleotidase), the homolog of eukaryotic ATPase ring complex, have advanced our knowledge in understanding the protein unfolding process. It was proposed that a conserved aromatic hydrophobic (Ar-Φ) loop protrudes from every ATPase subunit into the pore of the ATPase ring. Upon ATP hydrolysis, conformational changes of the ATPase domains move the pore loops along the axis of the channel, providing the driving force for substrate unfolding and translocation (Sauer *et al.,* 2011).

1.4.2.2.4 Proteolysis

Once the unfolded substrates thread into the 20S catalytic chamber, they are subjected to proteolysis by the proteolytic beta-subunits, β_1, β_2 and β_5 (Finley *et al.,* 2012). All the catalytic β subunits belong to the family of threonine proteases, which harbor an active-site threonine residue (Tomko *et al.,* 2013). The mechanism of proteolysis involves a threonine-dependent nucleophilic attack of the substrate. The three catalytic subunits differ in their catalytic preference: β_1 cleaves after acidic or small hydrophobic amino acids, β_2 cuts after basic or small hydrophobic amino acids, while β_5 hydrolyzes the peptide bond after hydrophobic residues regardless of whether they are bulky or not (Dick *et al.,* 1998). In most cases, the proteasome cleaves protein substrates into small peptides with lengths of 3 and 23 amino acids (Kisselev *et al.,* 1999), and the peptides can be further hydrolyzed by downstream proteases and aminopeptidases (Glickman *et al.,* 2002). The products of proteasomal degradation can be utilized as amino acid sources for protein biosynthesis or for antigen presentation by major histocompatibility complex (MHC) class I molecules (Glickman *et al.,* 2002; Warnatsch *et al.,* 2013).

Notably, although the proteasome mainly breaks down the ubiubiquitinated protein substrates, it may also degrade a number of non-ubiquitinated substrates, *i.e.* ubiquitin-independent degradation by the proteasome. An exemplary non-ubiquitinated proteasome substrate is ornithine decarboxylase (ODC), a key enzyme in polyamine biosynthesis (Zhang *et al.,* 2003). It has been revealed that the proteasomal degradation of ODC is

mediated by its inhibitory partner, the antizyme (AZ) (Coffino 2001). Antizyme physiologically binds ODC and promotes its association with the proteasome, where the exposure of an unstructured region of ODC provides the initiation site for protein unfolding at the 19S RP, thereby facilitating further degradation by the 20S CP (Godderz *et al.,* 2011). In contrast to ODC, some proteins are degraded by the 20S CP without the participation of the 19S RP. Blm10, a 246-kDa HEAT-repeat protein, functions as a "CP activator" (Dange *et al.,* 2011). A certain amount of 20S CP (20% in yeast) is bound to Blm10 instead of 19S RP (Schmidt *et al.,* 2005). Blm10 binds to the 20S CP via its C-terminus, by which Blm10 regulates the gate opening of 20S CP. By doing so, Blm10 may preferentially mediate the degradation of proteins that can bypass the ATP-dependent unfolding step, *i.e.* the substrate spontaneously unfolds at a high frequency or is constitutively unfolded (Dange *et al.,* 2011).

1.4.3 Proteasome inhibitors

Because a great diversity of intracelluar proteins is degraded through the proteasome, proteasomal functions are profoundly involved in various biological processes, including protein quality control, antigen processing, signal transduction, cell cycle control, cell differentiation, and apoptosis (Glickman *et al.,* 2002). Thereby, proteasome inhibitors are of great biological significance in intervention of certain cellular pathways via modulating the proteasomal activity (Nalepa *et al.,* 2006). So far, five classes of proteasome inhibitors have been found, including peptide aldehydes, peptide vinyl sulphones, peptide boronates, peptide epoxiketones and β-lactones (Borissenko *et al.,* 2007). Of note, proteasome inhibitors have been found to exhibit potent anticancer efficacy. Particularly, bortezomib, a small-molecule inhibitor of the 20S proteasome particle, has been successfully developed to become an anti-neoplastic drug for the treatment of relapsed and refractory multiple myeloma (Adams 2004). Importantly, bortezomib and other proteasome inhibitors show selective cytotoxicity to cancerous cells compared to normal cells in both *in vitro* and *in vivo* assays. The selectivity and specificity of proteasome inhibitors on cancerous cells may be due to the rapid proliferation rate of many cancerous cells that might make these cells more dependent on the proteasome to remove misfolded or damaged proteins, the accumulation of which may induce apoptosis (Adams 2004).

1.4.4 The ubiquitin-proteasome system of *Plasmodium*

1.4.4.1 The UPS in *Plasmodium*

As eukaryotes, *Plasmodium* parasites are supposed to preserve the UPS as the major machinery for intraparasitic protein degradation (Chung *et al.,* 2010). In fact, independent lines of evidence indicate the presence of a functional UPS in *Plasmodium* parasites. Over half of the parasite proteins have been predicted to be targets for ubiquitination, especially the proteins found to be present in the trophozoite and schizont stages (Ponts *et al.,* 2011). Besides, annotation of the genome for *P. falciparum* has revealed a similar componential profile of the plasmodial UPS to those of higher eukaryotic organisms. Notably, the UPS pathway in *P. falciparum* was deduced by Dr. Hagai Ginsburg. (http://sites.huji.ac.il/malaria/maps/proteaUbiqpath.html). Recently, Ponts *et al.* have conducted a comprehensive *in silico* analysis of proteins predicted to be involved in the apicomplexan ubiquitin-mediated pathway. Their study revealed a set of essential components in the ubiquitin pathway of *P.*

falciparum, including a plasmodial homolog of ubiquitin and ubiquitin-like molecules, ubiquitination enzymes (E1, E2, and E3), and deubiquitinases (Ponts *et al.,* 2008). Consistent to the *in silico* studies, ubiquitin conjugates have been detected abundantly in *P. falciparum* of all intraerythorytic stages (Ponts *et al.,* 2011). Furthermore, purification of ubiquitin conjugates in *P. falciparum* using anti-conjugated ubiquitin antibody has allowed the identification of 437 ubiquitinated proteins in the intraerythrocytic parasites (Ponts *et al.,* 2011). Several ubiquitination components in *P. falciparum* have also been biochemically characterized. Importantly, Chung *et al.* have recently characterized a cascade of fully functional ubiquitination enzymes that are specifically involved in the endoplasmic reticulum-associated degradation (ERAD) pathway of *P. falciparum* (Chung *et al.,* 2012). Besides, two putative deubiquitinases of *P. falciparum*, PfUCH54 and PfUCHL3, have been characterized in detail (Artavanis-Tsakonas *et al.,* 2006; Artavanis-Tsakonas *et al.,* 2010). Interestingly, PfUCH54 was demonstrated to have an additional deneddylating activity *in vitro*, which is absent from its human counterpart (Artavanis-Tsakonas *et al.,* 2006).

In addition to the ubiquitination pathway, the eukaryotic 26S proteasome also appears to be present in *Plasmodium*. An *in silico* search (Basic Local Alignment Search Tool, BLAST) using human 26S proteasome components as queries has revealed that the *P. falciparum* genome encodes all essential 26S proteasome subunits sharing high similarities with corresponding counterparts in human 26S proteasome (Aminake *et al.,* 2012). In agreement, Sessler and coworkers have managed to separate and detect the 20S CP complex in the schizont stage of *P. falciparum* by using an approach based on the blue native polyacrylamide gel electrophoresis (BN-PAGE) (Sessler *et al.,* 2012). Consistently, by using a specific antibody against the *P. falciparum* β5 subunit, Aminake *et al.* have observed that the β5 subunit is abundantly localized in the cytoplasm and nucleus of parasite trophozoites and schizonts as well as in the cytoplasm of gametocytes (Aminake *et al.,* 2011). Interestingly, it has been suggested that the *P. falciparum* proteasome may somewhat differ from the human proteasome in the insertion of *Plasmodium*-specific domains in certain proteasomal subunits, for example the asparagine-rich domain found in the plasmodial Rpn6 subunit and a large insert in the plasmodial β1 subunit (Muralidharan *et al.,* 2011; Sridhar *et al.,* 2013).

1.4.4.2 Inhibition of the plasmodial proteasome

Due to the essential roles of the UPS in all eukaryotic cells and the successful application of proteasome inhibitors in cancer therapeutics, a number of human proteasome inhibitors have been tested for their antiparasitic efficacy against *Plasmodium* (Gantt *et al.,* 1998; Lindenthal *et al.,* 2005; Reynolds *et al.,* 2007; Czesny *et al.,* 2009; Aminake *et al.,* 2011). As expected, human proteasome inhibitors have been demonstrated to exhibit potent antiplasmodial activities. Their potency is reflected by their efficiency in inhibiting *Plasmodium in vitro* at nanomolar concentrations (**Table 1**). Accumulation of ubiquitinated protein was commonly observed in the parasite lysate after treatment of the parasites with proteasome inhibitors, providing indirect evidence that the plasmodial proteasome is affected (Lindenthal *et al.,* 2005; Aminake *et al.,* 2011).

A remarkable advantage of proteasome inhibitors is their capability to inhibit *Plasmodium* parasites across different life stages. Different proteasome inhibitors have been shown to inhibit parasite growth in erythrocytic

stages at low nanomolar concentrations (**Table 1**). Particularly, the proteasome inhibitors lactacystin and MLN273 (a compound related to bortezomib) have been reported to have antiparasitic effects on liver stage parasites. Both can block the development of exoerythrocytic forms in liver hepatoma cells *in vitro*, and lactacystin has been shown to inhibit the infectivity of *P. berghei* in a mouse model (Gantt *et al.,* 1998; Lindenthal *et al.,* 2005). Furthermore, MG132 and epoxomicin have been reported to exhibit *in vitro* gametocytocidal effects within nanomolar concentrations, indicating that proteasome inhibitors may be applicable in transmission blockage by targeting *Plasmodium* gametocytes (Czesny *et al.,* 2009; Aminake *et al.,* 2011). Of particular importance, it has been found that proteasome inhibitors are equipotent against chloroquine-resistant *Plasmodium* parasites, suggesting that targeting the plasmodial proteasome may be a promising strategy that may bypass the issue of chloroquine resistance in treating malaria parasites (Reynolds *et al.,* 2007; Kreidenweiss *et al.,* 2008; Prudhomme *et al.,* 2008; Aminake *et al.,* 2011).

Table 1. The antimalarial effect of proteasome inhibitors*.

	Liver stages	Blood stages	Gametocytes
	100% inhibition [μM]	IC_{50} [μM]	100% elimination [μM]
Bortezomib	n.d.	0.03–0.56	n.d.
Epoxomicin	n.d.	0.002–0.03	0.03
Lactacystin	9.0	1.2–1.5	n.d.
MG-132	n.d.	0.04–0.05	0.5
MLN273	1.0	0.04	n.d.
Salinosporamide A	n.d.	0.01	n.d.
Thiostrepton	n.d.	8.9–16.7	8.9

*Modified from (Aminake *et al.,* 2012)

1.5 Aim of the study

The thesis consists of two parts: the study of protein *S*-nitrosylation in *P. falciparum* and the characterization of the 26S proteasome network in *P. falciparum*. The aims of each part are described below.

1) Protein *S*-nitrosylation in *P. falciparum*

As discussed before, it is evident that during its life cycle in humans and mosquito vectors, *P. falciparum* is exposed to NO and NO-derived reactive nitrogen species, which certainly have impacts on the development of the parasites. However, the mode of action of NO and its targets in *P. falciparum* have hardly been characterized. A striking biochemical feature of NO is to induce protein *S*-nitrosylation, and this protein modification has emerged as a principal mechanism by which NO exerts diverse biological effects. We therefore speculate that protein *S*-nitrosylation could also serve as an important mechanism for NO to exert biological functions in *P. falciparum*. In the study, we aimed to globally identify *S*-nitrosylated proteins in *P. falciparum* in order to shed light on potential NO targets in the parasites. Furthermore, we planned to study how protein *S*-nitrosylation is regulated in the parasites with respect to protein transnitrosylation and denitrosylation. This study should

contribute to our knowledge and understanding of how NO acts in malaria parasites and what the mechanism of NO toxicity/signaling in the malaria parasite might be.

2) Characterization of the 26S proteasome network in *P. falciparum*

Although compelling data have indicated the presence of a functional 26S proteasome network in *P. falciparum*, the componential integrity and functionality of the plasmodial 26S proteasome has not yet been systematically studied in detail. Besides, what might be different in the plasmodial 26S proteasome network compared to that of humans remains totally unclear. Therefore, this study aims to characterize (i) important components in the plasmodial proteasome system, mainly focusing on the factors that mediate the substrate recognition by the plasmodial proteasome, (ii) the componential integrity of the plasmodial 26S proteasome complex, and (iii) to identify important proteasome-interacting partners. In order to achieve these goals, we aim to develop an affinity purification method to isolate the intact plasmodial 26S proteasome together with proteasome-interacting partners from *P. falciparum*. By doing so, we sought to provide an initial insight into the 26S proteasome network in *P. falciparum* and pave the way for developing novel antimalarial agents targeting the UPS.

2. MATERIALS

2.1 Chemicals

Chemical	Company
1,4-Dithiothreitol (DTT)	Roth, Karlsruhe
4-(2-hydroxyethyl)-1-piperazineethanesulfonic acid (HEPES)	Roth, Karlsruhe
6-Aminohexanoic acid	Roth, Karlsruhe
7-Amino-4-methylcoumarin (AMC)	Enzo life Science, Lörrach
Acetic acid Acrylamide and bis-acrylamide solution (30/0.8%)	Roth, KarlsruheBioRad, München
Acetonitrile	Sigma Aldrich, Steinheim
Adenosinetriphosphate (ATP)	Sigma Aldrich, Steinheim
Agarose	PeqLab, Erlangen
Albumax	Gibco, Karlsruhe
Alkynyl biotin	Invitrogen, USA
Ammonium acetate	Sigma Aldrich, Steinheim
Ammonium persulfate (APS)	Sigma Aldrich, Steinheim
Ammonium sulfate	Roth, Karlsruhe
Azido myristic acid	Invitrogen, USA
Bacto-Agar	Roth, Karlsruhe
Boric acid	Roth, Karlsruhe
Bovine serum albumin (BSA)	Roth, Karlsruhe
Bradford reagent	BioRad, München
Bromophenol blue	Sigma Aldrich, Steinheim
Bz-Val-Gly-Arg-AMC (Bz-VGR-AMC)	Enzo life Science, Lörrach
Calcium chloride	Roth, Karlsruhe
Carbenicillin	Roth, Karlsruhe
Complete protease inhibitors	Roche, Mannheim
Coomassie brilliant blue R250	Sigma Aldrich, Steinheim
Coumaric acid	Sigma, Steinheim
Cystatin	Roth, Karlsruhe
Dimethyl sulfoxide (DMSO)	Roth, Karlsruhe
Dipotassium phosphate (K_2HPO_4)	Roth, Karlsruhe
Disodium hydrogen phosphate (Na_2HPO_4)	Roth, Karlsruhe
dNTPs	Fermentas, St. Leon-Rot
Ethanol	Roth, Karlsruhe
Ethidium bromide	Sigma Aldrich, Steinheim
Ethylene glycol tetraacetic acid (EGTA)	Roth, Karlsruhe
Ethylenediaminetetraacetic acid (EDTA)	Roth, Karlsruhe
Formic acid	Sigma Aldrich, Steinheim
Gentamycin	Invitrogen, Karlsruhe
Giemsa (0.4%, w/v)	Sigma Aldrich, Steinheim
Glucose	Merck, Darmstadt
Glutathione disulfide (GSSG)	Sigma Aldrich, Steinheim
Glutathione reduced (GSH)	Sigma Aldrich, Steinheim
Glycerol	Roth, Karlsruhe

Glycin	Roth, Karlsruhe
Hydrochloric acid	Roth, Karlsruhe
Hydrogen peroxide	Sigma Aldrich, Steinheim
Imidazole	Roth, Karlsruhe
Iodoacetamide (IAA)	Sigma Aldrich, Steinheim
Iodoacetyl-PEG2-biotin	Thermo Scientific Pierce
Isopropanol	Roth, Karlsruhe
Isopropyl-β-D-thiogalactopyranoside (IPTG)	Roth, Karlsruhe
Kanamycin	Roth, Karlsruhe
Lactacystin	Enzo life Science, Lörrach
L-Arabinose	Sigma Aldrich, Steinheim
Luminol	Sigma Aldrich, Steinheim
Magnesium chloride	Roth, Karlsruhe
Methanol	Roth, Karlsruhe
Methyl methanethiosulfonate (MMTS)	Sigma Aldrich, Steinheim
MG132	Enzo life Science, Lörrach
Milk powder	Roth, Karlsruhe
Neocuproine	Sigma Aldrich, Steinheim
Nickel-nitrilotriacetic acid (Ni-NTA)	Qiagen, Hilden
Nicotinamide adenine dinucleotide (NAD^+)	Sigma Aldrich, Steinheim
PEG 3350 (Polyethylene glycol)	Roth, Karlsruhe
PEG 6000	Roth, Karlsruhe
Pepstatin A	Sigma Aldrich, Steinheim
Phenylmethylsulfonylfluoride (PMSF)	Sigma Aldrich, Steinheim
Phosphate buffered saline tablet	Sigma Aldrich, Steinheim
Phosphoenolpyruvate (PEP)	Sigma Aldrich, Steinheim
Potassium dihydrogen phosphate (KH_2PO_4)	Roth, Karlsruhe
Potassium hydroxide (KOH)	Roth, Karlsruhe
Potassiumchloride (KCl)	Roth, Karlsruhe
RPMI 1640 Gibco	Invitrogen, Karlsruhe
Saccharose	Roth, Karlsruhe
Saponin	Roth, Karlsruhe
S-nitrosoglutathione (GSNO)	Sigma Aldrich, Steinheim
Sodium acetate	Roth, Karlsruhe
Sodium ascorbate (NaAsc)	Sigma Aldrich, Steinheim
Sodium chloride (NaCl)	Roth, Karlsruhe
Sodium dihydrogen phosphate (NaH_2PO_4)	Roth, Karlsruhe
Sodium dodecyl sulphate (SDS)	Merck, Darmstadt
Sodium hydrogen carbonate ($NaHCO_3$)	Roth, Karlsruhe
Sodium orthovanadate (Na_3VO_4)	Sigma Aldrich, Steinheim
SoftLink™ Soft Release avidin	Promega, Mannheim
Sorbitol	Sigma Aldrich, Steinheim
Suc-Leu-Leu-Val-Tyr-AMC (Suc-LLVY-AMC)	Enzo life Science, Lörrach
Tetramethylethylenediamine (TEMED)	Sigma Aldrich, Steinheim

Tetramethylethylenediamine (TEMED)	Sigma Aldrich, Steinheim
Triethylamine hydrochloride (TEA-HCl)	Sigma, Steinheim
Tris(2-carboxyethyl)phosphine (TCEP)	Sigma Aldrich, Steinheim
Tris(hydroxymethyl)aminomethane (Tris)	Roth, Karlsruhe
Tris[(1-benzyl-1H-1,2,3-triazol-4-yl)methyl]amine (TBTA)	Sigma Aldrich, Steinheim
Triton X-100	Sigma Aldrich, Steinheim
Trypton	Roth, Karlsruhe
Tween 20	Merck, Darmstadt
Urea	Roth, Karlsruhe
Yeast extract	Oxoid LTD, U.K
Z-Leu-Leu-Glu-AMC (Z-LLE-AMC)	Enzo life Science, Lörrach

2.2 Biological materials

2.2.1 Antibodies

Antibody	**Source**
Mouse anti-histidine6-tag antibody	Dianova, Hamburg
HRP Anti-mouse IgG antibody	Pierce, Rockford
Anti-biotin antibody	Santa Cruz, California
Anti-ubiquitin antibody	Sigma Aldrich, Steinheim
Anti-GST-HRP conjugates	GE Healthcare, Freiburg

2.2.2 Plasmids

Plasmids	**Antibiotic resistance**	**Source**
pGEM-T Easy	Carbenicillin	Promega, Mannheim
pQE30	Carbenicillin	Qiagen, Hilden
pGEX-4T	Carbenicillin	GE Healthcare, Freiburg
pRSET	Carbenicillin	Invitrogen, USA

2.2.3 *E. coli* strains

***E. coli* strains**	**Usage**	**Source**
XL-1 Blue	Cloning and plasmid preparation	Stratagene, Amsterdam
BL21	Overexpression	Invitrogen, Karlsruhe
M15	Overexpression	Qiagen, Hilden

2.2.4 Enzymes

2.2.4.1 DNA polymerase

Enzyme	**Company**
AccuPrime^{TM} Taq DNA polymerase	Invitrogen, Karlsruhe
Pfu DNA polymerase	Promega, Mannheim
RedTaq® DNA polymerase	Sigma Aldrich, Steinheim

2.2.4.2 Restriction enzymes

Enzyme	Cleavage sequence	Source
BamHI	5'-G$^{\downarrow}$GATCC-3'	Fermentas, St. Leon-Rot
HindIII	5'-A$^{\downarrow}$AGCTT-3'	Fermentas, St. Leon-Rot
EcoRI	5'-G$^{\downarrow}$AATTC-3'	Fermentas, St. Leon-Rot

2.2.4.3 Other enzymes

Enzyme	Function	Source
DNaseI	DNA digestion	Roche, Mannheim
Lysozyme	Cell lysis	Sigma Aldrich, Steinheim
T4 Ligase	Nucleotide fragment ligation	Fermentas, St. Leon-Rot

2.2.5 Kits

Kit	Source
Bradford assay kit	Bio-Rad, München
QIAprep Spin Miniprep kit	Qiagen, Hilden
QIAprep Spin Maxiprep kit	Qiagen, Hilden
QIAquick PCR purification kit	Qiagen, Hilden
Silver staining kit	Pierce, Rockford

2.2.6 Materials of affinity chromatography

Material	Source
Nickel-nitrilotriacetate-agarose (Ni-NTA)	Qiagen, Hilden
GSH-sepharose 4B	GE Healthcare, Freiburg

2.2.7 *Plasmodium falciparum* strain

Plasmodium falciparum strain	Source
3D7 (Chloroquine-sensitive)	Prof. Lanzer, Heidelberg University

2.2.8 Medium for *E. coli* culture

Culture medium	Recipe
Lysogeny broth medium (LB), 1 L	10 g Tryptone 5 g Yeast extract 10 g NaCl
Terrific broth medium (TB), 1 L	12 g Tryptone 24 g Yeast extract 9,4 g K_2HPO_4 2,2 g KH_2PO_4 4 ml Glycerol

2.3 Buffers and solutions

2.3.1 Buffer for DNA electrophoresis

DNA Sample buffer	0.1%	Bromophenol blue
	60%	Saccharose

	1 mM	Tris
	pH 8.3	HCl (adjustment)
10 X TBE (electrophoresis buffer)	1 M	Tris
	1 M	Boric acid
	20 mM	EDTA
	pH 8.0	Acetic acid (adjustment)

2.3.2 Buffer for isolation of *P. falciparum* parasites

Saponin lysis buffer	7 mM	K_2HPO_4
	1 mM	$MgCl_2$
	1 mM	NaH_2PO_4
	11 mM	$NaHCO_3$
	58 mM	KCl
	56 mM	NaCl
	14 mM	Glucose
	0.02%	Saponin
	pH 7.4	HCl (adjustment)

2.3.3 Buffer for SDS-PAGE electrophoresis

Electrophoresis buffer	193 mM	Glycine
	25 mM	Tris
	0.1% (w/v)	SDS
	pH 8.3	HCl (adjustment)
SDS sample buffer (4X)	240 mM	1 M Tris-HCl, pH 6.8
	8% (w/v)	SDS
	40% (v/v)	Glycerol
	5% (v/v)	14.7 M β-Mercaptoethanol
	0.04% (w/v)	Bromophenol blue
Coomassie staining solution	0.2% (w/v)	Coomassie brillant blue R250
	40% (v/v)	2-Propanol
	10% (v/v)	Acetic acid
Coomassie destaining solution	10% (v/v)	Acetic acid
	40% (v/v)	Methanol

2.3.4 Buffer for Western blot

Trans-blotting buffer	25 mM	Tris
	192 mM	Glycerol
	20%	Methanol
TBS buffer	10 mM	Tris
	155 mM	NaCl
	pH 8.0	HCl (adjustment)
TBS-Tween (TBST)	0.05%	Tween 20 (in TBS buffer)

Ponceau S staining solution	1% (w/v)	Ponceau S
	5% (v/v)	Acetic acid
Ponceau S destaining solution	1% (w/v)	Acetic acid
Luminol solution (store in the dark at 4 °C)	1.25 mM	Luminol
	0.0093% (v/v)	H_2O_2
	0.1 M	Tris-HCl, pH 8.6

2.4 Instruments

Instruments	**Producer**
Analytical balance	Scaltec Instruments, Göttingen
Autoclave	Webeco, Bad Schwartau
Beckman Optima Max ultracentrifuge	Beckmann, Munich
Bio photometer	Eppendorf,Hamburg
Eppendorf Research® plus pipettes	Eppendorf, Hamburg
Eppendorf thermomixer	Eppendorf, Hamburg
FPLC software Unicorn	Amersham Bioscience, Freiburg
FPLC system ÄKTA-FPLC	Amersham Bioscience, Freiburg
Fraction collector Frac-100	Pharmacia Biotech, Freiburg
Freezer -86 °C	Heraeus Instruments, Hanau
Gene pulser Xcell Electroporation	BioRad, Munich
GEL DOC 2000 system	BioRad, Munich
HeraCell CO_2 incubator for *P. falciparum* culture	Heraeus Instruments, Hanau
Hitachi U-2001 spectrophotometer	Hitachi, Schwäbisch Gmünd
Magnetic stirrers RCT basic	IKA Werke, Staufen
Mastercycler® thermal cyclers	Eppendorf, Hamburg
Megafuge 1.0R centrifuge	Heraeus Instruments, Hanau
Mini-PROTEAN cell electrophoresis module	BioRad, Munich
Minispin® centrifuge	Eppendorf, Hamburg
Mitsubishi P91 photo printer	Mitsubishi, Ratingen
Neolab heating block	NeoLab, Heidelberg
Optima™ TLX ultracentrifuge	Beckmann, Munich
OptiMax X-ray film processor	Protec, Oberstenfeld
QuadroMACS® magnetic separator	Miltenyi Biotec GmbH, Bergisch Gladbach
Owl EasyCast B1A mini gel electrophoresis systems	Thermo Scientific, Dreieich
pH meter	Beckman, Munich
Pharmacia LKB Multiphor II NovaBlot	Amersham Pharmacia Biotech, Freiburg
Rotor Sorvall SLA 3000, SS34	Thermo Fisher Scientific, Waltham, USA
Sonopuls GM 70 ultrasonicator	BandelinElectronics, Berlin
Sorvall® RC5BPlus centrifuge	ThermoScientific, Waltham, USA
Thermomixer comfort	Thermo Life Sciences, Egelsbach
Tecan Infinite M200 PRO	Tecan, Switzerland
Ultra pure water system	MembraPure, Bodenheim
UV/Vis-Spectrophotometer Beckman DU® 650	Beckmann, Munich
Vortex minishaker MS2	IKA Werke, Staufen

3. METHODS

3.1 General methods

3.1.1 Preparation of competent *E. coli* cells

E. coli cells were inoculated into 3 mL LB medium and grown overnight (~ 15 hours) in a shaking incubator at 37 °C. Then 150 mL LB medium was inoculated with the overnight culture, and the cells were grown until the value of the optical density at a wavelength of 600 nM (OD600) of the culture mixture reached 0.6. The culture was then transferred into Falcon tubes and placed on ice for 10 min. After the culture was centrifuged at 4,000 *g* at 4 °C for 10 min, the cell pellet was resuspended in 10 ml ice-cold sterile resuspension buffer containing 0.1 M $CaCl_2$ and 10% glycerol and left on ice for 15 min. Then the cell pellet was resuspended with the resuspension buffer and the centrifugation was repeated. In the end, the pellet was resuspended in 1.5 ml ice-cold sterile resuspension buffer and aliquoted into sterile Eppendorf tubes and frozen in liquid nitrogen for 3 minutes. Then the cells were stored at -80 °C.

3.1.2 Cleavage of double strand DNA by restriction endonucleases and ligation

The DNA fragments of PCR products or plasmids were cleaved by restriction endonucleases, which has the function of recognizing and cutting DNA at a specific nucleotide sequence known as the restriction site (Roberts 1976). The DNA fragments were digested by the respective Fermentas restriction enzymes in an appropriate buffer at 37 °C for 1 hour according to the manufacture's instruction. The cleaved DNA was purified by a QIAquick PCR purification kit and further used for ligation. The DNA concentration was determined via measuring its absorption at 260 nm. The purity of the DNA sample was examined by the ratio of A260nm/A280nm, which normally ranges from 1.8 to 2.0.

The ligation of cleaved PCR products with plasmid was carried out by using a T4 ligation system. A T4 ligase catalyzes the linkage by forming a phosphodiester bond between the 5' phosphate group of one fragment and the 3' hydroxyl group of the other. Different molar ratios of the plasmid to the DNA fragment (insert) varied from 1:3 to 1:5 in the ligation system and 1 unit T4 ligase was used. The ligation mixture was left for 1 hour at RT (room temperature) or 4 °C overnight to complete the reaction. In some cases, the ligation can be finished within 10 min by using a quick ligation system.

3.1.3 Transformation of competent *E. coli* cells

Transformation was carried out to insert plasmid DNA to competent *E. coli* cells. For this purpose, about 100 µL of competent *E. coli* cells were completely thawed on ice and 1 µL plasmid DNA was added to the cells and carefully mixed. The *E. coli* cells were placed on ice for 30 min. Then the cells were heated for 90 sec at 42 °C to induce a heat shock forcing the *E. coli* cells to take up plasmid DNA. Afterwards, the cells were placed on ice again for 2 min before a 400 µL of LB medium was added. The cells were incubated at 37 °C for one hour. Finally, the *E. coli* cells were plated on agar plates containing the appropriate antibiotics, and incubated at 37 °C overnight. Colonies were normally observed after 16-24 hours.

3.1.4 Sodium dodecyl sulfate-polyacrylamide gel electrophoresis (SDS-PAGE)

The sodium dodecyl sulfate-polyacrylamide gel electrophoresis (SDS-PAGE) was used to separate protein mixtures based on their molecular weights. Under denaturing conditions, SDS renders a negative charge to the proteins, resulting in the proteins being negatively charged in proportion to their molecular weights. Thus, within an electronic field, the proteins are fractionated by size (Laemmli 1970). Briefly, protein samples are mixed with 4× reducing SDS sample buffer and boiled at 95 °C for 5 min in order to denature the proteins. A 12% or 15% SDS-PAGE gel was placed in an electrophoresis tank, and the electrophoresis buffer was added. Under a 200 volt voltage, proteins migrated for about 40 min. Then the gel was subjected to Coomassie blue staining or silver staining to visualize the proteins in the gel. If western blot analysis was needed, the gel was directly used for trans-blotting proteins without staining.

3.1.5 Western blot analysis

Western blot analysis was generally used to detect either specific proteins or protein modifications with specific antibodies (Towbin *et al.,* 1992). Briefly, after proteins were separated in a gel by SDS-PAGE, the gel was soaked in the trans-blotting buffer (25 mM Tris, 192 mM glycine, 20% methanol) for 10 min. In parallel, a polyvinylidene difluoride (PVDF) membrane was activated with pure methanol. The PVDF membrane and four filter papers were equilibrated with the trans-blotting buffer. Then the transfer sandwich was assembled with two filter papers, the gel, a PVDF membrane, and another two filter papers in the order from the cathode to the anode. For protein transfer, a Mini Trans-Blot® electrophoretic transfer cell (Bio-Rad) was used. The transfer cassette was placed in a tank and filled with the trans-blotting buffer. The transfer process was performed at a constant current of 300 mA for 1 hour with a cooling system. After the transfer, the PVDF membrane was stained with Ponceau S solution for 1 min and destained with 1% acetic acid until protein bands appeared. Then the PVDF membrane was washed in TBST solution until no protein band was visible. The PVDF membrane was then blocked by 5% non-fat milk for 1 hour at RT or overnight at 4 °C. After blocking, the membrane was washed 3 times with TBST and incubated with a specific first antibody for 1 hour at RT with constant shaking. After the incubation with the first antibody, the membrane was intensively washed three times for 5 minutes each with TBST before a corresponding secondary antibody was added. After one-hour incubation, the membrane was again intensively washed, and an enhanced chemiluminescence (ECL) mixture containing 1 mL luminal solution and 10 µL coumaric acid was added to the PVDF membrane. The membrane was then placed in a film cassette and exposed to an X-ray film for an appropriate amount of time (30 sec to 1 min).

3.1.6 Chromatography purifications of recombinant proteins

The frozen resuspended *E. coli* pellet containing heterologously overexpressed recombinant proteins was first thawed and mixed with a small amount of DNAse and lysozyme (4 mg/g pellet). The mixture was then stirred on ice for 30 min to 1 hour, followed by ultra-sonication (three times for 30 sec each) to completely disrupt the cells and release proteins. The clear supernatant was taken out via centrifugation at 38,000 g for 30 min at 4 °C.

For the purification of recombinant proteins fused with six additional histidine residues (6×His tag), the

supernatant was applied onto a pre-equilibrated nickel-nitrilotriacetate (Ni-NTA) column with a 1-2 mL bed volume of the Ni-NTA agarose. After the supernatant passed though the column, the column was washed with a 20-column volume of an appropriate washing buffer. The bound proteins were then eluted using an appropriate elution buffer containing a gradient of imidazole concentrations (20-500 mM). The proteins in elution fractions were resolved via SDS-PAGE, and the purified proteins were checked with Coomassie blue staining.

For the purification of recombinant GST-tagged proteins, the supernatant was applied onto a pre-equilibrated GSH-sepharose column with an appropriate volume of GSH-sepharose 4B resin. After all supernatant passed though the column, the column was washed with a 20-column volume of PBS. The GST-tagged proteins were then eluted using an appropriate elution buffer containing 10 mM reduced glutathione together wit 1 mM DTT. The proteins in elution fractions were resolved via SDS-PAGE, and the purified proteins were checked with Coomassie blue staining.

To gain a high purity of the recombinant proteins, a gel filtration chromatography based on a 16/60 superdex200 prep grade column connected to an ÄKTA FPLC system (Amersham Pharmacia Biotech) was used. The protein sample was concentrated to a volume of 1-2 mL, which can be loaded onto the column. The proteins were then separated based on their molecular weights on the superdex200 column at a flow rate of 1 mL/min. Protein-containing fractions were detected spectrophotometrically at 280 nm and collected, followed by SDS-PAGE analysis. The fractions containing target proteins were pooled and concentrated for further experiments.

3.1.7 Protein concentration determination

Protein concentrations were measured by using the Bradford method, which is based on the shift of the maximal absorbance of the Coomassie Brilliant Blue G-250 dye from 465 nm to 595 nm when the protein-dye complex is formed (Bradford 1976). To prepare a calibration curve for calculating protein concentrations, a series of BSA concentrations as standards was prepared. Five microliters of each standard was mixed with 495 µl double-distilled water (ddH_2O). To each mixture, 125 µL of Bradford reagent (Bio-Rad) was added and immediately vortexed and incubated for 15 minutes at RT. The absorption at 595 nm of the respective standard sample was measured using a spectrophotometer. Then the calibration curve of absorption against the respective protein concentration was plotted. For the measurement of a sample, the same procedure was used and the protein concentration of the sample was be calculated according to the calibration curve.

For the sample with a limited volume and a low protein concentration, the Bradford microassay was used. A calibration curve covering low protein concentrations (0-200 µg/mL) was prepared by using a 10 µL reaction system, in which 8 µL of the standard sample was mixed with 2 µL of Bradford reagent. Similarly, 8 µL of the sample to be measured was used following the same procedure. The absorption at 595 nm of the sample was measured on a NanoDrop spectrophotometer (Thermo Scientific) using only 1 µL of the reaction mixture.

3.1.8 Cultivation of *P. falciparum* and isolation of the parasites

Intraerythrocytic stages of *P. falciparum* were grown in continuous culture as described by Trager and Jensen

(Trager *et al.,* 1976), with slight modifications. Parasites were maintained at 1 to 10% parasitemia and 3.3% hematocrit in an RPMI 1640 culture medium supplemented with A+ erythrocytes, 0.5% lipid-rich bovine serum albumin (Albumax), 9 mM (0.16%) glucose, 0.2 mM hypoxanthine, 2.1 mM L-glutamine, and 22 mg/ml gentamicin. All incubations were carried out at 37 °C in 3% O_2, 3% CO_2, and 94% N_2. Synchronization of parasites in culture to ring stages was carried out via treatment with 5% (w/v) sorbitol (Lambros *et al.,* 1979).

For experimental purposes, isolation and enrichment of *P. falciparum* parasites were performed. Trophozoite stage parasites were harvested by suspending red blood cells for 10 min at 37 °C in a 20-fold volume of saponin lysis buffer containing 7 mM K_2HPO_4, 1 mM NaH_2PO_4, 11 mM $NaHCO_3$, 58 mM KCl, 56 mM NaCl, 1 mM $MgCl_2$, 14 mM glucose, and 0.02% saponin, pH 7.4. After centrifugation at 1,500 g, the parasites pellet was washed with saponin lysis buffer followed by PBS. The parasite pellet can be kept frozen at -80 °C.

3.2 Protein *S*-nitrosylation methods

3.2.1 Preparation of *P. falciparum* cell extracts for protein *S*-nitrosylation analysis

To identify *S*-nitrosylated proteins in *P. falciparum*, the parasite cell extracts were prepared directly from the harvested parasites, which had been untreated or treated with 100 or 400 μM GSNO for 1h or 4h in the cell culture. The preparation of parasite cell extracts was carried out under protection from light. A parasite pellet was suspended in an equal volume of lysis buffer containing 50 mM Tris, 1 mM EDTA, 0.2 mM neocuproine, and complete protease inhibitor (Roche, Germany), pH 7.4. Cells were disrupted with four freezing-thawing cycles and ultrasonication. The contaminating hemozoin was first removed via a centrifugation at 15,000 g for 30 min at 4 °C, and then the clear supernatant was gained by an ultracentrifugation at 100,000 g for 30 min at 4 °C. The protein concentration of the cell extracts was determined via the Bradford assay. A typical protein concentration in the cell extracts was 6-8 mg/mL. Cell extracts were immediately subjected to a biotin-switch assay for the detection of endogenous *S*-nitrosylated proteins. For detecting *S*-nitrosylated proteins in the cell extracts treated with GSNO, freshly prepared cell extracts (4 mg total protein) were incubated with 40 or 100 μM GSNO at 25 °C for 1 hour. The residual GSNO was removed by passing the cell extracts through a Zeba desalting column (Thermo Scientific), and the *S*-nitrosylated proteins were detected via the biotin-switch assay (see below). The cell extracts treated with 100 μM GSNO were used for the identification of *S*-nitrosylated proteins by mass spectrometry.

3.2.2 Biotin-switch assay, detection of *S*-nitrosylated proteins, and purification of biotinylated proteins

The biotin-switch assay was performed as previously described with modifications (Han *et al.,* 2008; Forrester *et al.,* 2009; Huang *et al.,* 2010). *P. falciparum* cell extracts were diluted to 1 mg/mL with blocking buffer (8 M urea, 50 mM Tris, 1 mM EDTA, 0.1 mM neocuproine, pH 8.0) containing 200 mM methyl methanethiosulfonate (MMTS). The free cysteine thiols in cell extracts were blocked by MMTS via incubation at 50 °C for 30 min in the dark, with occasional vortexing. The reaction was stopped by adding three volumes of ice-cold acetone followed by protein precipitation at -20 °C for 30 min. After centrifugation at 5,000 g, the protein pellet was washed three times with 70% ice-cold acetone and completely dissolved in labeling buffer (4 M urea, 50 mM

Tris, 1 mM EDTA, 0.01 mM neocuproine, pH 8.0). The *S*-nitrosylated thiols were then switched to biotinylated thiols via incubation with 20 mM sodium ascorbate (NaAsc) and 0.2 mM iodoacetyl-PEG2-biotin (Pierce) for 1 h at 25 °C in the dark with constant shaking. A control sample without NaAsc was prepared in parallel. The reaction was stopped via protein precipitation in acetone, and the protein pellet was washed three times to remove residual biotinylating reagents.

To detect *S*-nitrosylated proteins, western blot analysis using anti-biotin antibodies was performed. Briefly, a protein pellet was dissolved in 0.2 mL labeling buffer and 2 µg of proteins per lane was subjected to sodium dodecyl sulfate-polyacrylamide gel electrophoresis (SDS-PAGE). After electrophoresis, proteins were transferred to a polyvinylidene difluoride (PVDF) membrane, which was then blocked overnight at 4 °C with 5% non-fat milk in Tris-buffered saline Tween-20 (TBST). Signals corresponding to *S*-nitrosylated proteins tagged with biotin were visualized via protein immunoblotting using anti-biotin antibodies (Santa Cruz, diluted 1:1,000 in 5% non-fat milk in TBST).

To purify biotinylated proteins, the protein pellet was completely dissolved in 0.2 mL labeling buffer and diluted to 1 mL with pull-down buffer (50 mM Tris, 150 mM NaCl, pH 8.0). Samples were further dialyzed against 100 mL pull-down buffer 3 times at RT. After dialysis, 150 µL of equilibrated SoftLink™ Soft Release avidin resin (Promega) was added and incubated with the samples overnight at 4 °C. The resin was collected and washed with 0.5 mL pull-down buffer six times in order to remove all unbound proteins. Biotinylated proteins were eluted by incubation of the resin with 0.5 mL pull-down buffer containing 5 mM biotin for 30 min at RT. The eluate was concentrated to 60 µL, and 15 µL were loaded into a 12% SDS-PAGE gel for silver staining. The rest was kept at -80 °C for the mass spectrometry analysis.

3.2.3. Sample preparation for mass spectrometry

Protein samples were present in 35-45 µL of buffer (50 mM Tris, 150 mM NaCl, 10 mM biotin) and had a concentration below the detection limit of a Bradford assay but were detectable via silver staining. Samples were diluted with 30 µL 16 M urea, 160 mM Tris pH 8.5; 3 µL of 100 mM TCEP (tris(2-carboxyethyl)phosphine) was added, and samples were incubated at RT for 20 min. Three microliters of 250 mM iodoacetamide (IAA) was added, and samples were incubated at RT for 20 min in the dark. Samples were diluted with 180 µL 100 mM Tris, pH 8.5, and trypsin was added (0.5 µg/µL). Samples were incubated at 37 °C overnight, and digestion was halted by adding 13.5 µL of 90% formic acid. Samples were spun for 20-30 min at 14,000 rpm and transferred to a new Eppendorf tube before pressure loading onto a microcapillary column.

3.2.4. Multidimensional protein identification technology (MudPIT)

The protein digest was pressure-loaded onto a fused silica capillary column containing 2.5 cm of Partisphere strong cation exchanger (Whatman, Clifton, NJ) followed by 2.5 cm of 10 µm Aqua C18 (Phenomenex, Ventura, CA) packed into a 250 µm inside diameter (i.d.) capillary (Polymicro Technologies, Phoenix, AZ) with a 1 µm frit. The column was washed for 60 min with buffer containing 95% water, 5% acetonitrile, and 0.1% formic acid. After washing, a 100-µm i.d. capillary with a 5-µm pulled tip packed with 15 cm 3-µm Aqua C18 material

(Phenomenex, Ventura, CA) was attached via a union, and the entire split column was placed in line with an Agilent 1100 quaternary high-performance liquid chromatography (HPLC) and analyzed using a modified 9-step separation similar to those described previously (Washburn *et al.,* 2001). The buffer solutions used were 5% acetonitrile/0.1% formic acid (buffer A), 80% acetonitrile/0.1% formic acid (buffer B), and 500 mM ammonium acetate/5% acetonitrile/0.1% formic acid (buffer C). Step 1 consisted of a 75 min gradient from 0% to 100% buffer B. Steps 2-9 had the following profile: 10 min of X% buffer C, a 15 min gradient from 0% to 5% buffer B, and a 95 min gradient from 15% to 100% buffer B. The 10 min buffer C percentages were 10%, 20%, 30%, 40%, 50%, 60%, 70%, and 100%, respectively, for the 9-step analysis.

As peptides eluted from the microcapillary column, they were electrosprayed directly into an Orbitrap velos mass spectrometer (ThermoFisher, SanJose, CA) with the application of a distal 2.4 kV spray voltage. A cycle of one full-scan mass spectrum (400-1400 m/z) followed by 15 data-dependent tandem mass spectrometry (MS/MS) spectra at a 35% normalized collision energy was repeated continuously throughout each step of the multidimensional separation. Application of mass spectrometer scan functions and HPLC solvent gradients were controlled by the XCalibur data system.

3.2.5. Analysis of tandem mass spectra

Protein and modification identifications were done with Integrated Proteomics Pipeline-IP2 (Integrated Proteomics Applications, Inc., San Diego, CA. http://www.integratedproteomics.com) using ProLuCID, DTASelect2, Census, DeBunker, and Ascore. Spectrum raw files were extracted into ms1 and ms2 files from raw files using RawExtract 1.9.9 (http://fields.scripps.edu/downloads.php) (McDonald *et al.,* 2004), and the tandem mass spectra were searched against a *Plasmodium falciparum* database (release date 01/10/12). In order to accurately estimate peptide probabilities and false discovery rates, we used a decoy database containing the reversed sequences of all the proteins appended to the target database (Peng *et al.,* 2003). Tandem mass spectra were matched to sequences using the ProLuCID algorithm with 50 ppm peptide mass tolerance (Xu *et al.,* 2006). ProLuCID searches were done on an Intel Xeon cluster running under the Linux operating system. The search space included all fully and half-tryptic peptide candidates that fell within the mass tolerance window with no miscleavage constraint. Modifications of: (i) +45.987722 on C (reversible label); (ii) +415.201515 on C (iodoacetyl-PEG2-biotin label); (iii) +146.081719 on C (fragment of biotin label); (iv) + 59.013305 on C (fragment of biotin label); and +57.02146 on C (iodoacetamide) were considered to be variable modifications.

The validity of peptide/spectrum matches (PSMs) was assessed in DTASelect (Tabb *et al.,* 2002; Cociorva *et al.,* 2007) using two SEQUEST (Eng *et al.,* 1994) defined parameters, the cross-correlation score (XCorr), and a normalized difference in cross-correlation scores (DeltaCN). The search results were grouped by charge state (+1, +2, +3, and greater than +3) and tryptic status (fully tryptic, half-tryptic, and non-tryptic), resulting in 12 distinct sub-groups. In each one of these sub-groups, the distribution of Xcorr, DeltaCN, and DeltaMass values for (a) direct and (b) decoy database PSMs was obtained; then the direct and decoy subsets were separated by discriminant analysis. Full separation of the direct and decoy PSM subsets is not generally possible; therefore, peptide match probabilities were calculated based on a nonparametric fit of the direct and decoy score

distributions. A peptide confidence of 99.5% was set as the minimum threshold, and only peptides with a delta mass less than 10 ppm were accepted. The false discovery rate was calculated as the percentage of reverse decoy PSMs among all the PSMs that passed the 99.5% confidence threshold. After this last filtering step, we estimate that the peptide false discovery rate was below 1%.

3.2.6 Preparation of recombinant plasmodial proteins

Recombinant His-tagged *P. falciparum* glyceraldehyde 3-phosphate dehydrogenase (PfGAPDH), pyruvate kinase (PfPK), lactate dehydrogenase (PfLDH), and phosphoglycerate mutase (PfPGM) were overexpressed and purified as previously described (Kehr *et al.,* 2011). The following recombinant His-tagged proteins were overexpressed and purified as described previously: recombinant wild type *P. falciparum* thioredoxin 1 (PfTrx1-WT), cysteine-mutated PfTrx1^{C33S}, PfTrx1$^{C30S/C33S}$ (Kanzok *et al.,* 2000), PfTrx1^{C43S} (Krnajski *et al.,* 2001), thioredoxin reductase (PfTrxR) (Kanzok *et al.,* 2002), peroxiredoxin 6 (PfPrx6), peroxiredoxin 1a (PfPrx1a) (Akerman *et al.,* 2003), and glutaredoxin 1 (PfGrx1) (Rahlfs *et al.,* 2001).

3.2.7 Protein immunoblotting analysis

Recombinant PfGAPDH, PfPK, PfLDH, PfPGM, PfTrx1-WT, PfTrx1^{C33S}, PfTrx1$^{C30S/C33S}$, and PfTrx1^{C43S} were reduced by incubation with 5 mM DTT for 30 min at RT, and the residual DTT was removed via gel filtration (Zeba^{TM}, Thermo Scientific) at 4 °C. The reduced proteins (0.2 mg) were then incubated with different concentrations of GSNO in 0.5 mL buffer of 50 mM Tris, 1 mM EDTA, 0.2 mM neocuproine, pH 7.4 for 1 h at RT in the dark. The reaction was stopped by adding 1.5 mL ice-cold acetone followed by protein precipitation at -20 °C for 30 min and centrifugation. After washing, the protein pellet was resolved in blocking buffer with 200 mM MMTS and subjected to a biotin-switch assay. Controls were performed without adding NaAsc into the assay. For detecting *S*-nitrosylated proteins, two microgram proteins were used in a western blot analysis, using anti-biotin antibody as mentioned before. Ponceau S staining of proteins was set as a loading control.

3.2.8 Enzyme treatments and enzymatic assays

Pre-reduced PfGAPDH, PfPK, and PfLDH were incubated with different concentrations of GSNO (0.1 mM to 1 mM) in 50 mM Tris, 1 mM EDTA, 0.2 mM neocuproine, pH 7.4 at RT in the dark. At different incubation time points, aliquots were taken and assayed for the enzymatic activity.

The PfGAPDH activity was measured as previously described (Kehr *et al.,* 2011). Briefly, the assay mixture contained 40 mM triethanolamine, 50 mM Na_2HPO_4, 0.2 mM EDTA, pH 7.4, PfGAPDH (0.48 µg/mL), 2 mM NAD^+, and 2 mM glyceraldehyde 3-phosphate (GAP, prepared from glyceraldehyde 3-phosphate diethyl acetal barium salt according the manufacturers' instructions; Sigma Aldrich). The production of NADH catalyzed by PfGAPDH was monitored at 340 nm at 25 °C.

To test whether GAP and NAD^+ can protect PfGAPDH activity from inhibition by *S*-nitrosylation, PfGAPDH was incubated with 1 mM GAP or 2 mM NAD^+ for 5 min at 25 °C prior to incubation with 0.2 mM GSNO. The PfGAPDH activity was then measured. The enzymatic activities of PfPK and PfLDH were determined as

previously described (Kehr *et al.,* 2011). All enzyme activity assays were carried out in at least three independent experiments using a Hitachi U-2001 spectrophotometer.

3.2.9. Denitrosylation assays

S-nitrosylated proteins in *P. falciparum* cell extracts were generated by incubating parasite cell extracts (0.2 mg protein) with 1 mM GSNO in the buffer containing 50 mM Tris, 1 mM EDTA, and 0.2 mM neocuproine (pH 7.4) at RT for 30 min in the dark. The residual GSNO was removed by passing the cell extracts through a Zeba desalting column (Thermo Scientific). Sixty micrograms of pre-reduced recombinant PfTrx1 was added to the cell extracts and incubated at 37 °C for 30 min in the dark for the denitrosylation. In another sample, 0.2 μM PfTrxR and 200 μM NADPH were added along with PfTrx1. For control samples, PfTrxR/NADPH alone or 1 mM reduced glutathione were added to the cell extracts. After denitrosylation, proteins were precipitated and washed with acetone and then subjected to a biotin-switch assay. The residual *S*-nitrosylated proteins were detected via anti-biotin western blot analysis as described above. A western blot analysis of *P. falciparum* glutathione *S*-transferase (PfGST) in cell extracts was employed as a loading control.

For denitrosylating PfGAPDH, PfGAPDH was first *S*-nitrosylated by incubating the 2 mg recombinant PfGAPDH with 1 mM GSNO in 0.5 mL buffer containing 50 mM Tris, 1 mM EDTA, and 0.2 mM neocuproine (pH 7.4) at RT for 30 min in the dark. After removing residual GSNO via gel filtration, 0.2 mg PfGAPDH (11 μM) was taken out and incubated with a 2 or 5-fold molar excess of pre-reduced PfTrx1 and different PfTrx1 cysteine mutants at 37 °C for 30 min in the dark for denitrosylation. The residual *S*-nitrosylated PfGAPDH was then analyzed via a biotin-switch assay followed by an anti-biotin western blot.

In order to enzymatically study the denitrosylation of PfGAPDH, PfGAPDH was *S*-nitrosylated via incubation with 1 mM GSNO for 30 min at 25 °C. The residual GSNO was removed by desalting PfGAPDH using a Zeba desalting column. The GSNO-treated PfGAPDH was incubated with different-fold molar excess of recombinant wild type PfTrx1 (with or without 0.2 μM PfTrxR and 200 μM NADPH) and cysteine-mutated PfTrx1 variants. Aliquots were taken at different incubation time points to monitor PfGAPDH activity as described above.

3.2.10 Transnitrosylation assays

Briefly, *S*-nitrosylated PfTrx1-WT and PfTrx1$^{C30S/C33S}$ were generated by incubating respective recombinant proteins with 1 mM GSNO for 30 min at 25 °C. After residual GSNO was removed, 20 μM *S*-nitrosylated PfTrx1-WT and PfTrx1$^{C30S/C33S}$ were incubated with *P. falciparum* cell extracts (0.2 mg) in 0.5 mL buffer containing 50 mM Tris, 1 mM EDTA, and 0.2 mM neocuproine, pH 7.4 for 1 h at 25 °C in the dark. For the transnitrosylation of PfGAPDH, a 2 or 5-fold molar excess of *S*-nitrosylated PfTrx1-WT and PfTrx1$^{C30S/C33S}$ were incubated with 11 μM PfGAPDH for 30 min at 25 °C in the dark. After transnitrosylation, proteins were subjected to the biotin-switch assay. The resulting *S*-nitrosylated proteins in cell extracts and the *S*-nitrosylated PfGAPDH were detected via anti-biotin western blot analysis. To compare the transnitrosylation efficiency of PfTrx1 and GSNO, pre-reduced PfTrx1$^{C30S/C33S}$ was *S*-nitrosylated with a 50-fold molar excess of GSNO for 30 min and then desalted to remove residual GSNO. In 300 μL buffer system (50 mM Tris, 1 mM EDTA, and 0.2

mM neocuproine, pH 7.4), 2.4 μg PfGAPDH was mixed with the same molar amounts of GSNO and *S*-nitrosylated PfTrx1$^{C30S/C33S}$ individually; 60 μL mixture was taken out every 5 min to measure the PfGAPDH activity.

3.3 Proteasome methods

3.3.1 Cloning of ubiquitin receptor domains of *P. falciparum*

In order to clone putative PfUIM domains from a putative PfRpn10 subunit, a domain of PfRpn10 which contains two PfUIM domains was first amplified from a blood stage cDNA library of *P. falciparum* (3D7) by PCR using two primers (5'-GTTTTGAATTCATTTTTAAATAATAATG-3' and 5'-ACTTGTTGTGTCTTTATTT TCTAATT-3'). The PCR-amplified fragment was purified with a QIAquick PCR Purification Kit (Qiagen) and ligated to a pGEM-T easy vector (Promega). The constructed plasmid was further transformed into *E. coli* XL-1 blue cells. Colonies were inoculated into 3 mL LB medium supplemented with carbenicillin (100 μg/mL) and grown overnight. The plasmids were extracted from the cells, and inserts can be analyzed by digesting the plasmids with *EcoRI*. The plasmids with inserts at the right size were sent for sequencing for verification.

The PfUIM1 domain, PfUIM2 domain, and the domain containing both PfUIMs (PfUIM1+2) were then individually amplified from the verified construct using different primers described in **Table 2**. After purification and cleavage of the PfUIM domains with respective restriction enzymes, the respective PfUIM domain was cloned into either a cleaved pQE30 vector or a cleaved pRSET expression vector. Both vectors add an N-terminal 6×His-tag to the recombinant protein. The plasmids containing right inserts were verified via sequencing analysis.

Table 2. Primers used for cloning the putative PfUIM domains.

Target domains	Primers*
PfUIM1	5'-ATATGGATCCGTTTTGAATTCATTTTTAAATAATAATG-3'
	5'-ATATAAGCTT CATATGCTGACTTTCTTCCAAAG-3'
PfUIM2	5'-ATATGGATCC ACAACTAATAATAATGACTTACC-3'
	5'-ATATAAGCTT TTTATTTTCTAATTTATTCTTTTCTG-3'
PfUIM1+2	5'-ATATGGATCCGTTTTGAATTCATTTTTAAATAATAATG-3'
	5'-ATATAAGCTT TTTATTTTCTAATTTATTCTTTTCTG-3'

*The restriction enzyme cleavage sites of *BamHI* and *HindIII* were underlined.

The putative Pru domain of a putative PfRpn13 subunit was amplified from the blood stage cDNA library of *P. falciparum* (3D7) by PCR using the primers 5'-ATATGGATCCGATTCAGCAAAGATACATTTACA-3' and 5'-ATATAAGCTTTTCGTCCTTCGAATCATCATAA-3', which have restriction sites of *BamHI* and *HindIII* (underlined). After the PCR product (320 bp) was purified and digested with *BamHI* and *HindIII*, the cleaved PCR product was directly ligated into a pQE30 plasmid cleaved with the same restriction enzymes. The constructed plasmid was transformed into *E. coli* XL-1 blue cells and the *E. coli* colonies were inoculated in 3

mL LB medium supplemented with carbenicillin (100 μg/mL) and grown overnight. After the constructed plasmids were extracted from the cell and purified, they were digested with *BamHI* and *HindIII* for 1 h at 37 °C and analyzed by an agarose gel (1.5%) electrophoresis. The plasmids with inserts at the right size were sent to sequencing analysis for verification.

3.3.2 Cloning of ubiquitin-like domains from putative PfRad23 and PfDsk2

The ubiquitin-like (UBL) domain from the putative PfRad23 was amplified from a blood stage cDNA library of *P. falciparum* (3D7) by using PCR with two primers: '-ATATGAATTCTTATTCCTTTTGATTATTTTTATTA ATAATTC-3' and 5'-ATATGGATCCAAAATAAAAGTAAGAACACTACAAAAC-3' with the cleavage sites of *EcoRI* and *BamHI* (underlined). Then the PCR product was purified and digested with *EcoRI* and *BamHI*, and directly ligated into a GST fusion protein expression vector (pGEX-4T) cleaved with the same restriction enzymes. The constructed plasmid was transformed into *E. coli* XL-1 blue cells, and the *E. coli* colonies were picked up and inoculated in 3 mL LB medium supplemented with carbenicillin (100 μg/mL) and grown overnight. After the constructed plasmids were extracted and purified, they were digested with *EcoRI* and *BamHI* for 1 h at 37 °C and analyzed by an agarose gel (1.5%) electrophoresis. The plasmids with inserts at the right size were sent to sequencing analysis for verification.

For cloning another UBL domain from the putative PfDsk2, a similar cloning procedure was carried out. For the amplification of the fragment, the following primers were used: 5'-ATATGGATCCGTAATAAATGTATC TTTTAAAGTTAC-3' and 5'-ATATGAATTCTTAATTACTTCTAACTAAATGCATAGTATT-3' with the restriction sites for *BamHI* and *EcoRI* underlined.

3.3.3 Heterologous expression and purification of ubiquitin receptor domains of *P. falciparum*

The plasmids of PfUIM2/pQE30 and PfUIM1+2/pQE30 were individually transformed into *E. coli* M15 cells. Colonies were inoculated in the tubes containing 3 mL of sterile LB medium supplemented with the antibiotics kanamycin (50 μg/mL) and carbenicillin (100 μg/mL) and grown at 37 °C for about 10 h. Then the culture mixture was transferred into a flask containing 50 mL sterile LB medium supplemented with the two antibiotics, and the cells were grown in a shaking incubator at 37 °C overnight. The overnight pre-culture mixture was then transferred into 1 L sterile LB medium supplemented with the two antibiotics and grown at 37 °C on the shaking incubation. The culture was induced with 1 mM IPTG when an optical density (OD600) of the culture mixture reached 0.9. After induction, the cells continued to grow for 4 h at 37 °C and then were harvested via centrifugation at 10,000 g for 15 min at 4 °C. The *E. coli* cell pellet was resuspended with a resuspension buffer (50 mM sodium phosphate, 300 mM NaCl, pH 8.0) supplemented with protease inhibitors PMSF (100 μM), pepstatin (3 μM) and cystatin (80 nM), and stored at -20 °C. The purification of the recombinant domains were performed based on the Ni-NTA affinity purification followed by the gel filtration chromatography as described in 3.1.6. Two milliliter Ni-NTA resin was used to purify the recombinant PfUIM2 expressed in 1 L culture, whereas only one milliliter resin was used to purify the recombinant PfUIM1+2 expressed in 1 L culture. The proteins were finally stored at 4 °C in a buffer containing 25 mM HEPES/KOH, 5 mM $MgCl_2$, 10% glycerol, pH

7.4.

For the heterologous overexpression of PfUIM1 domain, the plasmid PfUIM1/pRSET was transformed into *E. coli* BL21 cells. The cells were inoculated in a tube containing 3 mL of sterile LB medium supplemented with 100 µg/mL carbenicillin and grown at 37 °C for about 10 h. Then the culture mixture was transferred into a flask containing 50 mL sterile TB medium supplemented with 100 µg/mL carbenicillin, and the cells were grown in a shaking incubator at 37 °C overnight. The overnight pre-culture mixture was then transferred into 1 L sterile TB medium supplemented with 100 µg/mL carbenicillin, and cells were grown at 37 °C until its OD600 value reached 0.7. Then the cells continued to grow at RT. When the OD600 value reached 1.0, 0.5 mM IPTG was added to induce the expression of PfUIM1. After 20 h, the cells were harvested and resuspended in the resuspension buffer (50 mM sodium phosphate, 300 mM NaCl, pH 8.0) supplemented with protease inhibitors PMSF (100 µM), pepstatin (3 µM) and cystatin (80 nM). PfUIM1 was purified following the same procedure as described for the purification of PfUIM1+2.

For the heterologous overexpression of the PfPru domain, the plasmid PfPru/pQE30 was transformed into *E. coli* M15 cells. Colonies were inoculated in the tubes containing 3 mL of sterile LB medium supplemented with the antibiotics kanamycin (50 µg/mL) and carbenicillin (100 µg/mL) and grown at 37 °C for about 10 h. Then the culture mixture was transferred into a flask containing 50 mL sterile TB medium supplemented with the two antibiotics, and the cells were grown at 37 °C overnight. The overnight pre-culture mixture was then transferred into 1 L sterile TB medium supplemented with antibiotics, and the cells were grown at 37 °C until its OD600 value reached 1.3. Then the cells continued to grow at RT. When the OD600 value reached 1.6, 0.2 mM IPTG was added to induce the expression of PfPru. After 20 h, the cells were harvested and resuspended in a resuspension buffer (50 mM HEPES, 500 mM KCl, 20 mM imidazole, 10 % glycerol and 1% Triton X-100, pH 8.0) supplemented with protease inhibitors PMSF (100 µM), pepstatin (3 µM) and cystatin (80 nM). The recombinant His-tagged PfPru domain was purified with the Ni-NTA affinity chromatography followed by gel filtration as described in 3.1.6. Half milliliter of Ni-NTA resin was used to purify PfPru expressed in 1 L culture. The purified and concentrated PfPru was stored at 4 °C in a buffer containing 50 mM Tris, 150 mM NaCl, pH 8.0.

3.3.4 Heterologous overexpression and purification of ubiquitin-like domains from putative PfRad23 and PfDsk2

The plasmid constructs containing UBL domains from putative PfRad23 and PfDsk2 were individually transformed into *E. coli* BL21 cells. Colonies were inoculated in the tubes containing 3 mL of sterile LB medium supplemented with 100 µg/mL carbenicillin and grown at 37 °C for about 10 h. Then the culture mixture was transferred into a flask containing 50 mL sterile LB medium supplemented with 100 µg/mL carbenicillin and the cells were grown in a shaking incubator at 37°C overnight. The overnight pre-culture mixture was then transferred into 1 L sterile LB medium supplemented with 100 µg/mL carbenicillin. The culture was induced with 1 mM IPTG when an optical density (OD600 nm) of the culture mixture reached 0.9. After induction, the cells continued to grow for 4 h at 37 °C and were then harvested by centrifugation at 10,000 g for 15 min at 4 °C.

The *E. coli* cell pellet was resuspended with PBS supplemented with protease inhibitors (100 µM PMSF, 3 µM pepstatin and 80 nM cystatin), and stored at -20 °C.

The purification of the recombinant GST-tagged UBL domains was carried out based on the GSH-sepharose purification followed by the gel filtration chromatography as described in 3.1.6. Two milliliters of GSH-sepharose 4B resin was used to purify the recombinant UBL domains expressed in 1 L culture. The proteins were finally stored at 4 °C in a buffer containing 25 mM HEPES/KOH, 5 mM $MgCl_2$, 10% glycerol, pH 7.4.

Besides the full-length product, a truncated UBL domain of PfRad23 with a complete N-terminal GST tag can be co-purified. This truncated product cannot be separated from the full-length product via the chromatography purifications that we currently applied as well as by adding a C-terminal His-tag to the full-length product in order to purify the full-length GST-UBL by additional chromatography purification with Ni-NTA.

3.3.5 *In vitro* ubiquitin- and UBL-binding assays

Purified His-tagged *P. falciparum* ubiquitin receptor domains (18 µM) were mixed individually with 1.8 µM GST-tagged UBL domains (from the putative PfRad23 and PfDsk2) together with 20 µL (bed volume) pre-equilibrated Ni-NTA resin in 0.8 mL PBS buffer supplemented with 2 mg/mL BSA, 10 mM imidazole, 0.5% Triton-X100 (v/v). After incubation for 1 h at 4 °C with constant mixing, each incubation mixture was poured into a clean centrifuge tube (0.8 mL, Pierce) and centrifuged at 1,500 g for 1 min to discard the flow through. Then the Ni-NTA beads were intensively washed with 0.5 mL PBS seven times. The bound proteins were eluted with 0.8 mL PBS supplemented with 500 mM imidazole. The elution fraction was concentrated to 80 µL by a Vivaspin centrifugal concentrator with a molecular weight cut off of 3,000 Da. The sample was mixed with 20 µL 5×SDS-PAGE loading buffer and heated at 95 °C for 4 min. Then 12 µL sample was loaded into a 12% gel and proteins were fractionated by the SDS-PAGE and probed with an anti-GST HRP conjugate (GE Healthcare).

To test for ubiquitin-binding abilities, 4.5 µM purified His-tagged *P. falciparum* ubiquitin receptor domains was incubated with 5 µg of K48-linked polyubiquitin chains ranging from one to seven (Boston Biochem Inc.) in the Ni-NTA pull down assay. The ubiquitin chains were probed with an anti-ubiquitin antibody (sigma U5379, 1:1,000 dilution in 5% non-fat milk), followed by a second anti-goat antibody (1:20,000 dilution in 5% non-fat milk) and developed by the ECL method.

3.3.6 Preparation of *P. falciparum* cell extracts for purifications of the *P. falciparum* 26S proteasome

P. falciparum (3D7) cultivated in 24 large culturing plates (45 mL) were collected while they were in trophozoite and early schizont stages, and the parasitemia reached 8-10%. To do this, parasites from every two large culturing plates were collected in a 50 mL Falcon separately and subjected to saponin lysis as described in 3.1.8. After washing two times with PBS, two Falcons of parasites were pooled and subsequently incubated with 10 mL PBS containing 1% formaldehyde (v/v) to cross-link the parasites for 10 min at RT. The cross-linking was stopped by centrifuging the parasites at 1,500 g for 10 min and washing the parasite pellet with 10 mL PBS containing 0.125 M glycine. After a centrifugation at 1,500 g for another 10 min, the parasite pellet was washed

twice with PBS and immediately used or kept at -80 °C.

When the parasite pellet is to be used, the pellet was resuspended with an equal volume of a pre-cooled proteasome purification buffer (25 mM HEPES/KOH, 5 mM $MgCl_2$, 10% glycerol, 1 mM DTT, 10 mM ATP and 1 mM Na_3VO_4, pH 7.4). To avoid possible disruptions of the plasmodial 26S proteasome complex, a mild protein extraction method was used to prepare *P. falciparum* cell extracts. The resuspended parasites were first passed through a needle with a diameter of 0.55 mm in a syringe (B.Braun Sterican, Melsungen, Germany). Then the parasites were passed eight times through a needle with the diameter of 0.4 mm within the same syringe on ice to lyse the parasites. After a 30 min centrifugation at 100,000 g at 4 °C, the supernatant was taken out and subsequently passed though a 0.45-µm filter (Whatman) to remove residual cell debris and was collected in a 15 mL Falcon. The protein concentration of the cleared cell extracts was measured via the Bradford assay. Typically, about 8.5 mg total proteins can be obtained in the parasites extracts generated from 24 large culturing plates of parasites. The cell extracts were kept on ice, protected from the light and immediately used in the purification of the plasmodial proteasome.

3.3.7 Affinity purification of the *P. falciparum* 26S proteasome

The *P. falciparum* 26S proteasome complex was purified by an adopted chromatography method based on the affinity of the plasmodial proteasome to the UBL domain of the putative PfRad23 (Besche *et al.,* 2009; Scanlon *et al.,* 2009). The cleared *P. falciparum* cell extracts (~8.5 mg) were incubated with 2 mg purified GST-tagged UBL domain (GST-UBL) together with 0.4 mL (bed volume) of GSH-sepharose (GE Healthcare) for 3 h at 4 °C with constant mixing. Then the suspension was poured into a 5 mL empty column, and the flow through was collected for analysis. The GSH-sepharose was intensively washed with 10 mL pre-cooled proteasome purification buffer containing 2 mM ATP. In the elution step, excess of His-tagged PfUIM2 was used to compete with the proteasomes in binding to the GST-UBL affinity matrix, therefore eluting the proteasome from the GSH-sepharose. For elution, the GSH-sepharose was carefully agitated with 0.5 mL proteasome purification buffer containing 2 mM ATP and 1 mg purified His-tagged PfUIM2 and incubated for 20 min at RT. The elution step was repeated, and the column was washed once with 0.5 mL buffer without the PfUIM2 to elute residual proteasomes. All elution fractions (1.5 mL) were combined and supplemented with 0.25 mL (bed volume) of Ni-NTA resin (Invitrogen), and incubated for 45 min with constant mixing at 4 °C to completely remove residual His-tagged PfUIM2. After the incubation, the mixture was poured into a clean centrifuge tube (0.8 mL, Pierce), and the flow through containing the purified proteasome was collected. Finally, the proteasome sample was concentrated by a Vivaspin centrifugal concentrator with a molecular weight cut-off of 3,000 Da to a final volume of approximately 100 µL. The purified proteasome samples were immediately used in the proteasomal activity measurements without freezing. The remaining samples were kept at -80 °C until used for the MS analysis. The mock purification with GST as the bait protein was carried out in the same procedure.

3.3.8 Sample preparation for mass spectrometry

Proteasome samples (10 µg) were diluted to 120 µL with 200 mM Tris, pH 8.5 and solid urea was added to 8 M

(57 µg). Samples were reduced and alkylated by addition of 6 µL of 100 mM TCEP and incubated with shaking at RT for 20 minutes, followed by addition of 6 µL of 250 mM IAA, and incubated with shaking in the dark at RT for 20 minutes. One microgram (1 µg/µL) of endoproteinase-LysC was added and the reaction was allowed to proceed for 4 hours at 37 °C. Samples were diluted with 360 µL 100 mM Tris pH 8.5 and 2 µg of trypsin (1 µg/µL) was added. Samples were incubated with shaking at 37 °C for 18 hours and digestion was halted with the addition of 25 µL of 90% formic acid. Samples were spun for 20 min at 14,000 rpm and transferred to a new Eppendorf tube.

3.3.9 Multidimensional protein identification technology (MudPIT) for proteasome sample analysis

The protein digest was pressure-loaded onto a fused silica capillary column containing 2.5 cm of Partisphere strong cation exchanger (Whatman, Clifton, NJ) followed by 2.5 cm of 10 µm Aqua C18 (Phenomenex, Ventura, CA) packed into a 250 µm inside diameter (i.d.) capillary (Polymicro Technologies, Phoenix, AZ) with a 1 µm frit. The column was washed for 60 min with buffer containing 95% water, 5% acetonitrile, and 0.1% formic acid. After washing, a 100-µm i.d. capillary with a 5-µm pulled tip packed with 15 cm 3-µm Aqua C18 material (Phenomenex, Ventura, CA) was attached via a union, and the entire split-column was placed in line with an Agilent 1100 quaternary high-performance liquid chromatography (HPLC) and analyzed using a modified 9-step separation similar to those described previously (Washburn *et al.,* 2001). The buffer solutions used were 5% acetonitrile/0.1% formic acid (buffer A), 80% acetonitrile/0.1% formic acid (buffer B), and 500 mM ammonium acetate/5% acetonitrile/0.1% formic acid (buffer C). Step 1 consisted of a 90 min gradient from 0% to 100% buffer B. Steps 2-9 had the following profile: 10 min of X% buffer C, a 15 min gradient from 0% to 5% buffer B, and a 95 min gradient from 15% to 100% buffer B. The 10 min buffer C percentages were 10%, 20%, 30%, 40%, 50%, 60%, 70%, and 100%, respectively, for the 9-step analysis. As peptides eluted from the microcapillary column, they were electrosprayed directly into an Orbitrap Velos mass spectrometer (ThermoFisher, SanJose, CA) with the application of a distal 2.4 kV spray voltage. A cycle of one full-scan mass spectrum (400-1400 m/z) followed by 15 data-dependent MS/MS spectra at a 35% normalized collision energy was repeated continuously throughout each step of the multidimensional separation. Application of mass spectrometer scan functions and HPLC solvent gradients were controlled by the XCalibur data system.

3.3.10 Analysis of tandem mass spectra of proteasome samples

Protein identifications were done with Integrated Proteomics Pipeline-IP2 (Integrated Proteomics Applications, Inc., San Diego, CA. http://www.integratedproteomics.com) using ProLuCID (Xu *et al.,* 2006) and DTASelect2.0 (Tabb *et al.,* 2002; Cociorva *et al.,* 2007). Spectrum raw files were extracted into ms1 and ms2 files from raw files using RawExtract 1.9.9 (http://fields.scripps.edu/downloads.php) (McDonald *et al.,* 2004), and the tandem mass spectra were searched against a *Plasmodium falciparum* database (release date 01/10/12). In order to accurately estimate peptide probabilities and false discovery rates, we used a decoy database containing the reversed sequences of all the proteins appended to the target database (Peng *et al.,* 2003). Tandem mass spectra were matched to sequences using the ProLuCID algorithm. ProLuCID searches were done on an

Intel Xeon cluster running under the Linux operating system. The search space included all fully and half-tryptic peptide candidates that fell within the mass tolerance window with no miscleavage constraint. Modification of +57.02146 on C (iodoacetamide) was considered to be a static modification.

The validity of peptide/spectrum matches (PSMs) was assessed in DTASelect2.0 using two SEQUEST defined parameters (Eng *et al.,* 1994), the cross-correlation score (XCorr), and a normalized difference in cross-correlation scores (DeltaCN). The search results were grouped by charge state (+1, +2, +3, and greater than +3) and tryptic status (fully tryptic, half-tryptic), resulting in 8 distinct sub-groups. In each one of these sub-groups, the distribution of Xcorr and DeltaCN values for (a) direct and (b) decoy database PSMs was obtained; then the direct and decoy subsets were separated by a quadratic discriminant function which was used to compute a confidence score and achieve a user-specified false discovery rate. Full separation of the direct and decoy PSM subsets is not generally possible; therefore, peptide match probabilities were calculated based on a nonparametric fit of the direct and decoy score distributions. The false discovery rate was calculated as the percentage of reverse decoy PSMs among all the PSMs that passed the confidence threshold. Identified proteins were required to have minimum two peptides with a mass accuracy of up to 20 ppm. Under such filtering conditions, the estimated false discovery rate was below 1% at the peptide and protein level.

3.3.11 Proteasome activity assay

The three peptidolytic activities of the *P. falciparum* 26S proteasome were determined by a fluorogenic peptide cleavage assay using three specific peptide substrates: Suc-LLVY-AMC, Bz-VGR-AMC and Z-LLE-AMC (Enzo life Science). The assay is based on detection of the fluorophore 7-amino-4-methylcoumarin (AMC) after cleavage from the labeled substrates by the proteasome (Scanlon *et al.,* 2009). The released AMC fluorescence can be dynamically quantified using a 380/460 nm filter in a fluorometer. Generally, a standard AMC calibration curve has to be generated, and then the specific activity of the proteasome on a particular substrate is determined by measuring its response against the standard AMC calibration curve.

Briefly, appropriate amount of respective substrate was dissolved in DMSO to prepare a 10 mM stock solution of each substrate. To prepare a 100 µM substrate working solution, 20 µL of substrate stock solution was mixed with 980 µL assay buffer (50 mM Tris, 5 mM $MgCl_2$, 1 mM DTT, pH7.5). In parallel, 1 mM AMC working solution was prepared with the same assay buffer. Due to the auto-hydrolysis of AMC-containing peptide substrates, it is necessary to create the standard AMC curve for each of the substrates in serial dilution of AMC in the presence of the substrate. For this purpose, the AMC/substrate standard solution containing 16 µM AMC and 100 µM of respective substrates was prepared by adding 16 µL of AMC working solution (1 mM) and 10 µL stock solution (10 mM) of the respective substrate to 974 µL assay buffer. For the preparation of the AMC calibration curve for each substrate, the serial dilutions of AMC according to **Table 3** were prepared in duplicate in a 96-well black plate (Greiner Bio-One, Frickenhausen, Germany). After 30 min of incubation at 37 °C, the fluorescence of AMC of each well was read at 460 nm (excited at 380 nm) by a Tecan Infinite 200 fluorescent photometer. Then the AMC standard curve was produced by plotting the fluorescence intensity against the molar amount of AMC (**Figure 13**).

To measure the proteasomal activity, 5-10 µL of purified *P. falciparum* proteasome sample was mixed with 100 µM of respective substrate in 100 µL of assay buffer with or without 10 µM MG132 or lactacystin (Enzo life Science). In parallel, control wells only containing the respective substrates were set as blanks. The AMC fluorescence was read immediately after all samples were prepared. After 30 min incubation at 37 °C, AMC fluorescence was read again. The increased fluorescence intensity (△F) of blanks was subtracted from the △F of the respective samples. Then the respective proteasomal activities of the purified proteasome samples were calculated according to the AMC standard curve.

Table 3. Standard AMC concentrations with substrates in a 96-well plate used for creating AMC calibration curves*.

	1	2	3	4	5	6
A	16 µM AMC + 100 µM Suc-LLVY-AMC		16 µM AMC + 100 µM Bz-VGR-AMC		16 µM AMC + 100 µM Z-LLE-AMC	
B	8 µM AMC + 100 µM Suc-LLVY-AMC		8 µM AMC + 100 µM Bz-VGR-AMC		8 µM AMC + 100 µM Z-LLE-AMC	
C	4 µM AMC + 100 µM Suc-LLVY-AMC		4 µM AMC + 100 µM Bz-VGR-AMC		4 µM AMC + 100 µM Z-LLE-AMC	
D	2 µM AMC + 100 µM Suc-LLVY-AMC		2 µM AMC + 100 µM Bz-VGR-AMC		2 µM AMC + 100 µM Z-LLE-AMC	
E	1 µM AMC + 100 µM Suc-LLVY-AMC		1 µM AMC + 100 µM Bz-VGR-AMC		1 µM AMC + 100 µM Z-LLE-AMC	
F	0.5 µM AMC + 100 µM Suc-LLVY-AMC		0.5 µM AMC + 100 µM Bz-VGR-AMC		0.5 µM AMC + 100 µM Z-LLE-AMC	
G	0.25 µM AMC + 100 µM Suc-LLVY-AMC		0.25 µM AMC + 100 µM Bz-VGR-AMC		0.25 µM AMC + 100 µM Z-LLE-AMC	
H	0.125 µM AMC + 100 µM Suc-LLVY-AMC		0.125 µM AMC + 100 µM Bz-VGR-AMC		0.125 µM AMC + 100 µM Z-LLE-AMC	

* A total volume of the mixture in each well is 50 µL.

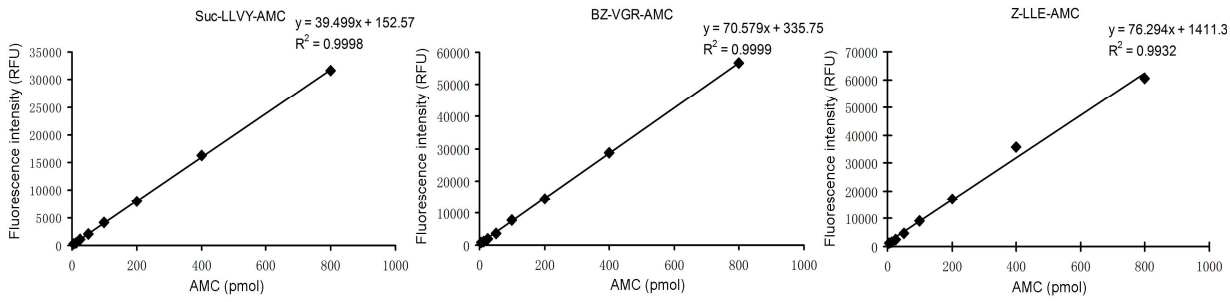

Figure 13. AMC calibration curves with respect to the peptide substrates used in the proteasome activity assay.

4. RESULTS

4.1 Protein *S*-nitrosylation in *P. falciparum*

4.1.1 Detection and isolation of *S*-nitrosylated proteins in *P. falciparum*

To detect *S*-nitrosylated proteins in *P. falciparum*, the biotin-switch assay coupled with anti-biotin western blot analysis was used. The biotin-switch assay involves the blocking of free protein thiols, specific reduction of *S*-nitrosothiols and subsequent biotinylation of the nascent thiols **(Figure 14A)**. To ensure the unbiased identification of *S*-nitrosylated proteins, the sufficiency of thiol blockage and the specificity of the assay were tested for *P. falciparum* samples **(Figure 14B)**. *P. falciparum* cell extracts were incubated with DTT (5 mM) to reduce and expose all protein thiols, which were then blocked with or without methyl methanethiosulfonate (MMTS, 200 mM) before biotinylation. The minimal anti-biotin immunoreactivity in MMTS-blocked cell extracts (Figure 14B, lane 8) compared to the strong immunoreactivity in unblocked cell extracts (Figure 14B, lane 1) indicated the minimization of false-positives by efficient blockage of free thiols. Additionally, the biotin-switch assay lacked the ability to recognize protein disulfides and protein *S*-glutathionylation, two major types of thiol-based redox modifications induced by hydrogen peroxide (H_2O_2) and oxidized glutathione (GSSG), respectively (Figure 14B, lanes 3, 2).

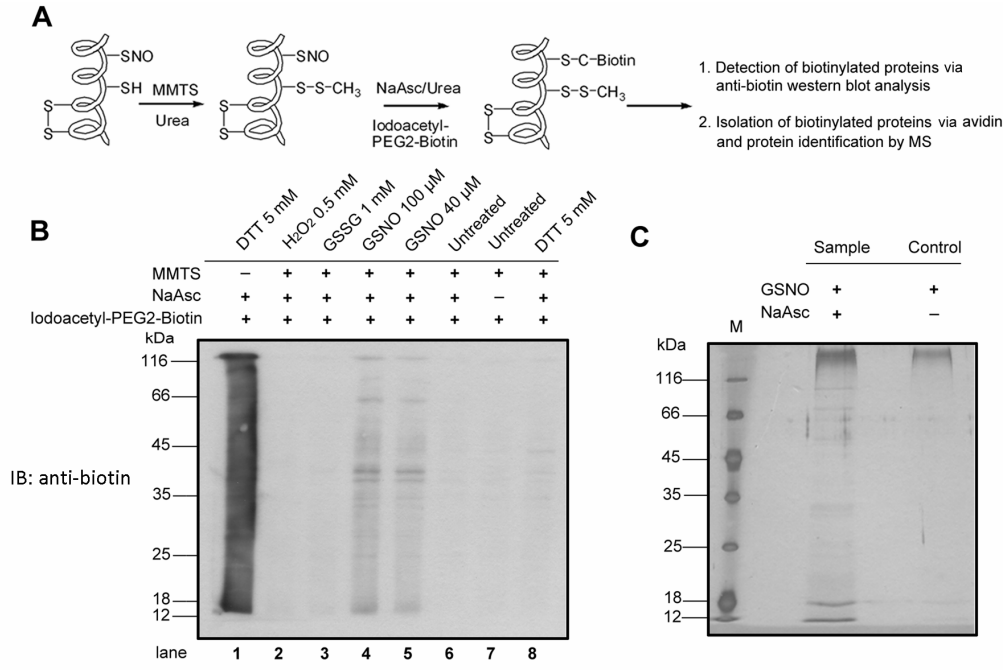

Figure 14. Analysis of *S*-nitrosylated proteins in *P. falciparum* cell extracts. (**A**) Schematic diagram of the biotin-switch assay used for the analysis of *S*-nitrosylated proteins. (**B**) Evaluation of the biotin-switch assay and the detection of *S*-nitrosylated proteins in *P. falciparum* cell extracts. (**C**) A representative silver-stained gel shows the avidin-purified *S*-nitrosylated proteins from *P. falciparum* cell extracts treated with 100 µM GSNO. A control sample without reduction of *S*-nitrosothiols by NaAsc was included in parallel. MMTS: methyl methanethiosulfonate; GSSG: glutathione disulfide. NaAsc: sodium ascorbate. (Wang *et al.,* 2013)

After the specificity of the biotin-switch assay was verified, we first applied the assay to detect *S*-nitrosylated proteins in unstressed and intact parasites. For this experiment, trophozoite-stage *P. falciparum* parasites were

isolated, directly lysed, and the cell extracts were immediately subjected to the biotin-switch assay. A control sample without the reduction of *S*-nitrosothiols by ascorbate was produced in parallel. Western blots indicated a rather low abundance of endogenous *S*-nitrosylated proteins in *P. falciparum* (Figure 14B, lanes 6 and 7), which is consistent with observations in other organisms (Lindermayr *et al.,* 2005; Lam *et al.,* 2010; Murray *et al.,* 2011). Incubation of parasitized erythrocytes with GSNO, a naturally occurring NO donor that promotes SNO (Broniowska *et al.,* 2013), did not significantly enhance the signals, which is likely due to the presence of high hemoglobin concentrations and multiple cell membranes surrounding the parasites (Sobolewski *et al.,* 2005). Therefore we decided to determine targets of *S*-nitrosylation in *P. falciparum* cell extracts treated with GSNO (40 and 100 µM). As a result, anti-biotin immunoblotting signals were clearly observed (Figure 14B, lanes 4 and 5), indicating that a group of *S*-nitrosylated proteins was specifically detected.

The *S*-nitrosylated proteins in the *P. falciparum* cell extracts treated with 100 µM GSNO were pulled down by avidin and visualized in gels via silver staining. In parallel, a stringent control sample that omitted the reduction of *S*-nitrosothiols by ascorbate was set, representing biotinylated proteins derived from blocking-resistant thiols and non-specific avidin-binding proteins. As shown in the silver-stained gel, a number of bands belonging to isolated *S*-nitrosylated proteins emerged in the GSNO-treated cell extracts but not in the control sample, indicating that *S*-nitrosylated proteins were specifically isolated (**Figure 14C**).

4.1.2 Identification of *S*-nitrosylated proteins in *P. falciparum* cell extracts

The *S*-nitrosylated proteins isolated from the 100 µM GSNO-treated *P. falciparum* cell extracts were trypsin-digested and identified using a linear trap quadrupole (LTQ)-Orbitrap mass spectrometer. Only proteins for which at least two peptides were detected in at least two independent experiments were included in the target list. Proteins that were also abundantly detected in control samples (without reduction of *S*-nitrosothiols) were subtracted. Meeting these strict criteria, 267 *S*-nitrosylated annotated proteins **(Appendix Table 1)** and 52 *S*-nitrosylated hypothetical proteins **(Appendix Table 2)** were identified as potential SNO targets in *P. falciparum*. In parallel, the MS/MS analysis revealed 37 *S*-nitrosylation sites from 34 proteins. Categorization of the identified proteins according to their gene ontology annotated in PlasmoDB (version 9.2) has revealed that *S*-nitrosylated proteins participate in a wide range of biological processes in *P. falciparum* and also differ in molecular functions (**Figure 15**).

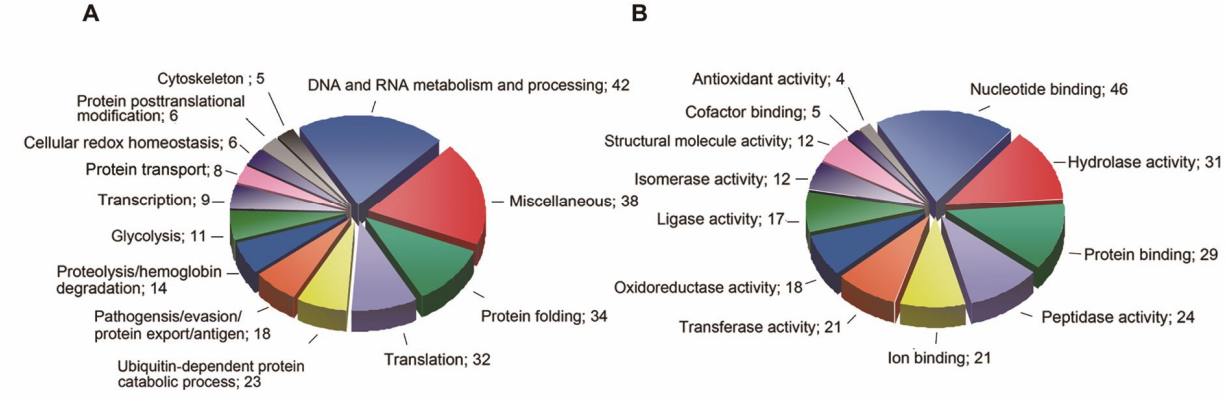

Figure 15. Functional classification of identified *S*-nitrosylated proteins in *P. falciparum*. The identified *S*-nitrosylated

proteins were categorized according to their gene ontology (GO) annotations in biological processes **(A)** and molecular functions **(B)**. Only annotated proteins were used in the analysis, and the most predominant GO terms were shown using the program PatternLab for Proteomics (Kehr *et al.,* 2011). (Wang *et al.,* 2013)

4.1.3 Glycolytic enzymes as targets for *S*-nitrosylation in *P. falciparum*

Interestingly, all eleven enzymes contributing to glycolysis were identified as potential SNO targets **(Appendix Table 1)**, indicating that glycolysis appears to be affected by *S*-nitrosylation. In order to reveal the effects of SNO on plasmodial glycolysis, *S*-nitrosylation on four glycolytic enzymes was characterized in more detail, including *P. falciparum* glyceraldehyde-3-phosphate dehydrogenase (PfGAPDH), phosphoglycerate mutase (PfPGM), pyruvate kinase (PfPK), and lactate dehydrogenase (PfLDH).

The enzymes were heterologously overexpressed in *E. coli* and purified to homogeneity. The pure proteins were incubated with different concentrations of GSNO and then subjected to the biotin-switch assay followed by anti-biotin western blot analysis. Consistent with the large-scale study, the glycolytic enzymes were all susceptible to *in vitro S*-nitrosylation by GSNO in a concentration-dependent manner, whereas *P. falciparum* thioredoxin reductase (PfTrxR) and glutathione *S*-transferase (PfGST), which were not identified as SNO targets in the study, were not *S*-nitrosylated in the assay (**Figure 16A**). Furthermore, the effects of *S*-nitrosylation on the enzymatic activities of PfGAPDH, PfPK, and PfLDH were tested. Interestingly, GSNO-induced *S*-nitrosylation resulted in a concentration and time-dependent inhibition of PfGAPDH activity (**Figure 16B**), whereas incubation with GSNO (up to 1 mM) did not significantly influence PfPK and PfLDH activities (data not shown).

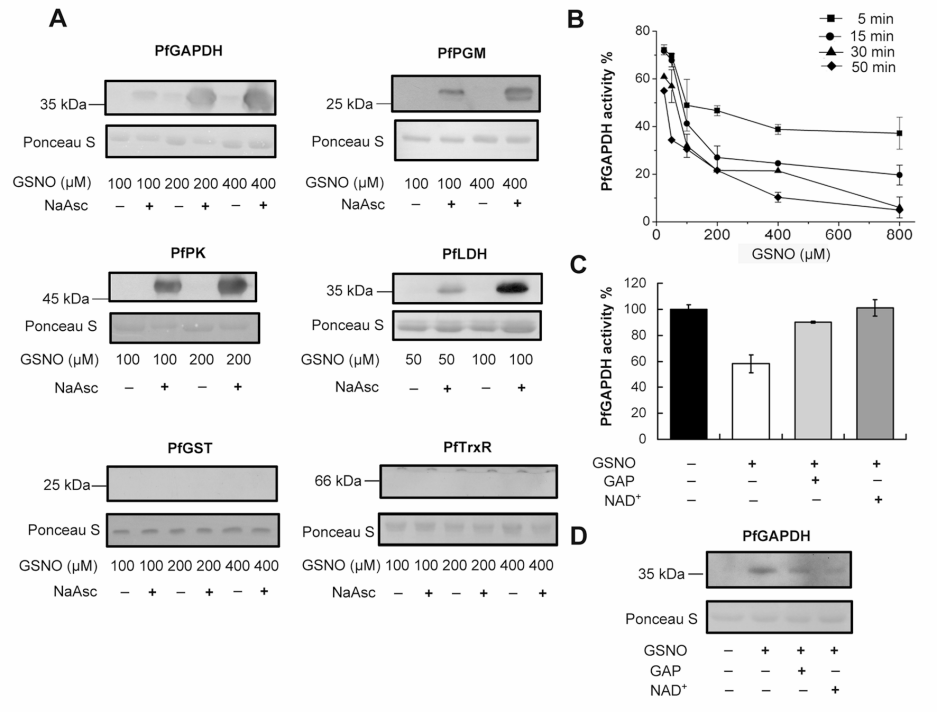

Figure 16. *S*-nitrosylation of glycolytic enzymes of *P. falciparum*. (**A**) Analysis of *S*-nitrosylation on PfGAPDH, PfPGM, PfPK, and PfLDH. Pre-reduced recombinant enzymes were incubated with different concentrations of GSNO at 25 °C for 1 h and subjected to a biotin-switch assay with or without NaAsc (as a control). *S*-nitrosylated enzymes were detected by the

anti-biotin western blot analysis. Ponceau S staining shows equal amounts of protein loaded into each lane. *P. falciparum* glutathione *S*-transferase (PfGST) and thioredoxin reductase (PfTrxR), which were not identified as SNO targets, served as negative controls were indeed not *S*-nitrosylated under the conditions chosen; these results further underline the modification specificity of the assay. (**B**) Concentration and time-dependent inhibition of PfGAPDH activity by *S*-nitrosylation induced by GSNO. Enzymatic activity is given as the percentage of PfGAPDH incubated without GSNO. (**C**) Protection of PfGAPDH activity from GSNO by the substrate glyceraldehyde 3-phosphate (GAP) and the cofactor nicotinamide adenine dinucleotide (NAD^+). PfGAPDH was incubated with 1 mM GAP or 2 mM NAD for 5 min prior to the treatment with 0.2 mM GSNO. Data are represented as mean ± standard deviation from at least three independent determinations. (**D**) Protection of PfGAPDH from GSNO-induced *S*-nitrosylation by preincubation with GAP and NAD^+ as revealed by anti-biotin western blot analysis. (Wang *et al.,* 2013)

It is known that PfGAPDH uses its active site cysteine (Cys153) to metabolize its substrate glyceraldehyde 3-phosphate (GAP) in the presence of the adjacently bound cofactor, nicotinamide adenine dinucleotide (NAD^+) (Robien *et al.,* 2006). To assess whether Cys153 is the target for *S*-nitrosylation, PfGAPDH was pre-incubated with GAP or NAD^+ for 5 min before it was exposed to GSNO treatment. Indeed, pre-incubation with either substrate or cofactor markedly protected PfGAPDH from inhibition by GSNO (**Figure 16C**). In parallel, western blot analysis of *S*-nitrosylated PfGAPDH also showed a reduced level of *S*-nitrosylation of PfGAPDH, which had been pre-incubated with GAP or NAD^+ (**Figure 16D**). The results indicate that GAP and NAD^+ competed with GSNO at the active site, thus protecting PfGAPDH from *S*-nitrosylation. Therefore the results strongly suggest that Cys153 is the target site for *S*-nitrosylation in PfGAPDH.

4.1.4 Redox-regulating proteins as targets for *S*-nitrosylation in *P. falciparum*

Several thiol-based redox-regulating proteins have been identified as potential SNO targets in *P. falciparum* **(Appendix Table 1)**. Several important redox-regulating proteins, including *P. falciparum* peroxiredoxin 6 (PfPrx6), glutaredoxin 1 (Grx1) and peroxiredoxin 1a (PfPrx1a) were tested in an *in vitro S*-nitrosylation assay. As a result, all the tested proteins can be dose-dependently *S*-nitrosylated by GSNO (**Figure 17**).

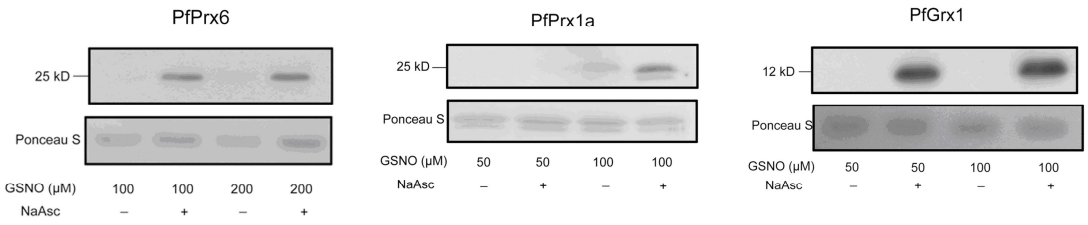

Figure 17. *In vitro S*-nitrosylation of recombinant *P. falciparum* PfPrx6, PfGrx1 and PfPrx1a. Pre-reduced recombinant proteins were incubated with different concentrations of GSNO at 25 °C for 1 h and subjected to a biotin-switch assay with or without NaAsc (as a control). *S*-nitrosylated proteins were detected via the anti-biotin western blot analysis. Ponceau S staining shows equal amounts of protein loaded in each lane. (Wang *et al.,* 2013)

More importantly, *P. falciparum* thioredoxin 1 (PfTrx1, the major cytosolic thioredoxin), a ubiquitous protein disulfide oxidoreductase, was identified as a target of *S*-nitrosylation in *P. falciparum*. Similar to human Trx1 (hTrx1), PfTrx1 contains a pair of active site cysteines in the conserved sequence Cys-Gly-Pro-Cys and a third cysteine (Cys43) (Krnajski *et al.,* 2001). Importantly, it has been shown for hTrx1 that distinct responses of its different cysteine residues to nitrosylating stress direct denitrosylating and transnitrosylating activities of hTrx1 in the regulation of SNO (Barglow *et al.,* 2011; Wu *et al.,* 2011). In order to explore possible regulatory roles of PfTrx1 in SNO, it is thus important to investigate susceptibilities of different cysteines of PfTrx1 to *S*-nitrosylation.

For this purpose, recombinant wild type and different cysteine-mutated PfTrx1s were pre-reduced with DTT followed by GSNO treatments. The *S*-nitrosylation of these proteins was detected by using the biotin-switch assay coupled to western blot analysis. As shown in **Figure 18**, wild type PfTrx1 (PfTrx1-WT) was detected to be *S*-nitrosylated by high concentrations of GSNO (more than 200 µM). Mutation of the resolving active site cysteine (Cys33) to serine in PfTrx1 ($PfTrx1^{C33S}$) showed an increased susceptibility to *S*-nitrosylation, as revealed by the *S*-nitrosylation of the mutant upon relatively low concentrations of GSNO (100 µM). Interestingly, PfTrx1 with both active site cysteines mutated to serine ($PfTrx1^{C30S/C33S}$) was concentration-dependently *S*-nitrosylated by GSNO, implying that Cys43 is an important site for *S*-nitrosylation. This was further evidenced by the finding that a single mutation of Cys43 in PfTrx1 ($PfTrx1^{C43S}$) completely abrogated *S*-nitrosylation of the protein, despite the fact that high concentrations of GSNO were used. Collectively, the results suggest that Cys43 of PfTrx1 is site-specifically targeted by *S*-nitrosylation, whereas the active site cysteines are not major sites of *S*-nitrosylation. The site-specific *S*-nitrosylation of PfTrx1 clues a potential of this protein in the regulation of SNO in *P. falciparum*.

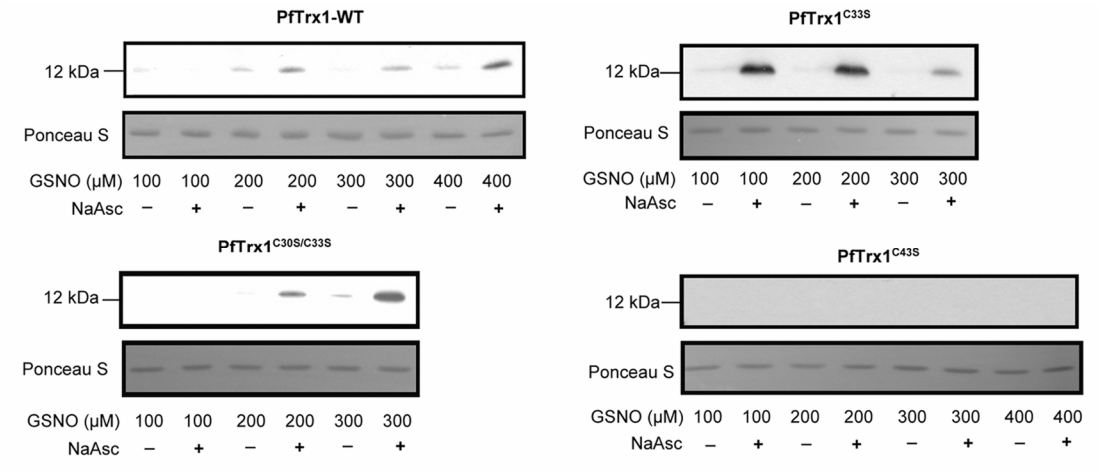

Figure 18. Characterization of the *S*-nitrosylation site in PfTrx1. Recombinant wild type PfTrx1 (PfTrx1-WT) and different PfTrx1 variants with cysteine mutated to serine were pre-reduced and incubated with different concentrations of GSNO for *S*-nitrosylation at 25 °C for 1 h. Proteins were then subjected to a biotin-switch assay with or without NaAsc (as a control) followed by anti-biotin western blot analysis. Ponceau S staining shows equal amounts of protein loaded into each lane. (Wang *et al.,* 2013)

4.1.5 Denitrosylation by *P. falciparum* thioredoxin 1

In order to understand how SNO is regulated in *P. falciparum*, we began to study denitrosylation by searching for a plasmodial homolog of GSNO reductase (GSNOR). However, bioinformatic analysis using the Basic Local Alignment Search Tool (BLAST) revealed that *Plasmodium* genomes lack the sequence encoding a putative GSNOR (data not shown). Considering the fact that *P. falciparum* also possesses a functional thioredoxin system and having learned about the site-specific response of PfTrx1 to *S*-nitrosylating stress, we hypothesized that PfTrx1 functions as a denitrosylase. To test this, we examined whether PfTrx1 is able to denitrosylate proteins at a biochemical level**.** A large variety of *S*-nitrosylated proteins was generated in *P. falciparum* cell extracts treated with GSNO and incubated with recombinant wild type PfTrx1 for denitrosylation. The residual *S*-nitrosylated proteins were then detected by the biotin-switch assay followed by anti-biotin western blot analysis. It was found that PfTrx1 dramatically reduced the levels of *S*-nitrosylated plasmodial proteins. Incubation of PfTrx1 along with PfTrx reductase (PfTrxR) and NADPH nearly eliminated all *S*-nitrosylation signals. This treatment was approximately equipotent to treatment with 1 mM GSH. On the contrary, incubation only with PfTrxR and NADPH showed no obvious denitrosylating effect, implying that PfTrxR has a catalytic effect in the PfTrx1-mediated denitrosylation by reducing PfTrx1 (**Figure 19A**).

To investigate the denitrosylation mechanism in more detail, we assessed activities of PfTrx1 and its cysteine-mutated variants in the denitrosylation of PfGAPDH by using both protein immunoblotting and enzymatic assays. Recombinant PfGAPDH was incubated with 1 mM GSNO to generate *S*-nitrosylated PfGAPDH, which was then incubated with pre-reduced wild type PfTrx1 and different cysteine-mutated PfTrx1 variants for denitrosylation. *S*-nitrosylation levels of PfGAPDH were analyzed with a biotin-switch assay followed by anti-biotin western blots **(Figure 19B)**. We found that PfTrx1 harboring intact active site cysteines (PfTrx1-WT and PfTrx1^{C43S}) significantly denitrosylated PfGAPDH with an efficiency comparable to 5 mM DTT. However, mutations of one or both active site cysteines in PfTrx1 markedly reduced its denitrosylating activity on PfGAPDH, though a slight denitrosylation was observed, which might be due to protein-protein transnitrosylation from *S*-nitrosylated PfGAPDH to PfTrx1. In the enzymatic assay, wild type PfTrx1 recovered the activity of *S*-nitrosylated PfGAPDH in a dose and time-dependent manner, whereas active site cysteine-mutated PfTrx1 variants did not **(Figure 19C)**. The results clearly suggest that active site cysteines of PfTrx1 are mainly responsible for the denitrosylating activity of PfTrx1. Furthermore, we found that the presence of PfTrxR substantially promoted the PfGAPDH-denitrosylating activity of PfTrx1, reflected by the accelerated recovery of PfGAPDH activity **(Figure 19D)**. This implied that an active site disulfide in PfTrx1 was formed in the catalysis of PfGAPDH denitrosylation and in turn reduced by PfTrxR. This result indicates that denitrosylation by PfTrx1 is based on a dithiol-disulfide exchange mechanism (Krnajski *et al.,* 2001). Collectively, the results clearly suggest a denitrosylating activity of PfTrx1 mediated by its active site cysteines.

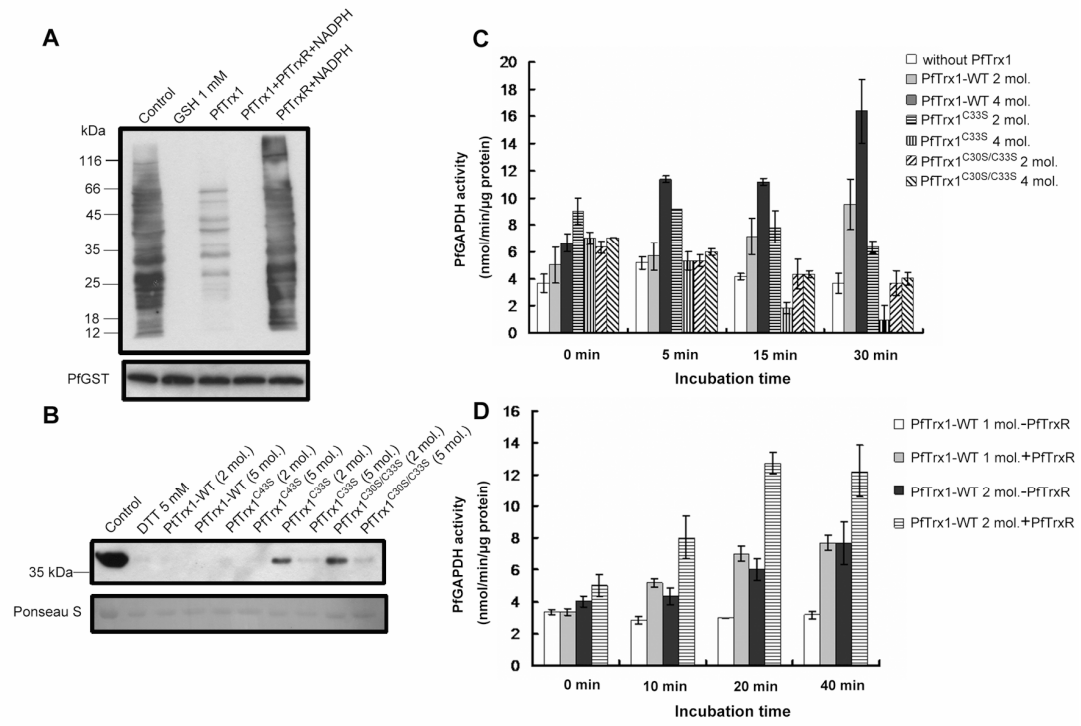

Figure 19. *In vitro* denitrosylation of plasmodial proteins by PfTrx1. (**A**) Denitrosylation of a large variety of *S*-nitrosylated proteins in *P. falciparum* cell extracts by PfTrx1 together with or without a back-up system containing PfTrxR and NADPH. Incubation of GSH and PfTrxR/NADPH alone was set as positive and negative controls, respectively. Immunoblotting of *P. falciparum* glutathione S-transferase (PfGST) in cell extracts was used as a loading control. (**B**) Denitrosylation of PfGAPDH by PfTrx1. The molar ratio of PfTrx1 proteins to PfGAPDH in the denitrosylation assay system was 2:1 or 5:1. *S*-nitrosylated PfGAPDH without denitrosylation was set as a control. Ponceau S staining shows an equal amount of PfGAPDH loaded into each lane. (**C**) The enzymatic activity of *S*-nitrosylated PfGAPDH was restored by wild type PfTrx1 in both concentration and time-dependent manners but not by active site mutated PfTrx1 variants ($PfTrx1^{C33S}$ and $PfTrx1^{C30S/C33S}$). (**D**) PfTrxR accelerated the denitrosylation of PfGAPDH-mediated by PfTrx1. The molar ratio of wild type PfTrx1 to PfGAPDH in the denitrosylation assay system was 1:1 or 2:1. Data are represented as mean ± standard deviation from at least three independent determinations. Incubation with PfTrxR/NADPH alone did not recover the PfGAPDH activity. (Wang *et al.,* 2013)

4.1.6 Transnitrosylation by *P. falciparum* thioredoxin 1

Because PfTrx1 can be *S*-nitrosylated at Cys43, we further tested whether PfTrx1 has a transnitrosylating activity mediated by the *S*-nitrosylated Cys43 residue. Wild type PfTrx1 and the PfTrx1 variant with double mutated active site cysteines ($PfTrx1^{C30S/C33S}$) were *S*-nitrosylated by GSNO and then incubated with *P. falciparum* cell extracts. Analyzed by the biotin-switch assay coupled with an anti-biotin western blot, a number of *S*-nitrosylated proteins in cell extracts emerged upon the incubation of *S*-nitrosylated wild type PfTrx1, indicating that numerous plasmodial proteins were transnitrosylated by PfTrx1 (**Figure 20A**). Compared to wild type PfTrx1, the similar immunoblotting pattern of *S*-nitrosylated proteins induced by *S*-nitrosylated $PfTrx1^{C30S/C33S}$ indicated that Cys43 is responsible for the transnitrosylating activity of PfTrx1. Additionally, by using PfGAPDH as a transnitrosylation substrate, we found that both wild type PfTrx1 and $PfTrx1^{C30S/C33S}$ were

able to transnitrosylate PfGAPDH in a dose-dependent manner (**Figure 20B**). Furthermore, it was found that PfGAPDH activity was more rapidly inhibited by the *S*-nitrosylated PfTrx1$^{C30S/C33S}$ than by the same molar amount of GSNO, indicating a higher efficiency of PfTrx1 in the protein transnitrosylation compared to the *in vivo* NO donor GSNO (**Figure 20C**). Taken together, the results strongly indicate a transnitrosylating activity of PfTrx1, which is mediated by its Cys43 residue.

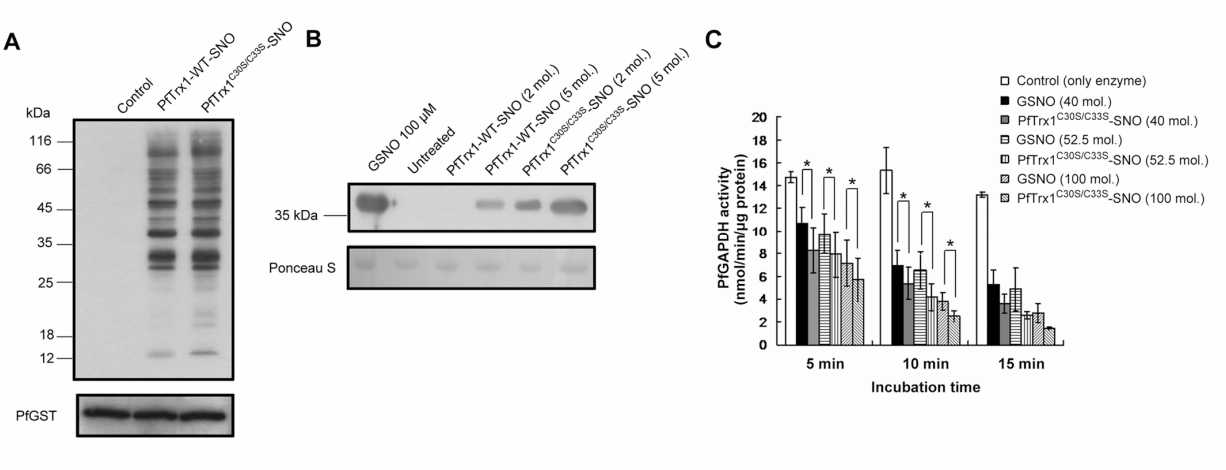

Figure 20. *In vitro* transnitrosylation of plasmodial proteins by PfTrx1. (A) Protein transnitrosylation in *P. falciparum* cell extracts by *S*-nitrosylated wild type PfTrx1 and active site cysteine-mutated PfTrx1 (PfTrx1$^{C30S/C33S}$). Immunoblotting of PfGST in cell extracts was used as a loading control. **(B)** Transnitrosylation of PfGAPDH by *S*-nitrosylated PfTrx1 and PfTrx1$^{C30S/C33S}$. The molar ratio of PfTrx1 proteins to PfGAPDH in the transnitrosylation assay system was 2:1 or 5:1. Incubation of 100 μM GSNO with PfGAPDH was used as a positive control. Ponceau S staining shows an equal amount of PfGAPDH loaded into each lane. (**C**) Comparison of the transnitrosylation efficiency of PfTrx1$^{C30S/C33S}$ with GSNO by using PfGAPDH as a substrate. Equal molar amounts of *S*-nitrosylated PfTrx1$^{C30S/C33S}$ and GSNO were individually incubated with PfGAPDH (molar ratio of both agents to PfGAPDH were 40:1, 52.5:1, and 100:1). A time-dependent inactivation of PfGAPDH was monitored to reflect the transnitrosylation efficiency. PfTrx1-WT-SNO, *S*-nitrosylated wild type PfTrx1; PfTrx1$^{C30S/C33S}$-SNO, *S*-nitrosylated PfTrx1$^{C30S/C33S}$; *, statistically significant difference $P<0.05$ (student *t*-test). (Wang *et al.,* 2013)

4.2 Characterization of the 26S proteasome network in *P. falciparum*

4.2.1 Identification of intrinsic ubiquitin receptors in the *P. falciparum* 26S proteasome

The intrinsic ubiquitin receptors of the eukaryotic 26S proteasome are critical for the substrate recognition at the 26S proteasome. As introduced before, the eukaryotic 26S proteasomes mainly equip two distinct ubiquitin-binding entities for docking ubiquitin or ubiquitin-like molecules, i.e. the UIM domain and the Pru domain located at the 19S Rpn10 and Rpn13 subunits, respectively (Tomko *et al.,* 2013). In order to understand the mechanism of substrate recognition at the plasmodial 26S proteasome, we aimed to identify and characterize the intrinsic ubiquitin receptors of the *P. falciparum* 26S proteasome.

4.2.1.1 *In silico* searching of intrinsic ubiquitin receptors in the *P. falciparum* 26S proteasome

In silico analysis based on the Basic Local Alignment Search Tool (BLAST) using human UIM and Pru domains as queries was carried out in order to search for putative ubiquitin receptors in the corresponding counterparts of the *P. falciparum* 26S proteasome. The human Rpn10 (S5a) has two UIM sequences which are separated by about 40 residues (Mueller *et al.,* 2003). By using a BLAST analysis with the sequence of the S5a domain (amino acids 203-310) containing two UIMs, two putative *P. falciparum* UIMs (PfUIMs) were predicted in a *P. falciparum* homolog of Rpn10 (PF08_0109, putative PfRpn10) (**Figure 21A**). Sequence alignment of the predicted PfUIMs with human UIMs revealed that PfUIMs preserve the key residues that have been demonstrated to be essential for binding ubiquitin or ubiquitin-like molecules (**Figure 21B**). Additionally, we found that the putative plasmodial UIMs appear to be conserved in other *Plasmodium* species, with the second UIM (UIM2) being more conserved among *Plasmodium* species (**Figure 21C**).

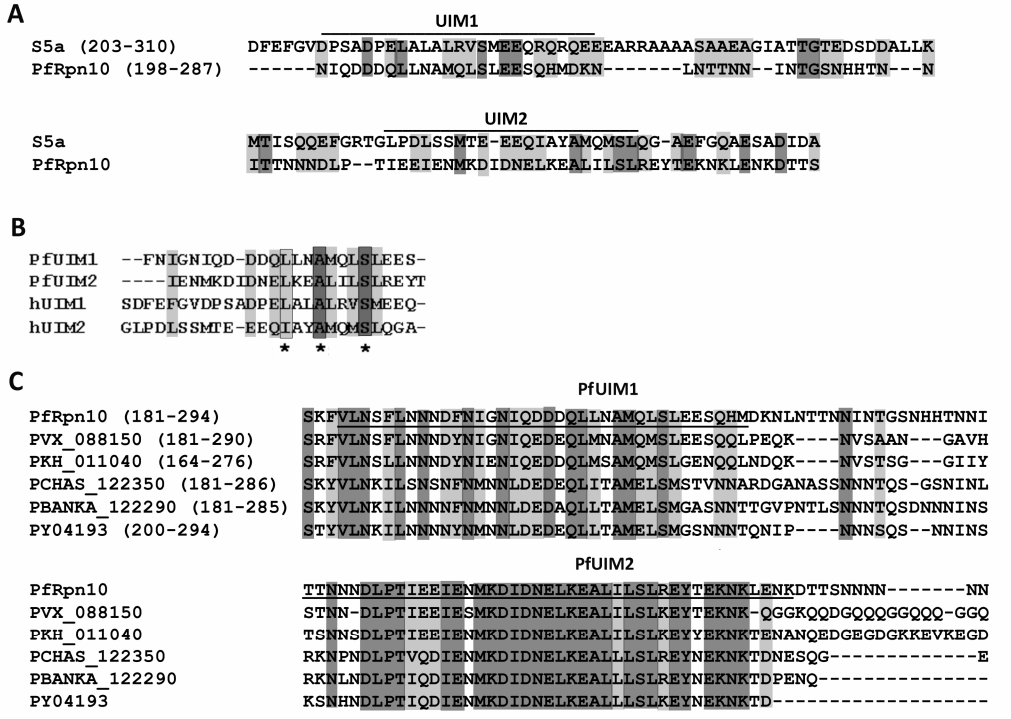

Figure 21. Identification of putative UIM domains in a *P. falciparum* homolog (PF08_0109) of S5a/Rpn10. (A) Sequence alignment of human $S5a_{203-301}$ with PF08_0109 (putative PfRpn10). The amino acid sequences of two human UIMs are indicated. **(B)** Multiple sequence alignment of the identified putative *P. falciparum* UIMs (PfUIMs) with human

UIMs. The most conserved leucine/isoleucine, alanine and serine residues found in both human UIMs and putative PfUIMs were labeled with asterisks. **(C)** Multiple sequence alignment of PfRpn10$_{181-294}$ with its counterparts in other *Plasmodium* species: PVX_088150 (*P. vivax*), PKH_011040 (*P. knowlesi*), PCHAS_122350 (*P. chabaudi*), PBANKA_122290 (*P. berghei*) and PY04193 (*P. yoelii*). The sequences of putative PfUIM domains that were subjected to cloning and heterologous overexpression are underlined. The conserved residues are labeled with gray color, with the intensity of the color indicating the degree of conservation of the residues.

Furthermore, searching for the Pru domain in the *P. falciparum* genome with BLAST predicted a putative Pru domain at the N-terminus of a *P. falciparum* homolog of Rpn13 (PF14_0138, PfRpn13) (**Figure. 22A**). This putative Pru domain has a 58% sequence similarity with the human Pru domain, highly suggesting that a functional Pru domain is present in PfRpn13. The putative plasmodial Pru domain was also found to be conserved in the corresponding counterparts of other *Plasmodium* species (**Figure 22B**).

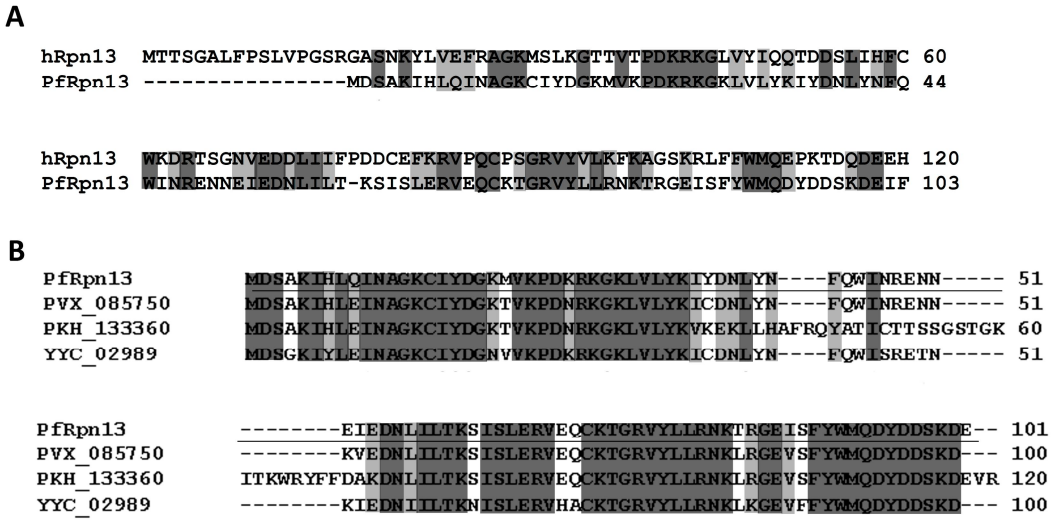

Figure 22. Identification of putative Pru domain in a *P. falciparum* homolog (PF14_0138) of Rpn13. (A) Sequence alignment of the Pru domain of human Rpn13 with the N-terminal sequence of PF14_0138 (putative PfRpn13). **(B)** Multiple sequence alignment of the N-terminal sequence of PF14_0138 with its counterparts in other *Plasmodium* species: PVX_085750 (*P. vivax*), PKH_133360 (*P. knowlesi*) and YYC_02989 (*P. yoelii*). The sequence of the putative PfPru domain that was subjected to cloning and heterologous expression is underlined. The conserved residues are labeled with gray color, with the intensity of the color indicating the degree of conservation of the residues.

4.2.1.2 Cloning, heterologous overexpressions and purifications of the putative ubiquitin receptor domains of *P. falciparum*

The putative PfUIM domains, the domain containing both PfUIM1 and PfUIM2 (PfUIM1+2) as well as the PfPru domain were successfully amplified from a blood stage cDNA library using the specific primers described in the Methods. For the heterologous overexpression of His-tagged recombinant domains, the PfUIM2, PfUIM1+2, and PfPru domains were individually cloned into a pQE30 expression vector, and the PfUIM1 domain was cloned into a pRSET vector in order to increase its expression yield (see Methods). Both expression

vectors render a His-tag to the N-terminus of the respective recombinant domains. The ubiquitin receptor domains were heterologously overexpressed in *E. coli* and purified via Ni-NTA affinity chromatography followed by gel filtration. The recombinant, His-tagged PfUIM1, PfUIM1+2, and PfPru were further verified via western blot analyses with anti-His antibodies (**Figure 23**).

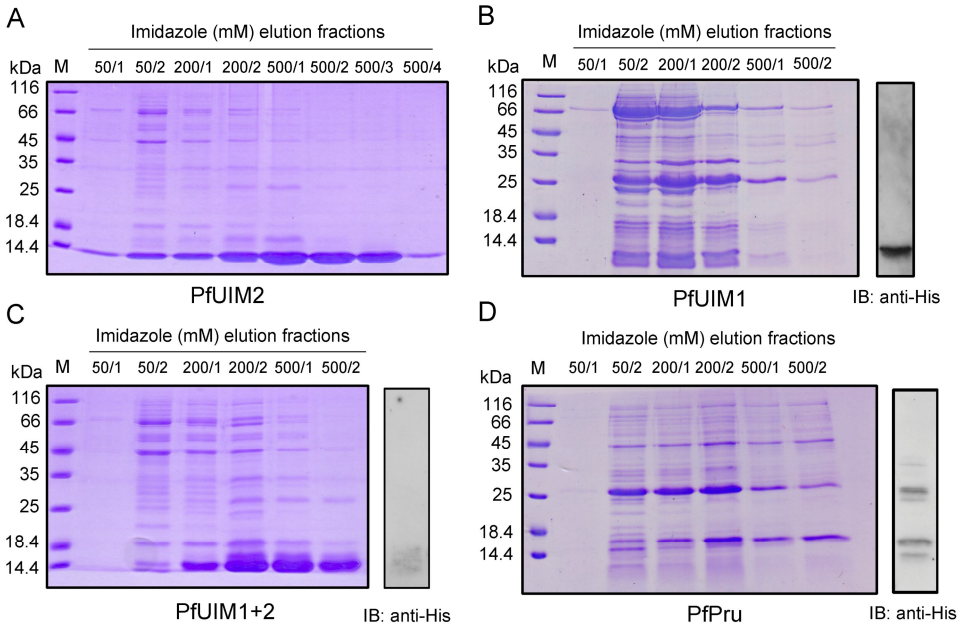

Figure 23. Ni-NTA purifications of recombinant ubiquitin receptor domains of *P. falciparum*. (A-D) SDS-PAGE analysis and Coomassie staining of the purified PfUIM1, PfUIM2, PfUIM1+2, and PfPru domains in imidazole elution fractions. The purified PfUIM1, PfUIM1+2, and PfPru were confirmed by the western blot analysis using an anti-His antibody. In the western blot analysis of Pru, a protein detected by the anti-His antibody at the size of 27 kDa is most likely a dimer of the recombinant PfPru.

4.2.2 Identification of the ubiquitin-like domains from two putative UBL-UBA proteins in *P. falciparum*

The ubiquitin receptors of the eukaryotic 26S proteasome have been reported not only to bind to (poly)ubiquitin but also to the ubiquitin-like (UBL) domains of several proteasomal substrate shuttle factors, i.e. the UBL-UBA proteins (Mueller *et al.,* 2003; Husnjak *et al.,* 2008). The best studied UBL-UBA proteins are Rad23 and Dsk2. By using the sequences of human Rad23 and Dsk2 as inquiries in the BLAST, we found that *P. falciparum* encodes two proteins (PF10_0114 and PF11_0142), which are highly homologous to human Rad23 and Dsk2, respectively (data not shown). Sequence alignments of the UBL domains from human Rad23 and Dsk2 with the corresponding N-terminal parts of the two proteins suggested putative UBL domains are conserved in the two plasmodial proteins (**Figure 24**).

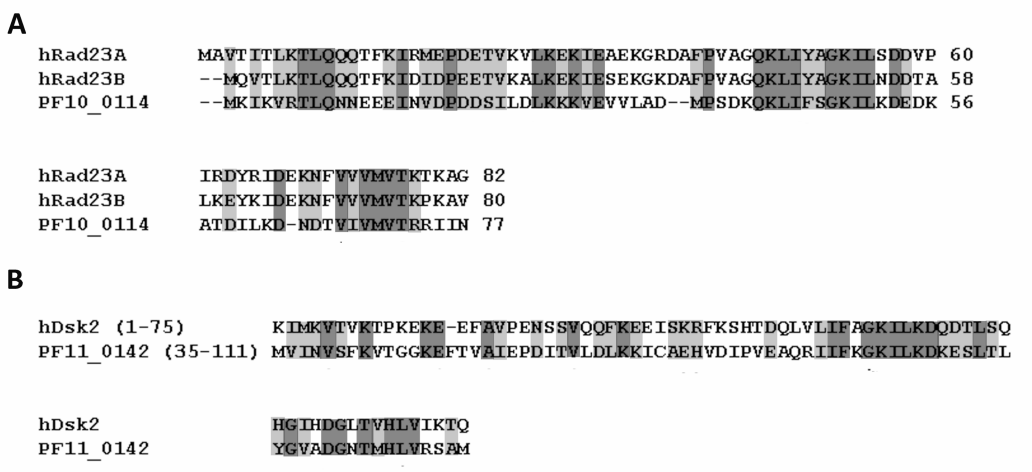

Figure 24. Identification of putative UBL domains in PF10_0114 (putative PfRad23) and PF11_0142 (putative PfDsk2). (A) Sequence alignment of the UBL domains of human RAD23A and RAD23B with the N-terminal sequence of PF10_0114. **(B)** Sequence alignment of the UBL domain of human Dsk2 with PF11_0142$_{35\text{-}111}$. The conserved residues are labeled with gray color, with the intensity of the color indicating the degree of conservation of the residues.

The putative UBL domains of PF10_0114 and PF11_0142 were individually amplified and cloned into a GST-fusion protein expression vector. The GST-fused UBL domains were heterologously overexpressed in *E. coli* and purified via GSH-sepharose 4B affinity chromatography followed by gel filtration (**Figure 25**). It should be noted that the GST-fused UBL domain of PF10_0114 forms a truncated product with intact GST tag during the heterologous expression, which can be revealed via western blot analysis using the anti-GST antibody. The truncated product could not be further separated from the full-length product via normal chromatographic purifications, possibly due to the fact that they form a stable heterodimeric complex via their GST parts.

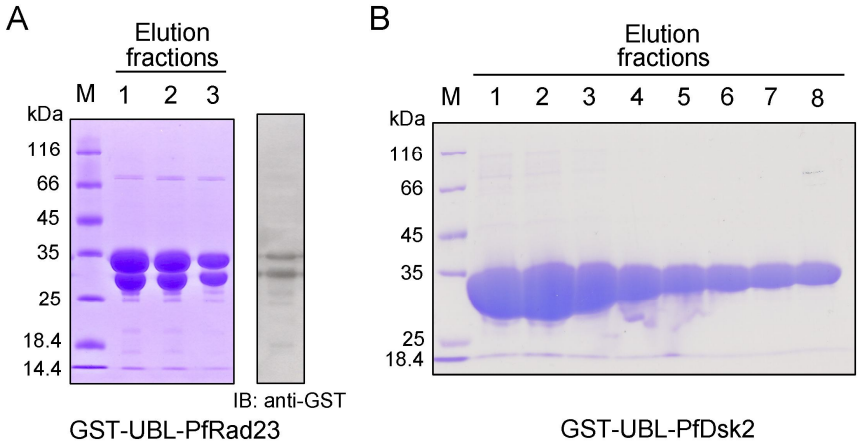

Figure 25. GSH-sepharose 4B purifications of recombinant GST-tagged UBL domains from the putative PfRad23 and PfDsk2. (A) SDS-PAGE analysis and Coomassie staining of the purified GST-tagged UBL domain from putative PfRad23 (GST-UBL-PfRad23). The purified GST-UBL-PfRad23 can be confirmed via a western blot analysis using the anti-GST antibody. A truncated product with a complete GST tag can be co-purified and detected. **(B)** SDS-PAGE analysis and Coomassie staining of the purified GST-tagged UBL domain from putative PfDsk2 (GST-UBL-PfDsk2).

4.2.3 Verification of the identified *P. falciparum* ubiquitin receptor domains

To verify the identified ubiquitin receptor domains, the *in vitro* binding of the ubiquitin receptors with UBL domains or ubiquitin were assessed in a Ni-NTA-based pull-down assay. First, equal molar amounts of His-tagged ubiquitin receptor domains together with Ni-NTA resin were used to pull down the GST-fused UBL domains of PfRad23 and PfDsk2. As a result, it was found that the recombinant PfUIM and PfPru domains can pull down the GST-fused ubiquitin-like domains derived from PfRad23 and PfDsk2, whereas an equal molar amount of recombinant His-tagged PfTrx1 cannot. In the control experiment, GST itself was hardly pulled down by PfUIMs and PfPru, thus indicating that the ubiquitin receptor domains directly interact with the plasmodial UBL domains in the assay (**Figure 26A**).

Next, we incubated the identified ubiquitin receptor domains with a mixture of K-48 linked polyubiquitin chains containing mono-ubiquitin and polyubiquitin molecules up to hepta-ubiquitin (Ub_{1-7}) in the pull down assay. In the control experiments, either the equal molar amount of His-tagged PfTrx1 or only Ni-NTA resin was incubated with the polyubiquitin chains. The pulled-down ubiquitin molecules were detected via western blot analysis using anti-ubiquitin antibodies. As a result, it was found that PfUIM2 and PfUIM1+2 domains successfully pulled down the polyubiquitin chains ranging from diubiquitin to hepta-ubiquitin, but not the mono-ubiquitin. In strong contrast, the PfUIM1 and PfPru domains did not pull down any ubiquitin molecules. Using a 3-fold molar amount of PfUIM1 and PfPru in the pull-down assay was still unable to pull down polyubiquitin chains (data not shown), indicating that they lack the ability to bind ubiquitin and polyubiquitin chains. No ubiquitin molecules were pulled down by the His-tagged PfTrx1 or only by the Ni-NTA resin (**Figure 26B**).

Taken together, the *in vitro* binding assays confirmed the UBL domain-binding capabilities of all identified *P. falciparum* ubiquitin receptor domains. However, only the PfUIM2 domain pocesses the capability to bind high-molecular-weight ubiquitin chains, strongly suggesting that the PfUIM2 domain of PfRpn10 is the major site for the direct recognition of ubiquitin conjugates at the *P. falciparum* 26S proteasome.

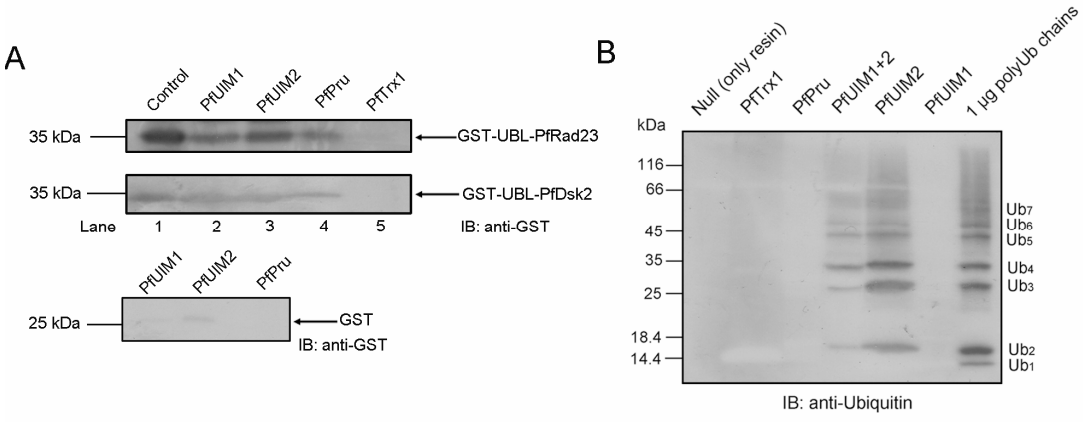

Figure 26. *In vitro* binding of the UBL domains and the K48-linked polyubiquitin chains by *P. falciparum* ubiquitin receptor domains. (A) The recombinant His-tagged PfUIM1, PfUIM2, and PfPru domains (18 µM) were individually used to pull down GST-tagged UBL domains or GST (1.8 µM) together with 25 µL Ni-NTA resin. The western blot analysis using an anti-GST antibody was used to detect GST or GST-tagged UBL domains. One microgram of the respective purified

GST-tagged UBL domains were loaded as positive controls (lane 1). Pull down of GST-tagged UBL domains with an equal amount of His-tagged PfTrx1 were set as control experiments (lane 5). **(B)** The recombinant His-tagged PfUIM1, PfUIM2, UIM1+2, and PfPru domains (4.5 µM) were individually used in the pull down of 5 µg K-48 linked polyubiquitin chains (Ub_{1-7}). The western blot analysis using an anti-ubiquitin antibody was used to detect ubiquitin molecules. One microgram of polyubiquitin chains was loaded as a positive control. As negative controls, equal molar amounts of His-tagged PfTrx1 or only Ni-NTA resin (Null) were used in the pull-down assay.

4.2.4 Affinity purification of the *P. falciparum* 26S proteasome

To characterize the componential integrity and functionality of the *P. falciparum* 26S proteasome complexes, we developed an affinity purification method to isolate the *P. falciparum* 26S proteasome complex. The method is based on the interaction of the PfUIM2 domain with the GST-tagged UBL (GST-UBL) domain of PfRad23. The experimental design is shown in **Figure 27A**. Formaldehyde was used to cross-link the intact parasites before lysis in order to stabilize the assembly of the whole 26S complex and maximize the identification of putative proteasome-interacting proteins (PIPs) (Bousquet-Dubouch *et al.,* 2009).

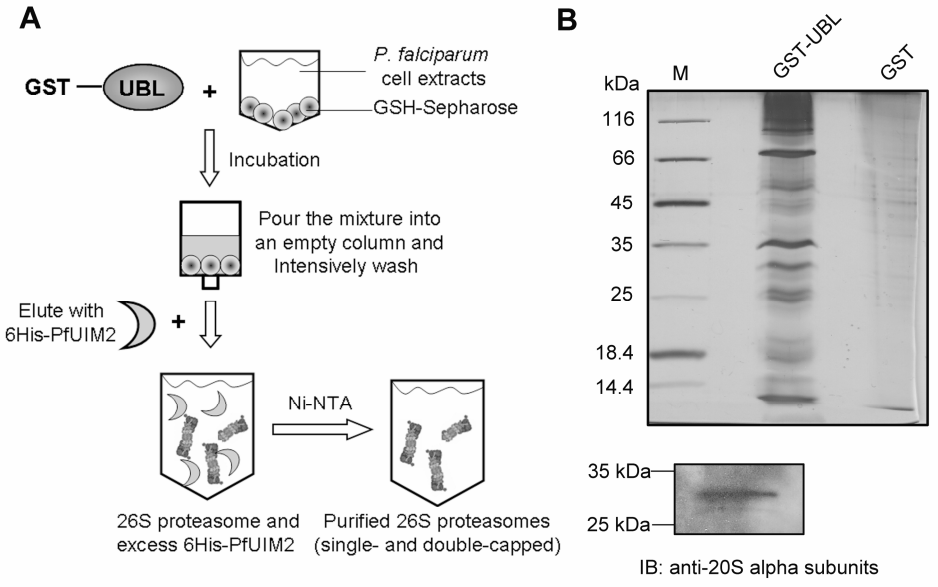

Figure 27. Affinity purification of the *P. falciparum* 26S proteasome. (A) The experimental workflow of the affinity purification of the *P. falciparum* 26S proteasome is based on the interaction of PfUIM2 with the UBL domain of PfRad23. See Methods for experimental details. The scheme has been modified from (Besche *et al.,* 2012) **(B)** The SDS-PAGE (12%) and silver staining analysis of the proteins in the purified *P. falciparum* 26S proteasome sample. A control sample from a mock purification by using GST was included in parallel. The presence of the 20S subunits in the purified proteasome sample was confirmed by a western blot analysis with an antibody against 20S alpha subunits.

Analysis of the purified proteasome sample in a silver-stained gel revealed that a number of proteins emerged in the GST-UBL-based purification but not in the mock purification with GST itself (**Figure 27B**). Additionally, the presence of 20S subunits can be detected via western blot analysis using an anti-20S α-subunit antibody. A typical yield of the purified 26S proteasome sample was about 15 µg from 6 mg parasite extracts. Furthermore,

determined by the fluorogenic peptide cleavage assay, the specific chymotrypsin-like, trypsin-like, and PGPH activities of the purified *P. falciparum* 26S proteasome were shown to be 54.6±8.8 pmol/μg/h, 76.08±17.5 pmol/μg/h, and 35.62±3.9 pmol/μg/h, respectively. The respective proteasomal activities were also shown to be inhibited by the human proteasome inhibitors MG132 and lactacystin (**Figure 28**). No proteasomal activities were detected in the control sample from the GST mock purification (data not shown).

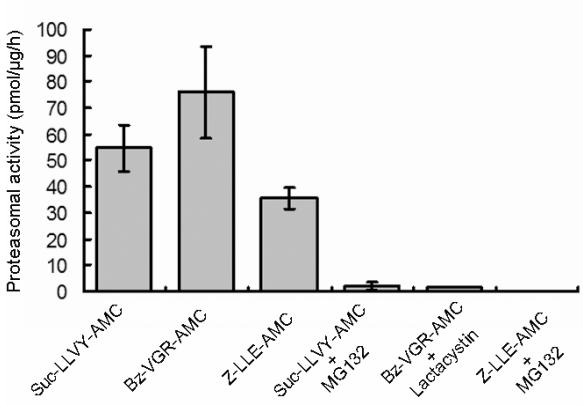

Figure 28. The proteasomal activities of the affinity purified *P. falciparum* 26S proteasome. The specific chymotrypsin-like, trypsin-like, and PGPH activities of the purified *P. falciparum* 26S proteasome were determined by using the fluorogenic proteasomal substrates Suc-LLVY-AMC, Bz-VGR-AMC, and Z-LLE-AMC in a peptide cleavage assay, respectively. Inhibitory effects of the human proteasome inhibitors MG132 and lactacystin (10 μM) were tested on the proteasomal activities of the purified *P. falciparum* 26S proteasome. Ten percent of the purified sample was used in each measurement.

The proteins in the purified *P. falciparum* 26S proteasome samples from four independent GST-UBL-based purifications together with a control sample from a mock purification with GST were trypsin-digested and identified using a linear trap quadrupole (LTQ)-Orbitrap mass spectrometer **(Table 4)**. Proteins that were abundantly detected in the control sample were subtracted. In total, 33 proteasomal proteins covering all putative subunits of the *P. falciparum* 26S proteasome were abundantly and reproducibly identified in the samples but not in the control, demonstrating the robustness of the purification method for isolating plasmodial 26S proteasomes. The overall abundance of the identified 19S subunits appeared to be higher than that of the 20S subunits. This is probably due to the fact that the affinity is generated to the 19S sub-complex, resulting in the capture of both single and double-capped 26S proteasomes. Besides, a putative plasmodial subunit of the proteasome activator complex (PA28) was also identified. No human 26S proteasome subunits were detected, indicating the specificity of the affinity purification method.

Table 4. Proteasomal components identified in the affinity purification of the *P. falciparum* 26S proteasome

PlasmoDB Accession No.	Descriptive name[1]	Unique Peptides[2]	Coverage %[3]
19S RP			
Non-ATPase subunits			
PFB0260w	Proteasome 26S regulatory subunit, putative (Rpn1)	55/43/28/19	38.3/32.6/24.7/25.1
PF14_0632	26S proteasome regulatory subunit, putative (Rpn2)	48/34/23/18	38.5/31.9/27.2/26.5
MAL13P1.190	Proteasome regulatory subunit, putative (Rpn3)	28/19/16/6	41/34.8/40.4/19.7
PFC0785c	Proteasome regulatory protein, putative (Rpn4/P27)	4/5/3	19.1/19.1/18.2
PF10_0174	26s proteasome regulatory subunit p55, putative (Rpn5)	25/14/17/14	39/22.3/29.8/23.1
PF14_0025	Proteosome subunit, putative (Rpn6)	22/19/15/11	27/24.2/23.9/15.3
PF11_0303	26S proteasome regulatory subunit, putative (Rpn7)	13/18/7/4	31.6/25.4/18.1/15
PFI0630w	26S proteasome regulatory subunit, putative (Rpn8)	17/14/11/7	49.1/36.1/34.3/31.4
PF10_0298	26S proteasome regulatory subunit, putative (Rpn9)	16/11/5/5	34.9/30/17/16.5
PF08_0109	Proteasome subunit alpha type 5, putative (Rpn10)	27/17/20/9	38.7/48.4/33.1/32.4
MAL13P1.343	Proteasome regulatory subunit, putative (Rpn11)	17/15/13/13	50.8/45.7/42.8/51.1
PFC0520w	26S proteasome regulatory subunit S14, putative (Rpn12)	5/3/3/2	15.8/8.9/8.9/8.9
PF14_0138	26S proteasome regulatory subunit, putative (Rpn13)	7/3/4	43.1/19.8/24.9
ATPase subunits			
PF13_0063	26S proteasome regulatory subunit 7, putative (Rpt1)	31/31/19/19	41.4/50.5/33.6/39.3
PF10_0081	26S proteasome regulatory subunit 4, putative (Rpt2)	42/36/37/23	62.5/60.3/53.6/52.7
PFD0665c	26S proteasome AAA-ATPase subunit, putative (Rpt3)	45/29/31/15	58.7/48/59.9/37.8
PF13_0033	26S proteasome regulatory subunit, putative (Rpt4)	19/20/13/9	41.2/37.2/33.1/29.3
PF11_0314	26S proteasome regulatory subunit 6a, putative (Rpt5)	55/49/44/30	60.4/60.1/65.4/64.5
PFL2345c	26S proteasome regulatory subunit 8, putative (Rpt6)	30/25/27/19	46.9/49/49/40.5
20S CP			
Alpha-subunits			
MAL8P1.128	Proteasome subunit alpha, putative (α1)	16/12/8/9	53.8/46.9/28.1/35.4
PFF0420c	Proteasome subunit alpha type 2, putative (α2)	14/12/13/8	52.8/43.8/52.8/43.8
PF13_0282	Proteasome subunit, putative (α3)	15/10/11/6	59.8/51.2/42.3/45.1
MAL13P1.270	Proteasome subunit, putative (α4)	23/19/10/10	38.6/45.6/37.8/44.4
PF07_0112	Proteasome subunit alpha type 5, putative (α5)	15/15/11/12	39.5/46.5/35.5/37.1
PF14_0716	Proteosome subunit alpha type 1, putative (α6)	15/8/10/9	43.7/25.2/43.7/42.5
PFC0745c	Proteasome component C8, putative (α7)	6/6/7/3	23.8/20.6/25.8/15.9
Beta-subunits			
PFI1545c	Proteasome precursor, putative (β1)	15/11/8/3	27.3/28/26.2/21.3
PF13_0156	Proteasome subunit beta type 7 precursor, putative (β2)	3/2	13.3/4.1
PFA0400c	Beta3 proteasome subunit, putative (β3)	13/10/7/5	32.4/41.7/20.6/31.4
PF14_0676	20S proteasome beta 4 subunit, putative (β4)	8/7/4/3	40/40/23.6/17.9
PF10_0111	20S proteasome beta subunit, putative (β5)	7/4/4/2	27.3/15.9/15.1/12.5
PFE0915c	Proteasome subunit beta type 1, putative (β6)	8/5/8/4	32.9/18.3/32.5/18.8
MAL8P1.142	20S proteasome beta subunit (β7)	30/25/14/16	44.2/44.2/38.1/45.3
Proteasome activator			
PFI0370c	Subunit of proteasome activator complex, putative, PA28	9/5/4/7	42.3/21.5/17.2/31.2

[1]The descriptive names of the proteins were annotated in the PlasmoDB. The assignments of the subunits of the *P. falciparum* 26S proteasome complex were referred to the "Malaria Parasite Metabolic Pathways" (http://priweb.cc.huji.ac.il/malaria/). [2,3]The number of unique peptides and the corresponding sequence coverage identified by the MS/MS analysis were given for each identified protein. Values from four independently conducted experiments were listed.

4.2.5 Identification of putative *P. falciparum* proteasome-interacting proteins (PIPs)

Besides the proteasomal components, a number of additional plasmodial proteins were identified in the MS/MS analysis, indicating the co-purification of these proteins with the *P. falciparum* 26S proteasome **(Table 5)**. It is well known in the mammalian and plant system that a variety of PIPs dynamically interact with the 26S proteasome (Bousquet-Dubouch *et al.,* 2009; Saeki *et al.,* 2009). Thus, we speculate that many of the co-purified proteins might be putative PIPs of the *P. falciparum* 26S proteasome. Supporting this, a large group of the co-purified proteins consist of many conserved proteins whose mammalian and plant counterparts have been reported to be PIPs in other affinity purifications of the eukaryotic 26S proteasomes. For example, the putative PfRad23 and PfDsk2, whose mammalian counterparts are well characterized proteasome interactors, were identified in at least three independent purifications. Additionally, several proteins that belong to the plasmodial UPS were identified in the purified proteasome sample, including the plasmodial polyubiquitin, one E1 enzyme and four E2 enzymes, and several deubiquitinases. Of great significance, a putative ubiquitin carboxyl-terminal hydrolase (PFE1355c) were abundantly and reproducibly identified with a large number of peptides and high sequence coverage in the MS/MS analysis, highly suggesting a specific interaction of the protein with the plasmodial 26S proteasome. Furthermore, a variety of proteins involved in the protein folding and quality control, protein translation, glycolysis, ribosomal function, and *Plasmodium*-specific processes were also identified to be co-purified with the plasmodial 26S proteasome. Many of the proteins have mammalian and plant counterparts that are validated PIPs or have been shown to be co-purified with the 26S proteasome by similar purification strategies or other biochemical approaches. These proteins include heat shock proteins, proteasome-assembling chaperones, T-complex proteins, elongation factors, some glycolytic enzymes, and ribosomal proteins **(Table 5)**. These proteins appear to be present in high abundance among total co-purified proteins, indicating the effectiveness of the affinity purification method to co-isolated putative PIPs of the *P. falciparum* 26S proteasome. Of course, the interactions of the identified putative PIPs with the plasmodial 26S proteasome need to be validated in further investigations.

Table 5. Co-purified proteins identified in the affinity purification of the *P. falciparum* 26S proteasome.

PlasmoDB Accession No.	Descriptive name[1]	Peptides number[2]	Coverage %[3]
Ubiquitin and ubiquitin domain containing proteins			
PFL0585w	Polyubiquitin※	2	6.6
PF10_0114	DNA repair protein RAD23, putative※	2/2/2	5.6/5.9/5.6
PF11_0142	Ubiquitin domain containing protein※	4/4/4/2	18/18/22.2/17
Ubiquitination enzymes			
PFL1245w	Ubiquitin-activating enzyme e1, putative	5/5/2/10	5.1/5.9/2.3/16.1
PFE1350c	Ubiquitin conjugating enzyme 13, putative	3/7/5/4	24.3/63.8/52.6/52
PFL0190w	Ubiquitin conjugating enzyme E2, putative	4/5/3/4	18.4/18.4/18.4/18.4
PFI0740c	Ubiquitin conjugating enzyme, putative	2/3	35.8/35.8
PF13_0301	Ubiquitin conjugating enzyme, putative	2/2/3	26.2//21.8/34.2
Deubiquitinases			
PFE1355c	Ubiquitin carboxyl-terminal hydrolase, putative※	34/24/26/12	39.7/30.2/39.8/22.5

PlasmoDB Accession No.	Descriptive name[1]	Peptides number[2]	Coverage %[3]
MAL7P1.147	Ubiquitin carboxyl-terminal hydrolase, putative	2	1.2
PFA0220w	Ubiquitin carboxyl-terminal hydrolase, putative	2	1.5
PF11_0177	Deubiquinating/deneddylating enzyme※	2/5	7.7/14
Protein folding and quality control			
PFF0940c	Cell division cycle protein 48 homologue, putative※	12/13/20/23	19.2/23.9/29.1/27.7
PF14_0046	Conserved *Plasmodium* protein, unknown function▲	18/12/11/19	42.1/42.1/45.5/53.9
PF11_0055	Conserved protein, unknown function▲	10/8/21/16	24.8/21/34/34.7
PF11_0098	Endoplasmic reticulum-resident calcium binding protein▲	37/28/38/36	71.7/75.8/73.5/66.5
PFL1070c	Endoplasmin homolog precursor, putative▲	24/33/38/34	31.2/48.7/48.2/40.7
PF07_0033	Heat shock protein 110※	13/12/14/13	20.8/18.1/23.6/21
MAL13P1.540	Heat shock protein 110, putative▲	22/19/52/48	32.3/25.6/51.1/48.5
PFI0875w	Heat shock protein 70※	172/119/238/197	83.6/70.2/88.8/75.9
PF08_0054	Heat shock protein 70※	47/47/59/51	55.1/53.3/67.7/58.3
PF11_0351	Heat shock protein 70※	17/16/44/32	30.6/26.5/49.6/41.9
PF07_0029	Heat shock protein 90※	51/76/58/61	45/56.5/52.8/49.9
PF14_0359	HSP40, subfamily A, putative	14/4/9/9	35.1/18.2/30.7/28.1
PF14_0324	HSP70/HSP90 organizing protein, putative	9/14/16/7	20.7/30.5/28.9/15.4
PFF1050w	Nascent polypeptide associated complex alpha chain, putative※▲	11/8/4/5	56.5/47.8/37.5/48.9
PF11_0164	Peptidyl-prolyl cis-trans isomerase, cyclophilin▲	6/4/8/7	35.9/19.0/51.8/46.2
MAL8P1.17	Protein disulfide isomerase▲	17/21/25/25	37.1/42.4/50.7/49.9
PFL1425w	T-complex protein 1, gamma subunit, putative※	12/11/9/12	27.7/28.4/20.5/22.1
PFC0285c	T-complex protein beta subunit, putative※	5/16/4/12	15.2/29.1/13.3/21.4
Protein translation			
PF14_0486	Elongation factor 2※	38/37/39/33	45.3/41.7/47.4/34.6
PF13_0304	Elongation factor 1-alpha※	62/63/58/63	59.8/65.9/55.1/65.9
PFI0645w	Elongation factor 1-beta※	17/13/12/11	55.8/51.1/43.1/50
PF13_0214	Elongation factor 1-gamma, putative	11/13/14/14	18/24.6/23.8/20.9
PFL0625c	Eukaryotic translation initiation factor-3 subunit 10, putative	10/15/7/7	10.8/14.7/9.7/9.8
PF14_0104	Eukaryotic translation initiation factor 2 γ-subunit, putative	10/10/6/7	26.2/23.4/18.3/22.2
Glycolysis			
PFI0755c	6-phosphofructokinase※	17/13/41/40	19.9/15.3/31/32
PF10_0155	Enolase※	25/32/36/38	53.8/58.3/57.2/61.7
PF14_0425	Fructose-bisphosphate aldolase※	28/30/14/18	55.3/58.3/48.5/45.3
PF14_0598	Glyceraldehyde-3-phosphate dehydrogenase※	34/31/43/33	57.6/48.1/68/66.5
PF13_0141	L-lactate dehydrogenase	16/27/27/22	50.3/70.3/70.6/60.4
PFI1105w	Phosphoglycerate kinase	25/24/29/30	51/50.7/58.2/56
PF11_0208	Phosphoglycerate mutase, putative	8/14/16/20	35.6/48.8/56.8/57.2
PFF1300w	Pyruvate kinase※	27/22/26/38	39.5/41.9/39.3/58.1

PlasmoDB Accession No.	Descriptive name[1]	Peptides number[2]	Coverage %[3]
Ribosome complex			
PFE0810c	40S ribosomal protein S14, putative	10/12/11/13	52.3/70.9/68.9/52.3
PF11_0272	40S ribosomal protein S18, putative	12/8/11/13	51.3/38.5/46.2/46.2
PF14_0448	40S ribosomal protein S2, putative	16/12/10/12	50/29/31.6/32
PF10_0264	40S ribosomal protein S2B, putative	12/12/16/13	39.5/46/46/39.2
PF14_0627	40S ribosomal protein S3, putative※	13/14/12/15	42.5/44.8/40.7/40.7
PFC1020c	40S ribosomal protein S3A, putative	14/11/18/17	44.3/38.5/34.7/38.9
PF11_0065	40S ribosomal protein S4, putative	12/14/17/16	38.7/41.4/41/53.3
PF13_0228	40S ribosomal protein S6, putative※	20/13/17/19	37.9/27.8/32/40.5
PF14_0083	40S ribosomal protein S8e, putative	15/13/13/10	64.7/46.8/50.5/33.9
PFC0400w	60S acidic ribosomal protein P2, putative	23/17/12/13	75/65.2/65.2/75
PF14_0141	60S ribosomal protein L10, putative	13/13/9/10	32/32/31.5/31.5
PF10_0272	60S ribosomal protein L3, putative	13/19/15/19	26.9/33.9/30.1/33.4
PFE0350c	60S ribosomal protein L4, putative	23/19/23/18	33.6/32.4/37/33.1
PF14_0230	60S ribosomal protein L5, putative	12/13/10/9	35/38.1/38.4/34
PF13_0213	60S ribosomal protein L6-2, putative	8/11/11/12	41.6/42.1/41.2/48.4
PF11_0313	60S ribosomal protein P0※	20/24/21/26	52.8/70.9/63.9/57
PF11_0043	60S ribosomal protein P1, putative	22/13/21/19	69.5/72/69.5/69.5
Proteinases and *Plasmodium* surface protein			
PFI1475w	Merozoite surface protein 1	35/43/46/56	24.6/28.7/26.8/30.1
PF14_0075	Plasmepsin IV	17/13/19/15	37.6/35.4/38.1/33.2
MAL13P1.56	M1-family alanyl aminopeptidase	15/13/26/31	21.6/18.3/27/35.1
PF14_0078	Plasmepsin III, histo-aspartic protease	11/18/21/17	25.1/40.4/45.7/29.3
PF14_0077	Plasmepsin II	10/9/10/6	25.4/23.4/20.1/15.7

[1]The descriptive names of the proteins were annotated in the PlasmoDB.

[2,3]The number of peptides and the corresponding sequence coverage identified by the MS/MS analysis were given for each identified protein. Values from four independently conducted experiments were listed.

▲Proteins predicted to have endoplasmic reticulum retention sequences. Refer to the "Malaria Parasite Metabolic Pathways" (http://priweb.cc.huji.ac.il/malaria/)

※The proteins that have mammalian counterparts which were validated as PIPs or have been shown to be co-purified with eukaryotic 26S proteasomes (Wang *et al.,* 2008; Besche *et al.,* 2009; Bousquet-Dubouch *et al.,* 2009; Bousquet-Dubouch *et al.,* 2009; Scanlon *et al.,* 2009).

5. DISCUSSION

5.1 The *S*-nitrosoproteome of *P. falciparum*

In this thesis, we carried out the first comprehensive analysis of protein *S*-nitrosylation (SNO) induced by the NO donor GSNO in the human protozoan parasite *P. falciparum*. Based on a biotin-switch assay coupled to proteomic analysis, 319 potential protein targets and 37 sites for *S*-nitrosylation have been identified. The identified proteins give an initial insight into the *S*-nitrosoproteome of *P. falciparum*. It should be noted that although the *S*-nitrosylated proteins were identified in cell extracts of asexual intraerythrocytic *P. falciparum*, many proteins are expressed throughout the complete life cycle of the parasites, including the mosquito stages. Thus, the data may also contribute to the understanding of SNO in the mosquito stages, when the parasites encounter severe oxidative/nitrosative stresses (Luckhart *et al.,* 1998; Ascenzi *et al.,* 2002; Peterson *et al.,* 2007).

It is known that *S*-nitrosylated proteins are normally present in very low abundance in unstressed cells and are technically difficult to be directly detected and identified (Hess *et al.,* 2005). Therefore, the biotin-switch assay was invented to be the most commonly used method to study SNO**.** To increase sensitivity and facilitate sample handling, the assay typically requires cell extracts that are directly treated by NO donors (100 μM to 1 mM) or are extracted from the cells treated with NO donors (100 μM to 1 mM). Accordingly, in this study 100 μM GSNO was used to facilitate the detection and identification of SNO targets in the *P. falciparum* cell extracts. To our knowledge, the direct quantification of cellular RNS/GSNO levels is technically difficult, and the quantitative information of GSNO or RNS concentration that the malaria parasites are exposed to is so far unclear (Kalyanaraman *et al.,* 2012). However, Ostera G. and co-workers have detected RNS in both intraerythrocytic stages of the parasites and parasite gametocytes by using a specific fluorescent probe. Although no quantitative information of RNS was provided, they have observed that RNS are abundantly present around the food vacuole in the parasites, indicating that compartmentalized concentrations of intraparasitic RNS can probably be high (Ostera *et al.,* 2008). Besides, from the view of host-parasite interaction, malaria parasites are exposed to extracellular NO originating mainly from the NO synthase of host immune cells or mosquito vectors (Ferrari *et al.,* 2011; Marois 2011). It was determined that the NO concentration in the hemolymph of *Anopheles albimanus* infected with *P. berghei* (a rodent *Plasmodium* parasite) is about 17 μM, which is three times higher than that in uninfected mosquitoes (Herrera-Ortiz *et al.,* 2011). Another study reported that in CBA/Ca mice infected with *P. chabaudi* (another rodent *Plasmodium* parasite), the NO concentration in serum was 120 μM when a peak parasitemia appears (Legorreta-Herrera *et al.,* 2011). Furthermore, one study on malaria patients reported that the NO concentration in the plasma of patients infected with *P. falciparum* is about 7 μM (Lima-Junior *et al.,* 2012), whereas another study reported the NO concentration in patients' plasma to be about 60 μM (Nahrevanian *et al.,* 2006). These studies are indicative of the overall elevation of NO levels due to *Plasmodium* infection, suggesting that intraparasitic RNS/NO levels can dramatically increase when the parasites are directly exposed to an inflammatory level of ROS/RNS stress from the host immune response or near the parasitic origin where endogenous RNS are generated.

The identified plasmodial *S*-nitrosoproteome shares a similar pattern of composition with the

S-nitrosoproteomes from other organisms. In accordance with *S*-nitrosoproteomes of higher eukaryotic organisms [dbSNO, http://dbsno.mbc.nctu.edu.tw], the *P. falciparum S*-nitrosoproteome possesses many conserved proteins whose mammalian and plant counterparts have been reported as canonical *S*-nitrosylation targets. These proteins are mainly gene transcription and translation factors, protein chaperones, ribosome proteins, proteasome subunits, cytoskeletal and antioxidant proteins, and miscellaneous metabolic enzymes. The specificity of *S*-nitrosylation on these proteins is most likely due to the evolutionary conserved structure of these proteins in *P. falciparum* and higher eukaryotes, indicating that SNO may play similar regulatory roles in corresponding pathways.

5.2 Potential NO targets and affected pathways in *P. falciparum*

The identified *S*-nitrosylated proteins involved in diverse cellular processes and biological pathways provide a molecular basis for further studies on how NO exerts its action in *P. falciparum* and – at high concentrations – mediates parasite killing. For example, *S*-adenosylmethionine synthetase (SAMS), a key enzyme involved in methionine and polyamine metabolism, was identified to be *S*-nitrosylated at a cysteine residue conserved in both *P. falciparum* (Cys113, see Appendix Table 1) and rat (Cys121) (Chiang *et al.,* 1999; Perez-Mato *et al.,* 1999). It has been shown for rat SAMS that the acidic (Asp355) and basic (Arg357, Arg363) amino acids in the vicinity of Cys121 are critically involved in the deprotonation of the sulfur group of the cysteine and concertedly facilitate the GSNO-induced *S*-nitrosylation at Cys121 (Perez-Mato *et al.,* 1999; Hess *et al.,* 2005). Intriguingly, *P. falciparum* SAMS (PfSAMS) shares a sequence identity of 57% with rat SAMS and preserves the surrounding acidic/basic amino acids required for *S*-nitrosylation: Asp352, Arg354, and Gln360 (a conservative substitution of Arg363 in rat SAMS) (Chiang *et al.,* 1999). Thus, *S*-nitrosylation may occur at Cys113 of PfSAMS due to the coordination of surrounding acidic/basic amino acids in the same manner. More importantly, *S*-nitrosylation of Cys121 has been shown to markedly inactivate rat SAMS and result in a reduction of the *S*-adenosylmethionine (SAM) level in rat hepatocytes (Perez-Mato *et al.,* 1999). Regarding the similar metabolic function and the presence of the same *S*-nitrosylation site in PfSAMS compared to rat SAMS, it is reasonable to speculate that SNO may affect the SAM biosynthesis in *P. falciparum* by influencing PfSAMS activity. Because SAMS is a key precursor for polyamine biosynthesis, which is closely related to the proliferation of *P. falciparum* (Clark *et al.,* 2010), SNO on PfSAMS may correlate with the growth arrest of *Plasmodium* parasites caused by NO, which has been observed in several studies (Taylor-Robinson 1997; Balmer *et al.,* 2000). Of course, this hypothesis needs to be substantiated by further experiments.

Of particular interest, a series of essential proteases involved in the cascade of hemoglobin digestion were identified as potential SNO targets (Appendix Table 1). It is well known that hemoglobin digestion in the parasites' food vacuole is essential for *Plasmodium* parasites, providing a main source of amino acids during parasite growth (Goldberg 2005). Given that intraparasitic RNS are abundantly present around the food vacuole where many of these hemoglobinases reside (Ostera *et al.,* 2008), nitrosative stress-derived *S*-nitrosylation has a high likelihood of occurrence on these hemoglobinases. Indeed, the cysteine protease falcipain has been demonstrated to be substantially inactivated by 10 μM of NO donors due to *S*-nitrosylation of its active site

cysteine (Venturini *et al.,* 2000). The susceptibility of falcipain to NO has been linked to the growth inhibition of parasites under NO donor treatments (Venturini *et al.,* 2000; Nahrevanian 2006). Thus, it is likely that SNO influences hemoglobin digestion via modulating hemoglobinases, thereby being relevant to the inhibitory effects of NO on the proliferation of the parasites.

Glycolytic enzymes of *P. falciparum* appear to undergo multiple thiol-based redox regulations. We have shown previously that nine enzymes in the glycolysis pathway can be modified by GSH via *S*-glutathionylation *in vivo* (Kehr *et al.,* 2011). Moreover, PfPK, PfLDH, PfGAPDH, and PfHK (hexokinase) are regulated by the thioredoxin superfamily in *P. falciparum* (Sturm *et al.,* 2009). Strikingly, in this study we identified all eleven glycolytic enzymes of *P. falciparum* as potential SNO targets, suggesting that the glycolysis pathway is highly susceptible to redox modulation by NO. The importance of glycolysis to *P. falciparum* is highlighted by the fact that the uptake and consumption of glucose by parasitized erythrocytes is increased by a factor of ~100 compared to normal erythrocytes (Roth 1990). Additionally, because of the absence of a pyruvate dehydrogenase complex in mitochondria, *P. falciparum* becomes critically dependent upon glycolysis for energy production (Ralph 2005). Hence, perturbation of glycolysis may render detrimental effects on the proliferation of parasites as suggested before (van Schalkwyk *et al.,* 2008). We confirmed that four glycolytic enzymes, PfPK, PfLDH, PfPGM, and PfGAPDH were readily *S*-nitrosylated via protein immunoblotting analysis (**Figure 16A**). Furthermore, PfGAPDH was found to be significantly inhibited by *S*-nitrosylation at its conserved active site cysteine (Cys153) (**Figure 16B and C**). GAPDH is a central glycolytic enzyme responsible for the NAD^+-dependent phosphorylation of glyceraldehyde-3-phosphate to the product, 1,3-bisphosphoglycerate, a key step in the glycolytic pathway (Robien *et al.,* 2006). Thus, inhibition of PfGAPDH via SNO may indicate an inhibitory role of NO in the regulation of glycolysis in the parasite. Furthermore, it has been reported that reversible inactivation of GAPDH under oxidative stress may protect the enzyme from over-oxidation and re-route the metabolic flux from glycolysis to the pentose phosphate pathway (PPP), which is a critical process for generating reducing equivalents in the form of NADPH (Ralser *et al.,* 2007). Similarly, the reversible inactivation of PfGAPDH via *S*-nitrosylation is presumably also an early signaling event that redirects the carbohydrate flux to the PPP in order to generate more NADPH, which can be used to cope with oxidative and nitrosative stress in the parasites. For example, the plasmodial TrxR-Trx system may utilize NADPH to recover PfGAPDH activity via denitrosylation (**Figure 19**). In this way, *S*-nitrosylation of PfGAPDH may serve as a signaling switch to contribute to the parasitic tolerance to nitrosative stress.

5.3 Regulation of SNO in *P. falciparum*

Intracellular GSH, an abundant antioxidant tripeptide, detoxifies nitrosative stress by reacting with RNS (Broniowska *et al.,* 2013). This results in the formation of GSNO, which can be denitrosylated back to GSH by GSNOR as shown in higher eukaryotic cells (Benhar *et al.,* 2009). Although GSNOR seems to be conserved from bacteria to humans, a plasmodial homolog of GSNOR has not been identifiable in the genome of *P. falciparum* so far. The lack of GSNOR in the parasites may render RNS detoxification more dependent upon the thioredoxin system. Indeed, we have previously reported that PfTrx1 can efficiently reduce GSNO to GSH at a

biologically relevant rate (Kanzok *et al.,* 2000), suggesting that PfTrx1 might compensate for GSNOR to reduce GSNO *in vivo*. More importantly, we proved in this study that PfTrx1 functions as a general denitrosylase that can efficiently denitrosylate a large variety of proteins (**Figure 19A**), suggesting that PfTrx1 may protect proteins from NO stress. For example, the PfTrx1 system was demonstrated to be able to denitrosylate PfGAPDH and efficiently recover its glycolytic activity (**Figure 19B, C, and D**), indicating a role for the PfTrx1 system in protecting glycolysis from nitrosative stress. The active site cysteines were demonstrated to be responsible for the denitrosylating activity of PfTrx1, consistent with the denitrosylation mechanism of Trx in higher eukaryotic organisms (Wu *et al.,* 2011). Considering the fact that PfTrx1 is generally located in the parasites' cytosol and ubiquitously expressed in asexual and sexual stages of *P. falciparum* and also in parasite ookinetes (Kehr *et al.,* 2010; Turturice *et al.,* 2013), denitrosylation mediated by PfTrx1 may represent an important defense mechanism against nitrosative stress throughout the life cycle of *Plasmodium* parasites.

Whereas PfTrx1 mediates denitrosylation via active site cysteines, we demonstrate that PfTrx1 itself can be site-specifically *S*-nitrosylated at Cys43, which in turn mediates the transnitrosylating activity of PfTrx1 (**Figure 18 and Figure 20**). A number of proteins appear to be targets of transnitrosylation by PfTrx1. In contrast to denitrosylation, transnitrosylation by Trx has been reported to transduce NO stress and mediate NO signaling in cells (Wu *et al.,* 2011; Nakamura *et al.,* 2013). It is thus plausible that PfTrx1 plays dual roles in the regulation of SNO, which is closely associated with its site-specific response to NO stress. Based on these findings, we proposed a redox status-based model for PfTrx1 in protein denitrosylation and transnitrosylation (**Figure 29**): under normal conditions the reduced PfTrx1 is predominantly present in the parasites (Kanzok *et al.,* 2000; Krnajski *et al.,* 2001; Kanzok *et al.,* 2002). The model of denitrosylation by reduced PfTrx1 may represent a general mechanism by which reduced PfTrx1 protects the parasites from RNS/NO stress. This protective mechanism may explain, at least in part, the parasitic tolerance to nitrosative stress generated either endogenously or exogenously (Luckhart *et al.,* 1998; Ostera *et al.,* 2008); however, upon extreme NO stress or along with an increase in ROS/RNS stress together with a gradual loss of the recycling of reduced PfTrx1, PfTrx1 could be *S*-nitrosylated at the non-active-site cysteine (Cys43) to a significant extent, turning the overall role of PfTrx1 from denitrosylation to transnitrosylation for transducing NO stress/signaling. The transnitrosylation model of PfTrx1 is probably of more physiological relevance during parasite transmission between mosquito vectors and hosts, as the parasites are directly exposed to the host immune response in which inflammatory levels of NO are clearly involved (Ascenzi *et al.,* 2002; Ali *et al.,* 2010). For example, during the initial invasion of the mosquito midgut, the *Plasmodium* parasite ookinetes temporarily suffer NO stress generated by the mosquito NOS (Ali *et al.,* 2010). Although specific denitrosylation and transnitrosylation substrates of PfTrx1 are yet to be discovered, the model may give a first insight into possible regulatory potentials of PfTrx1 in the interplay of NO and the *Plasmodium* parasites within a specific redox milieu. It will be of great interest to identify and characterize denitrosylation and transnitrosylation substrates of PfTrx1 in *P. falciparum* in order to reveal specific pathways regulated by PfTrx1 upon nitrosative stress.

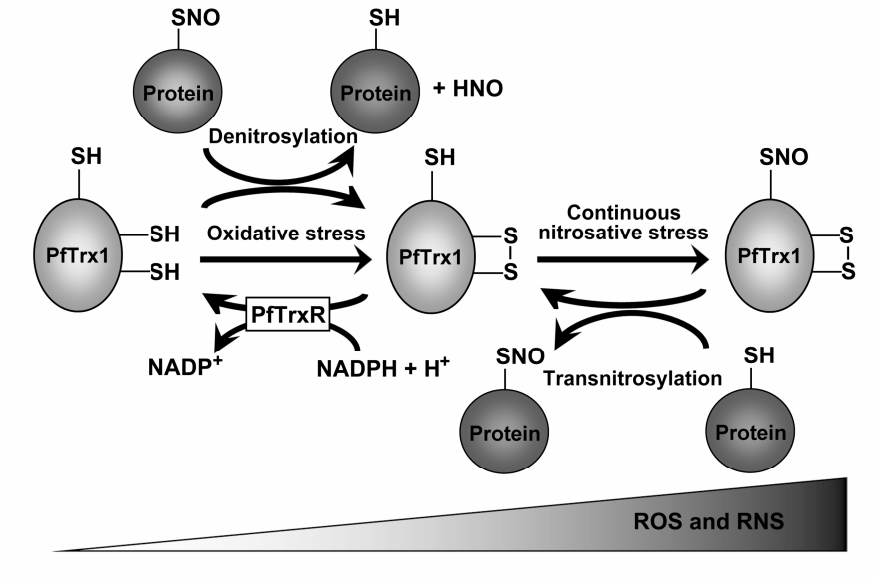

Figure 29. Proposed redox-based regulation of *S*-nitrosylation by PfTrx1. Upon mild to moderate nitrosative stress, the predominantly reduced PfTrx1 in cells mainly acts as a denitrosylase by catalyzing the denitrosylation of *S*-nitrosylated biomolecules via its active site cysteines. In this process, its active site cysteines are oxidized to a disulfide, which can be re-reduced by PfTrxR in the presence of NADPH. When parasite cells encounter severe and continuous oxidative/nitrosative stress (e.g. drug treatment) or local NO stress is severely enhanced (e.g. under NO burst generated from host iNOS), the reduction of oxidized PfTrx1 by PfTrxR can be compromised. Under these conditions, Cys43 of PfTrx1 can be *S*-nitrosylated to a significant extent and transnitrosylate other proteins, thus mediating NO stress. In addition to the processes shown in this scheme, *S*-nitrosylation of Cys43 in reduced PfTrx1 might also occur as well as transnitrosylation from *S*-nitrosylated proteins to PfTrx1. ROS, reactive oxygen species; RNS, reactive nitrogen species. (Wang *et al.,* 2013)

5.4 Mode of substrate recognition at the *P. falciparum* 26S proteasome

The recognition of the proteasomal substrates is a key component of the UPS and represents the initial signaling event that triggers downstream proteasomal functions. It has been well established in eukaryotes that the UPS employed three different classes of ubiquitin receptors for recognizing ubiquitinated substrates, including the intrinsic ubiquitin receptors harbored by the proteasome itself, the UBL-UBA shuttle factors that contain both ubiquitin-like (UBL) and ubiquitin-associated (UBA) domains, and the CDC48-based complexes, which are primarily involved in the endoplasmic reticulum-associated degradation (ERAD) pathway (Tomko *et al.,* 2013). In this study, we focused on the intrinsic ubiquitin receptors of the *P. falciparum* 26S proteasome, aiming to decipher the mechanistic context of the recognition of ubiquitin substrates by the plasmodial 26S proteasome. By taking advantage of current knowledge on eukaryotic ubiquitin receptors, we identified two PfUIM domains and a PfPru domain from the putative PfRpn10 and PfRpn13 subunits, respectively. All identified ubiquitin receptor domains were successfully cloned, heterologously overexpressed, and purified.

In an *in vitro* binding assay, the recombinant PfUIM domains were proved to bind UBL domains from putative PfRad23 and PfDsk2, which are plasmodial homologs of UBL-UBA shuttle factors. This result indicates that

both PfUIM domains may be involved in receiving proteasomal substrates carried by the UBL-UBA shuttle factors, for example, the PfRad23 and PfDsk2. However, only the PfUIM2 domain was found to be able to bind K48-linked polyubiquitin chains rather than mono-ubiquitin, whereas the PfUIM1 domain completely lacked the ubiquitin-binding capability under the same experimental conditions. Consistent with our results, three UIM domains have been found in *Arabidopsis* but only the N-terminal UIM1 domain of *Arabidopsis* is able to bind ubiquitin chains (Fu *et al.,* 1998; Fatimababy *et al.,* 2010).

Structural analyses of complexes of human UIMs with mono-ubiquitin or diubiquitin have revealed several structural determinants that affect their affinity. Although PfUIM1 preserves the key hydrophobic residues at the center of the ubiquitin-interacting surface, a strictly conserved N-terminal region of UIM1 (^{206}FGVDPS^{211} in human S5a) is missing from the PfUIM1 sequence (Zhang *et al.,* 2009). This region has been shown to be involved in the binding interface of S5a with diubiquitin. Lack of this region in PfUIM1 might be an explanation for its inability in binding ubiquitin chains. Of course, it cannot be ruled out that PfUIM1 has a weak ubiquitin-binding affinity that was not detected by the pull-down assay used in this study. Furthermore, both human UIMs (hUIM1 and hUIM2) have been reported to bind either mono-ubiquitin or polyubiquitin chains, with hUIM2 having a greater affinity over hUIM1 (Wang *et al.,* 2005). The higher binding affinity of hUIM2 could be attributed to an N-terminal region (P276-T282 in S5a) of hUIM2, which is important in forming a more compact and extensive binding interface with ubiquitin (Zhang *et al.,* 2009). Within this region, a key methionine residue (M281 in S5a) is involved in stabilizing the N-terminal patch of hUIM2 and its substitution by alanine dramatically reduces the polyubiquitin-binding ability of hUIM2 (Zhang *et al.,* 2009). Although no structural information of PfUIM2 was obtained, the sequence alignment of hUIM2 and PfUIM2 showed that PfUIM2 may also preserve such an N-terminal region in which the conserved methionine (M257 in PfRpn10) residue is located.

Another intriguing finding of this study is that, similar to PfUIM1, the PfPru domain was found to bind UBL domains of PfRad23 and PfDsk2 but not K48-linked polyubiquitin chains. In fact, the ubiquitin chain-binding properties of eukaryotic Pru domains vary significantly across species. Human Pru domain has been shown to strongly bind mono-ubiquitin and diubiquitin with dissociation constant (K_d) values of 300 nM and 90 nM, respectively (Husnjak *et al.,* 2008). However, the *S. cerevisiae* Pru domain (ScPru) has a markedly reduced affinity to mono-ubiquitin with a K_d value of 65 μM, and the *Arabidopsis* Pru domain has only a weak affinity to ubiquitin chains (Husnjak *et al.,* 2008; Fatimababy *et al.,* 2010). Although the PfPru domain is highly homologous to the human Pru domain, several key residues that are important for mammalian Pru domains for binding ubiquitin have been non-conservatively substituted in the PfPru domain. These conserved residues in the human Pru domain include Phe76, Asp78, and Phe98, which are replaced by Thr60, Lys61, and Asn81 in the PfPru domain, respectively (Schreiner *et al.,* 2008). It has been shown that individual mutations of these conserved residues in human Rpn13 drastically decreased the affinity of the human Pru domain to K48-linked polyubiquitin chains (Husnjak *et al.,* 2008; Schreiner *et al.,* 2008). Therefore, the inability of PfPru in binding ubiquitin chains might be attributed to the lack of several key residues that are essential for the Pru domain to bind ubiquitin.

Collectively, the current data clearly suggest divergent roles of the identified ubiquitin receptor domains in the recognition of ubiquitin substrates. Based on the binding affinity, a model of substrate recognition mediated by the ubiquitin receptors at the *P. falciparum* 26S proteasome was proposed (**Figure 30**). All identified ubiquitin receptor domains might be involved in receiving proteasomal substrates delivered by the UBL-UBA shuttle factors (mainly PfRad23 and PfDsk2). Considering the fact that the PfUIM2 domain appears to be highly conserved among *Plasmodium* species and has been shown to directly bind K-48 polyubiquitin chains, the PfUIM2 domain probably plays a major role in the direct recognition of polyubiquitinated substrates at the *P. falciparum* 26S proteasome.

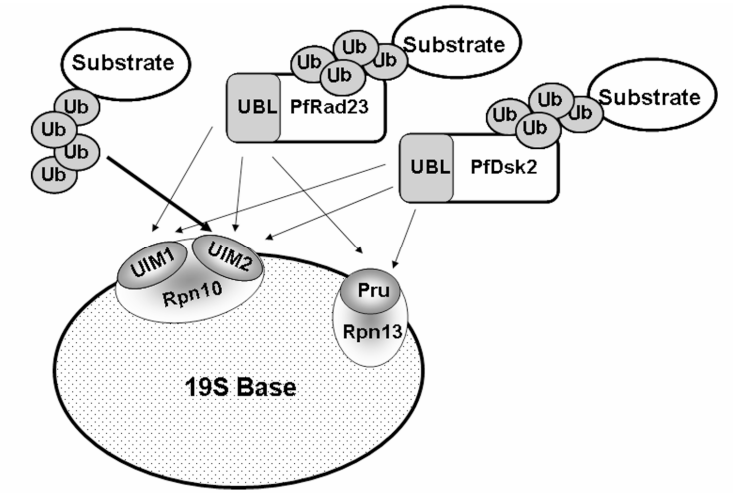

Figure 30. A proposed model of recognitions of polyubiquitinated substrates by the identified ubiquitin receptor domains in *P. falciparum*. The arrow heads indicate the possible recognition sites for polyubiquitin chains or UBL domains of substrate shuttle factors, the putative PfRad23 and PfDsk2. UBL: ubiquitin-like domain; Ub: ubiquitin; UIM: ubiquitin-interacting motif; Pru, pleckstrin-like receptor for ubiquitin.

5.5 The *P. falciparum* 26S proteasome complex

The notion of utilizing the binding affinity between UIM and UBL domains in the purification of 26S proteasomes have been approved by the purifications of mammalian 26S proteasomes from mouse muscle tissue and human embryonic kidney cells (Besche *et al.,* 2009; Scanlon *et al.,* 2009). Based on the affinity of PfUIM2 domain to the UBL domain of PfRad23, here we successfully adopted the affinity purification method to isolate the *P. falciparum* 26S proteasome complex from the parasite cell extracts. The use of PfUIM2 was due to the fact that it was shown to have the strongest affinity to both UBL domains and ubiquitin chains. To our knowledge, before this work there was no purification method available to purify the *P. falciparum* 26S proteasome. Li *et al.* reported that they have partially enriched the *P. falciparum* proteasome by using an anion exchange chromatography coupled to a size-exclusion chromatography (Li *et al.,* 2012). Another pull down assay using an anti-GFP (anti-green fluorescent protein) antibody has immunoprecipitated nearly 30 proteasomal components associated with the GFP-tagged Rpn6 subunit from the *P. falciparum* whole extracts

(Muralidharan *et al.,* 2011). However, such antibody-based purification methods require *in vivo* genetic modifications on a proteasomal subunit, which may have already perturbed the subunit associations (Wang *et al.,* 2007). In great contrast, our affinity-based purification method offers a simple and robust method to isolate the intact *P. falciparum* 26S complex together with many proteasome-interacting proteins. Additionally, *in vivo* formaldehyde cross-linking was included to stabilize the assembly of the whole 26S complex as well as weak and transient interactions of some interactors with the plasmodial proteasome. Indeed, the use of a cross-linking strategy significantly increased the peptide recovery of the plasmodial 20S subunits and the number of co-purified proteins, compared to our preliminary tests without cross-linking.

The established purification method has allowed us to take the first insight into the integral composition of the *P. falciparum* 26S proteasome complex. The MS/MS analysis of the purified proteasome samples has revealed all putative subunits of the *P. falciparum* 26S proteasome. It is acknowledged that high throughput liquid chromatography-MS/MS data frequently suffer from a lack of reproducibility and identify very low abundant proteins. However, most of the *P. falciparum* proteasomal subunits were reproducibly and abundantly identified from four independent purifications, suggesting that they are indeed proteasomal components and were selectively co-purified within a complex. Interestingly, in the MS/MS analysis the number of observed peptides and sequence coverage for the plasmodial Rpn13 subunit appeared to be typically low, indicating a low abundance of Rpn13 among the co-purified proteasomal subunits. Consistently, similar results have been reported in several affinity purifications of 26S proteasomes from other organisms (Besche *et al.,* 2009; Bousquet-Dubouch *et al.,* 2009; Scanlon *et al.,* 2009). These results are reminiscent of a recent finding that only one Rpn13 copy is present in a double-capped eukaryotic 26S proteasome, meaning a non-stoichiometric occupancy of Rpn13 in the majority of the 26S proteasome population (Berko *et al.,* 2014). This could be a reasonable explanation for the low abundance of Rpn13 observed in the purified proteasome samples. Therefore, our data not only support this notion but also highly suggest a similar asymmetric integrity in the *P. falciparum* 26S proteasome. Besides, a plasmodial homolog of a proteasomal activator PA28 (in human PSMD10) was reproducibly identified, indicating its association with the plasmodial proteasome. In eukaryotes, three isoforms of PA28 subunits have been found. They form a heteroheptamer or hexamer complex that can attach to either one or both outer α-rings of the 20S CP, thus activating the peptidolytic activities of the 20S CP (Jung *et al.,* 2013; Tomko *et al.,* 2013). Besides, hybrid proteasomes with one 19S RP and one PA28 complex at opposite ends of the 20S CP (19S-20S-PA28) have also been identified (Hendil *et al.,* 1998; Tanahashi *et al.,* 2000). Accordingly, PA28 has been observed to be co-purified in other affinity-based purifications of eukaryotic proteasomes (Besche *et al.,* 2009; Scanlon *et al.,* 2009). Although the role of the PA28 complex has not been studied in *P. falciparum*, the identification of plasmodial PA28 subunits suggests that 19S-20S-PA28 proteasomes may exist in the parasites and that their role in the plasmodial 20S CP activation might be also conserved.

Three major peptidolytic activities of eukaryotic proteasomes have been detected in the purified proteasome samples, indicating that our purification method is able to isolate plasmodial proteasomes in an active form. When compared to the reported values of proteasomal activities, the activities of the purified plasmodial

proteasome determined in the eluted fractions was generally lower, although the measured chymotrypsin-like activity was comparable to the one of 26S proteasomes purified from human erythrocytes (a product of Enzo Life Science, PW8720). However, it should be mentioned that the reported values of eukaryotic proteasomal activities vary significantly depending on the purification method and the assay components. Due to the existence of different forms of proteasomes in eukaryotes (*e.g.* free 20S proteasomes, single or double-capped 26S proteasomes and hybrid proteasomes) and the inherently labile association between the 20S and the 19S subcomplexes (Tomko *et al.,* 2013), different purification methods may result in a distinct composition of the isolated proteasomes. For example, conventional purifications of 20S proteasomes using multi-centrifugal procedures or affinity purifications via targeting the 20S subunits usually obtained a higher percentage of 20S proteasomes, which results in that the apparent proteasomal activities appear to be generally higher (Bousquet-Dubouch *et al.,* 2009). In comparison, affinity purifications of 26S proteasomes via targeting to the 19S subunits may result in a certain extent of loss of the 20S due to the reasons that a certain amount of 20S may not associate with the 19S or they dissociate from the 19S during the purification procedure. Furthermore, it has been shown that affinity purifications of eukaryotic 26S proteasomes usually co-purify a number of additional proteins (Besche *et al.,* 2009; Scanlon *et al.,* 2009; Tai *et al.,* 2010), which will be taken into account when calculating the proteasomal activities in the elution fractions. Besides the factor of purification method, different assay components appear to significantly influence proteasomal activities. For example, in some studies the proteasomal activities were measured within a buffer containing a proteasome-activating agent (SDS), which we did not use in our assays (Shibatani *et al.,* 1995; Scanlon *et al.,* 2009). Therefore, low proteasomal activities observed in the purified plasmodial proteasome samples may be due to the aforementioned factors, or even due to the origin itself.

5.6 Putative proteasome-interacting proteins (PIPs) in *P. falciparum*

Apart from proteasomal components, the affinity purification method has concomitantly purified a number of plasmodial proteins, which could be candidates of PIPs for the *P. falciparum* 26S proteasome. Supporting this, the most abundantly identified proteins have predicted roles either in the UPS or related to protein metabolism processes. In addition, supportive evidence could be seen in purifications of eukaryotic proteasomes from other organisms, in which a large portion of the co-purified plasmodial proteins have counterparts that have been validated as PIPs or found to be co-purified with eukaryotic proteasomes. However, it is possible that some proteins were co-purified not via binding to the plasmodial proteasome but via binding to the UBL domain of PfRad23 and eluted together with the proteasome. Another possibility is that some co-purified proteins are ubiquitinated substrates that were captured when they transiently bound to the proteasome for degradation. However, ubiquitinated substrates are unlikely to contribute to the majority of the co-purified proteins, because they are supposed to be removed by the excess eluting protein, the PfUIM2 domain which has been proved to bind polyubiquitin chains efficiently. Of course, it cannot be ruled out that some ubiquitinated substrates that were not completely trapped by PfUIM2 were left and identified.

5.6.1 Putative PIPs in the plasmodial UPS system

We noticed that several proteins belonging to the plasmodial UPS components were co-purified. This is in consistent with the results of other affinity purifications of eukaryotic proteasomes that UPS components are usually purified with the proteasome (Besche *et al.,* 2009; Scanlon *et al.,* 2009). Notably, the PfRad23 and PfDsk2 were identified, suggesting their interactions with the plasmodial proteasome and supporting the role of PfRad23 and PfDsk2 in transporting proteasomal substrates to the proteasome (**Figure 30**). Of greater significance, the affinity purification method has reproducibly co-purified two plasmodial deubiquitinases (DUBs), a deubiquinating/deneddylating enzyme, known as PfUCH54 (PFE1355c), and a putative ubiquitin carboxyl-terminal hydrolase (PF11_0177). The PfUCH54 has been characterized to be the plasmodial homolog of human Uch37, which is a validated proteasome-bound deubiquitinase (see Introduction) (Artavanis-Tsakonas *et al.,* 2006). Structural analysis has revealed that Uch37 utilizes its C-terminal region to bind to a Uch37-binding motif at the C-terminus of Rpn13, therefore being associated with the 19S complex to perform its ubiquitin-trimming functions (Yao *et al.,* 2006). Consistently, PfUCH54 was reported to preserve a C-terminus homologous to the one of Uch37 (Artavanis-Tsakonas *et al.,* 2006). Furthermore, a putative C-terminal Uch37-binding motif could also be recognized in PfRpn13 based on sequence homology analysis (data not shown). Thus, it is most likely that the PfUCH54 associates with the plasmodial proteasome via binding to PfRpn13. Similar to the case of PfRpn13, a low abundance of the identified PfUCH54 was observed in the purified proteasome samples, which might be a supportive indication of the association between PfUCH54 and PfRpn13. Interestingly, different from its mammalian counterparts, PfUCH54 has been found to additionally have a deneddylating activity (Artavanis-Tsakonas *et al.,* 2006). As there is limited information about the neddylation in the proteasomal degradation (Rabut *et al.,* 2008), the significance of the deneddylating activity of PfUCH54 at the plasmodial proteasome remains unclear and is worth being further investigated.

In contrast to PfUCH54, another putative ubiquitin carboxyl-terminal hydrolase with a predicted molecular weight of 70.7 kDa was among the most abundant co-purified proteins, strongly indicating its association with the plasmodial proteasome. Homology analysis of this protein strongly suggests that it is a plasmodial homolog of an important deubiquitinase known as Ubp6 in yeast or USP14 in human (unpublished work), and especially it has a putative N-terminal UBL domain, which is a key structural feature shared by Ubp6/USP14 homologs (Hu *et al.,* 2005). Mechanistic studies have revealed that Upb6/USP14 docks at the 19S via its UBL domain, which in turn activates its ubiquitin-trimming activities (Hu *et al.,* 2005). Thus, the co-purification of the plasmodial counterpart of Ubp6/USP14 highly suggests this uncharacterized protein is a proteasome-bound deubiquitinase in *P. falciparum*.

Importantly, human Uch37 and USP14 can be specifically targeted by small-molecular-weight inhibitors (Lee *et al.,* 2010; D'Arcy *et al.,* 2011). It has been shown that the inhibition of these proteasome-bound DUBs can significantly affect proteasomal functions and may have promising therapeutic implications in cancer and neurodegenerative diseases (Hanna *et al.,* 2006; Lee *et al.,* 2010; D'Arcy *et al.,* 2011). Consistently, in our preliminary tests, human Uch37/USP14 inhibitors have been shown to have potent antimalarial activities against intraerythrocytic stages of *P. falciparum* (data not shown). Further biochemical characterizations of these

plasmodial DUBs would be of great interest for developing *Plasmodium*-specific inhibitors, aiming to offer novel antimalarial strategies.

5.6.2 Other putative PIPs

Many co-purified plasmodial proteins with the plasmodial proteasome are not directly involved in the UPS pathway. Among the identified proteins are a number of abundant cellular proteins, such as heat shock proteins (HSPs), elongation factors, glycolytic enzymes, and ribosomal proteins. Due to the large quantity of these proteins present in cells, it is difficult to completely prevent their nonspecific purification. However, it should be emphasized that these proteins were significantly enriched in the GST-UBL-based affinity purifications but not in the GST-based mock purification, indicating they were selectively isolated via certain interactions either with the plasmodial proteasome or directly with the UBL domain of PfRad23. In good agreement with our results, affinity purifications of eukaryotic proteasomes from other organisms have co-isolated many homologs of the plasmodial proteins identified in our study (Wang *et al.,* 2008; Besche *et al.,* 2009; Bousquet-Dubouch *et al.,* 2009; Besche *et al.,* 2012). Although the proteasomal network has hardly been explored in *P. falciparum*, knowledge on PIPs identified in higher eukaryotic organisms could help when interpreting the co-isolation of some plasmodial proteins with the plasmodial 26S proteasome.

To date, extensive studies have shown that protein chaperones play important roles in modulating proteasomal functions. Several HSP70 members have been reported to be associated with the yeast 26S proteasome (Guerrero *et al.,* 2006; Wang *et al.,* 2008). Furthermore, in higher eukaryotes it has been shown that HSP70 members can facilitate the delivery of aggregation-prone substrates for proteasomal degradation by interacting with the 26S proteasome via adaptor proteins (Luders *et al.,* 2000; Wiederkehr *et al.,* 2002). Furthermore, HSP90 family members have been suggested to play roles in the proteasomal structural integrity and assembly through their interactions with eukaryotic 26S proteasomes (Imai *et al.,* 2003). The identification of plasmodial HSP70/90 members as abundant co-purified proteins suggests that the identified plasmodial HSPs may preserve such roles in *Plasmodium*. Besides heat shock proteins, two subunits of plasmodial T-complex protein 1 (TCP-1) were identified. In eukaryotes the TCP-1 complex is known as a heterooligomeric molecular chaperone that assists in folding some cytosolic proteins such as actin and tubulin (Valpuesta *et al.,* 2002). In accordance with our results, co-purification of TCP-1 subunits in affinity purifications of human 26S proteasomes has been reported (Wang *et al.,* 2008). Additionally, a study based on a comparative proteome analysis has confirmed a direct interaction of the TCP-1 complex with the 26S proteasome of goldfish (Horiguchi *et al.,* 2006).

Importantly, the plasmodial homolog of cell division cycle protein 48 (CDC48) was identified to be abundantly co-purified with the plasmodial 26S proteasome. It is well acknowledged that in eukaryotes the 26S proteasome has an important application in degrading aberrant and misfolded proteins from the ERAD pathway, in which CDC48 is a major player (Wolf *et al.,* 2012). It is generally thought that CDC48 forms complexes with several cooperators to extract and shuttle aberrant proteins from the ER to the 26S proteasome for degradation, thus linking ERAD and UPS pathways (Wolf *et al.,* 2012). In this regard, CDC48 has been known as a validated PIP and indeed has been abundantly co-purified in several affinity-based purifications of eukaryotic proteasomes

(Besche *et al.,* 2009; Scanlon *et al.,* 2009). Recently, it was found that eukaryotic CDC48 directly binds to the 20S in the place of 19S to form a CDC48-20S complex (Barthelme *et al.,* 2013). It is thus likely that hybrid CDC48-20S-19S proteasomes may exist and can be co-isolated with 26S proteasomes. Furthermore, direct association of CDC48 with the 60S ribosome has been reported to play a role in extracting aberrant nascent polypeptides for proteasomal degradation (Defenouillere *et al.,* 2013). Thus, it is also possible that the identification of plasmodial CDC48 was partially due to its association with plasmodial 60S ribosomal subunits, which were also abundantly co-purified.

In addition to CDC48, a number of co-purified proteins with predicted ER-retention sequences have been identified. Most of them have validated or predicted functions in protein folding and quality control. A human counterpart of the identified plasmodial α-chain subunit of nascent polypeptide associated complex has been reported to be a putative PIP (Bousquet-Dubouch *et al.,* 2009). Together with our results, the findings have a strong indication that proteasomal functions are tightly correlated with protein folding and quality control at the ER in eukaryotes, including *P. falciparum*. Similarly, plasmodial elongation factors were found to be among the most abundantly co-purified proteins. This agrees well with several reports that eukaryotic elongation factors can interact with both ubiquitinated substrates and the proteasome, therefore mediating the proteasomal degradation of co-translationally damaged proteins (Gonen *et al.,* 1996; Schmidt *et al.,* 2005). Based on our results, we speculate on a similar role for the co-purified plasmodial elongation factors in linking the pathways of protein synthesis and degradation in *P. falciparum.*

Some *Plasmodium*-specific proteins were co-purified, including merozoite surface protein 1 (MSP1) and several plasmepsins. Although they have been largely enriched in the GST-UBL-based purifications, there is currently no clue indicating their associations with the proteasome complex. As these plasmodial proteins were predicted to be potential ubiquitinylation targets and the *in vivo* polyubiquitination of plasmepsin II has been detected in *P. falciparum*, it is possible that these proteins may be proteasomal substrates that were trapped during the purification process (Ponts *et al.,* 2011).

In conclusion, in this work we successfully isolated, for the first time, the *P. falciparum* 26S proteasome together with a number of putative PIPs via a novel affinity-based purification method. The established method has been proved to be a simple and efficient tool that can be applied in further investigations on the structure and function of the *P. falciparum* 26S proteasome. More importantly, the co-purified putative PIPs may shed light on a profound network orchestrated by the plasmodial proteasome in malaria parasites. Further validations of the putative PIPs and investigations on their essentiality in the parasite growth would have great significance for providing novel antimalarial agents targeting the plasmodial UPS or related pathways.

6. REFERENCES

Adams, J. (2004). The proteasome: a suitable antineoplastic target. *Nat Rev Cancer* **4**: 349-360.

Akerman, S. E. and S. Muller (2003). 2-Cys peroxiredoxin PfTrx-Px1 is involved in the antioxidant defence of Plasmodium falciparum. *Mol Biochem Parasitol* **130**: 75-81.

Akman-Anderson, L., M. Olivier *et al.* (2007). Induction of nitric oxide synthase and activation of signaling proteins in Anopheles mosquitoes by the malaria pigment, hemozoin. *Infect Immun* **75**: 4012-4019.

Alderton, W. K., C. E. Cooper *et al.* (2001). Nitric oxide synthases: structure, function and inhibition. *Biochem J* **357**: 593-615.

Ali, M., E. M. Al-Olayan *et al.* (2010). Naturally occurring triggers that induce apoptosis-like programmed cell death in Plasmodium berghei ookinetes. *PLoS One* **5**.

Amerik, A. Y., S. J. Li *et al.* (2000). Analysis of the deubiquitinating enzymes of the yeast Saccharomyces cerevisiae. *Biol Chem* **381**: 981-992.

Aminake, M., H. D. Arndt *et al.* (2012). The proteasome of malaria parasites: A multi-stage drug target for chemotherapeutic intervention? *International Journal for Parasitology: Drugs and Drug Resistance* **2**: 1-10.

Aminake, M. N., S. Schoof *et al.* (2011). Thiostrepton and derivatives exhibit antimalarial and gametocytocidal activity by dually targeting parasite proteasome and apicoplast. *Antimicrob Agents Chemother* **55**: 1338-1348.

Anand, P. and J. S. Stamler (2012). Enzymatic mechanisms regulating protein S-nitrosylation: implications in health and disease. *J Mol Med (Berl)* **90**: 233-244.

Angeles, A., G. Fung *et al.* (2012). Immune and non-immune functions of the immunoproteasome. *Front Biosci (Landmark Ed)* **17**: 1904-1916.

Artavanis-Tsakonas, K., S. Misaghi *et al.* (2006). Identification by functional proteomics of a deubiquitinating/deNeddylating enzyme in Plasmodium falciparum. *Mol Microbiol* **61**: 1187-1195.

Artavanis-Tsakonas, K., W. A. Weihofen *et al.* (2010). Characterization and structural studies of the Plasmodium falciparum ubiquitin and Nedd8 hydrolase UCHL3. *J Biol Chem* **285**: 6857-6866.

Ascenzi, P. and L. Gradoni (2002). Nitric oxide limits parasite development in vectors and in invertebrate intermediate hosts. *IUBMB Life* **53**: 121-123.

Astier, J., A. Kulik *et al.* (2012). Protein S-nitrosylation: what's going on in plants? *Free Radic Biol Med* **53**: 1101-1110.

Atamna, H. and H. Ginsburg (1993). Origin of reactive oxygen species in erythrocytes infected with Plasmodium falciparum. *Mol Biochem Parasitol* **61**: 231-241.

Atamna, H. and H. Ginsburg (1995). Heme degradation in the presence of glutathione. A proposed mechanism to account for the high levels of non-heme iron found in the membranes of hemoglobinopathic red blood cells. *J Biol Chem* **270**: 24876-24883.

Balmer, P., H. M. Phillips *et al.* (2000). The effect of nitric oxide on the growth of Plasmodium falciparum, P. chabaudi and P. berghei in vitro. *Parasite Immunol* **22**: 97-106.

Barglow, K. T., C. G. Knutson *et al.* (2011). Site-specific and redox-controlled S-nitrosation of thioredoxin. *Proc Natl Acad Sci U S A* **108**: E600-606.

Barthelme, D. and R. T. Sauer (2013). Bipartite determinants mediate an evolutionarily conserved interaction between Cdc48 and the 20S peptidase. *Proc Natl Acad Sci U S A* **110**: 3327-3332.

Becker, K., S. M. Kanzok *et al.* (2003). Plasmoredoxin, a novel redox-active protein unique for malarial parasites. *Eur J Biochem* **270**: 1057-1064.

Becker, K., S. Rahlfs *et al.* (2003). Glutathione--functions and metabolism in the malarial parasite Plasmodium falciparum. *Biol Chem* **384**: 551-566.

Becker, K., L. Tilley *et al.* (2004). Oxidative stress in malaria parasite-infected erythrocytes: host-parasite interactions. *Int J Parasitol* **34**: 163-189.

Beckwith, R., E. Estrin *et al.* (2013). Reconstitution of the 26S proteasome reveals functional asymmetries in its AAA+ unfoldase. *Nat Struct Mol Biol* **20**: 1164-1172.

Benhar, M., M. T. Forrester *et al.* (2008). Regulated protein denitrosylation by cytosolic and mitochondrial thioredoxins. *Science* **320**: 1050-1054.

Benhar, M., M. T. Forrester *et al.* (2009). Protein denitrosylation: enzymatic mechanisms and cellular functions. *Nat Rev Mol Cell Biol* **10**: 721-732.

Berko, D., O. Herkon *et al.* (2014). Inherent asymmetry in the 26S proteasome is defined by the ubiquitin receptor Rpn13. *J Biol Chem*.

Besche, H. C. and A. L. Goldberg (2012). Affinity purification of mammalian 26S proteasomes using an ubiquitin-like domain. *Methods Mol Biol* **832**: 423-432.

Besche, H. C., W. Haas *et al.* (2009). Isolation of mammalian 26S proteasomes and p97/VCP complexes using the ubiquitin-like domain from HHR23B reveals novel proteasome-associated proteins. *Biochemistry* **48**: 2538-2549.

Bogdan, C. (2001). Nitric oxide and the immune response. *Nat Immunol* **2**: 907-916.

Borissenko, L. and M. Groll (2007). 20S proteasome and its inhibitors: crystallographic knowledge for drug development. *Chem Rev* **107**: 687-717.

Bousquet-Dubouch, M. P., E. Baudelet *et al.* (2009). Affinity purification strategy to capture human endogenous proteasome complexes diversity and to identify proteasome-interacting proteins. *Mol Cell Proteomics* **8**: 1150-1164.

Bousquet-Dubouch, M. P., S. Nguen *et al.* (2009). Chronic ethanol feeding affects proteasome-interacting proteins. *Proteomics* **9**: 3609-3622.

Bradford, M. M. (1976). A rapid and sensitive method for the quantitation of microgram quantities of protein utilizing the principle of protein-dye binding. *Anal Biochem* **72**: 248-254.

Broniowska, K. A., A. R. Diers *et al.* (2013). S-nitrosoglutathione. *Biochim Biophys Acta* **1830**: 3173-3181.

Buchholz, K., E. D. Putrianti *et al.* (2010). Molecular genetics evidence for the in vivo roles of the two major NADPH-dependent disulfide reductases in the malaria parasite. *J Biol Chem* **285**: 37388-37395.

Carney, C. K., A. C. Schrimpe *et al.* (2006). The basis of the immunomodulatory activity of malaria pigment (hemozoin). *J Biol Inorg Chem* **11**: 917-929.

Chernin, E. (1988). Sir Ronald Ross, malaria, and the rewards of research. *Med Hist* **32**: 119-141.

Chiang, P. K., M. E. Chamberlin *et al.* (1999). Molecular characterization of Plasmodium falciparum S-adenosylmethionine synthetase. *Biochem J* **344 Pt 2**: 571-576.

Chung, D. W. and K. G. Le Roch (2010). Targeting the Plasmodium ubiquitin/proteasome system with anti-malarial compounds: promises for the future. *Infect Disord Drug Targets* **10**: 158-164.

Chung, D. W., N. Ponts *et al.* (2012). Characterization of the ubiquitylating components of the human malaria parasite's protein degradation pathway. *PLoS One* **7**: e43477.

Clark, K., J. Niemand *et al.* (2010). Functional consequences of perturbing polyamine metabolism in the malaria parasite, Plasmodium falciparum. *Amino Acids* **38**: 633-644.

Cociorva, D., L. T. D *et al.* (2007). Validation of tandem mass spectrometry database search results using DTASelect. *Curr Protoc Bioinformatics* **Chapter 13**: Unit 13 14.

Coffino, P. (2001). Antizyme, a mediator of ubiquitin-independent proteasomal degradation. *Biochimie* **83**:

319-323.

Coux, O., K. Tanaka *et al.* (1996). Structure and functions of the 20S and 26S proteasomes. *Annu Rev Biochem* **65**: 801-847.

Czesny, B., S. Goshu *et al.* (2009). The proteasome inhibitor epoxomicin has potent Plasmodium falciparum gametocytocidal activity. *Antimicrob Agents Chemother* **53**: 4080-4085.

D'Arcy, P., S. Brnjic *et al.* (2011). Inhibition of proteasome deubiquitinating activity as a new cancer therapy. *Nat Med* **17**: 1636-1640.

Dalle-Donne, I., R. Rossi *et al.* (2007). S-glutathionylation in protein redox regulation. *Free Radic Biol Med* **43**: 883-898.

Dange, T., D. Smith *et al.* (2011). Blm10 protein promotes proteasomal substrate turnover by an active gating mechanism. *J Biol Chem* **286**: 42830-42839.

Defenouillere, Q., Y. Yao *et al.* (2013). Cdc48-associated complex bound to 60S particles is required for the clearance of aberrant translation products. *Proc Natl Acad Sci U S A* **110**: 5046-5051.

Deharo, E., D. Barkan *et al.* (2003). Potentiation of the antimalarial action of chloroquine in rodent malaria by drugs known to reduce cellular glutathione levels. *Biochem Pharmacol* **66**: 809-817.

Dick, T. P., A. K. Nussbaum *et al.* (1998). Contribution of proteasomal beta-subunits to the cleavage of peptide substrates analyzed with yeast mutants. *J Biol Chem* **273**: 25637-25646.

Doulias, P. T., J. L. Greene *et al.* (2010). Structural profiling of endogenous S-nitrosocysteine residues reveals unique features that accommodate diverse mechanisms for protein S-nitrosylation. *Proc Natl Acad Sci U S A* **107**: 16958-16963.

Ehlinger, A. and K. J. Walters (2013). Structural Insights into Proteasome Activation by the 19S Regulatory Particle. *Biochemistry* **52**: 3618-3628.

Elsasser, S. and D. Finley (2005). Delivery of ubiquitinated substrates to protein-unfolding machines. *Nat Cell Biol* **7**: 742-749.

Elsasser, S., R. R. Gali *et al.* (2002). Proteasome subunit Rpn1 binds ubiquitin-like protein domains. *Nat Cell Biol* **4**: 725-730.

Enayati, A. and J. Hemingway (2010). Malaria management: past, present, and future. *Annu Rev Entomol* **55**: 569-591.

Eng, J. K., A. L. McCormack *et al.* (1994). An approach to correlate tandem mass spectral data of peptides with amino acid sequences in a protein database. *J AM SOC MASS SPECTR* **5**: 976-989.

Fang, F. C. (2004). Antimicrobial reactive oxygen and nitrogen species: concepts and controversies. *Nat Rev Microbiol* **2**: 820-832.

Fatimababy, A. S., Y. L. Lin *et al.* (2010). Cross-species divergence of the major recognition pathways of ubiquitylated substrates for ubiquitin/26S proteasome-mediated proteolysis. *FEBS J* **277**: 796-816.

Ferrari, C. K., P. C. Souto *et al.* (2011). Oxidative and nitrosative stress on phagocytes' function: from effective defense to immunity evasion mechanisms. *Arch Immunol Ther Exp (Warsz)* **59**: 441-448.

Finley, D., H. D. Ulrich *et al.* (2012). The ubiquitin-proteasome system of Saccharomyces cerevisiae. *Genetics* **192**: 319-360.

Fisher, R. D., B. Wang *et al.* (2003). Structure and ubiquitin binding of the ubiquitin-interacting motif. *J Biol Chem* **278**: 28976-28984.

Forrester, M. T., M. W. Foster *et al.* (2009). Detection of protein S-nitrosylation with the biotin-switch technique. *Free Radic Biol Med* **46**: 119-126.

Frey, P. A. (1997). Radicals in enzymatic reactions. *Curr Opin Chem Biol* **1**: 347-356.

Fritz-Wolf, K., E. Jortzik *et al.* (2013). Crystal structure of the plasmodium falciparum thioredoxin

reductase-thioredoxin complex. *J Mol Biol* **425**: 3446-3460.

Fu, H., S. Sadis *et al.* (1998). Multiubiquitin chain binding and protein degradation are mediated by distinct domains within the 26 S proteasome subunit Mcb1. *J Biol Chem* **273**: 1970-1981.

Fujiwara, K., T. Tenno *et al.* (2004). Structure of the ubiquitin-interacting motif of S5a bound to the ubiquitin-like domain of HR23B. *J Biol Chem* **279**: 4760-4767.

Gantt, S. M., J. M. Myung *et al.* (1998). Proteasome inhibitors block development of Plasmodium spp. *Antimicrob Agents Chemother* **42**: 2731-2738.

Gardner, P. R., A. M. Gardner *et al.* (2004). Dioxygen-dependent metabolism of nitric oxide. *Methods Mol Biol* **279**: 133-150.

Giustarini, D., R. Rossi *et al.* (2004). S-glutathionylation: from redox regulation of protein functions to human diseases. *J Cell Mol Med* **8**: 201-212.

Glickman, M. H. and A. Ciechanover (2002). The ubiquitin-proteasome proteolytic pathway: destruction for the sake of construction. *Physiol Rev* **82**: 373-428.

Godderz, D., E. Schafer *et al.* (2011). The N-terminal unstructured domain of yeast ODC functions as a transplantable and replaceable ubiquitin-independent degron. *J Mol Biol* **407**: 354-367.

Goldberg, D. E. (2005). Hemoglobin degradation. *Curr Top Microbiol Immunol* **295**: 275-291.

Goldstein, G., M. Scheid *et al.* (1975). Isolation of a polypeptide that has lymphocyte-differentiating properties and is probably represented universally in living cells. *Proc Natl Acad Sci U S A* **72**: 11-15.

Gonen, H., D. Dickman *et al.* (1996). Protein synthesis elongation factor EF-1 alpha is an isopeptidase essential for ubiquitin-dependent degradation of certain proteolytic substrates. *Adv Exp Med Biol* **389**: 209-219.

Green, S. J., L. F. Scheller *et al.* (1994). Nitric oxide: cytokine-regulation of nitric oxide in host resistance to intracellular pathogens. *Immunol Lett* **43**: 87-94.

Griffith, O. W. and D. J. Stuehr (1995). Nitric oxide synthases: properties and catalytic mechanism. *Annu Rev Physiol* **57**: 707-736.

Gross, S. S. and M. S. Wolin (1995). Nitric oxide: pathophysiological mechanisms. *Annu Rev Physiol* **57**: 737-769.

Guerrero, C., C. Tagwerker *et al.* (2006). An integrated mass spectrometry-based proteomic approach: quantitative analysis of tandem affinity-purified in vivo cross-linked protein complexes (QTAX) to decipher the 26 S proteasome-interacting network. *Mol Cell Proteomics* **5**: 366-378.

Guillemin, J. (2002). Choosing scientific patrimony: Sir Ronald Ross, Alphonse Laveran, and the mosquito-vector hypothesis for malaria. *J Hist Med Allied Sci* **57**: 385-409.

Gyan, B., M. Troye-Blomberg *et al.* (1994). Human monocytes cultured with and without interferon-gamma inhibit Plasmodium falciparum parasite growth in vitro via secretion of reactive nitrogen intermediates. *Parasite Immunol* **16**: 371-375.

Hafalla, J. C., O. Silvie *et al.* (2011). Cell biology and immunology of malaria. *Immunol Rev* **240**: 297-316.

Han, P. and C. Chen (2008). Detergent-free biotin switch combined with liquid chromatography/tandem mass spectrometry in the analysis of S-nitrosylated proteins. *Rapid Commun Mass Spectrom* **22**: 1137-1145.

Hanna, J., N. A. Hathaway *et al.* (2006). Deubiquitinating enzyme Ubp6 functions noncatalytically to delay proteasomal degradation. *Cell* **127**: 99-111.

Haorah, J., D. Heilman *et al.* (2004). Alcohol and HIV decrease proteasome and immunoproteasome function in macrophages: implications for impaired immune function during disease. *Cell Immunol* **229**: 139-148.

Hara, M. R., N. Agrawal *et al.* (2005). S-nitrosylated GAPDH initiates apoptotic cell death by nuclear translocation following Siah1 binding. *Nat Cell Biol* **7**: 665-674.

Harwaldt, P., S. Rahlfs *et al.* (2002). Glutathione S-transferase of the malarial parasite Plasmodium falciparum:

characterization of a potential drug target. *Biol Chem* **383**: 821-830.

Hay, S. I., C. A. Guerra *et al.* (2004). The global distribution and population at risk of malaria: past, present, and future. *Lancet Infect Dis* **4**: 327-336.

Helms, C. and D. B. Kim-Shapiro (2013). Hemoglobin-mediated nitric oxide signaling. *Free Radic Biol Med* **61C**: 464-472.

Hendil, K. B., S. Khan *et al.* (1998). Simultaneous binding of PA28 and PA700 activators to 20 S proteasomes. *Biochem J* **332 (Pt 3)**: 749-754.

Herrera-Ortiz, A., J. Martinez-Barnetche *et al.* (2011). The effect of nitric oxide and hydrogen peroxide in the activation of the systemic immune response of Anopheles albimanus infected with Plasmodium berghei. *Dev Comp Immunol* **35**: 44-50.

Hess, D. T., A. Matsumoto *et al.* (2005). Protein S-nitrosylation: purview and parameters. *Nat Rev Mol Cell Biol* **6**: 150-166.

Hicke, L. (2001). Protein regulation by monoubiquitin. *Nat Rev Mol Cell Biol* **2**: 195-201.

Hiyama, H., M. Yokoi *et al.* (1999). Interaction of hHR23 with S5a. The ubiquitin-like domain of hHR23 mediates interaction with S5a subunit of 26 S proteasome. *J Biol Chem* **274**: 28019-28025.

Hogg, N. (2002). The biochemistry and physiology of S-nitrosothiols. *Annu Rev Pharmacol Toxicol* **42**: 585-600.

Horiguchi, R., H. Dohra *et al.* (2006). Comparative proteome analysis of changes in the 26S proteasome during oocyte maturation in goldfish. *Proteomics* **6**: 4195-4202.

Hu, M., P. Li *et al.* (2005). Structure and mechanisms of the proteasome-associated deubiquitinating enzyme USP14. *EMBO J* **24**: 3747-3756.

Huang, B. and C. Chen (2010). Detection of protein S-nitrosation using irreversible biotinylation procedures (IBP). *Free Radic Biol Med* **49**: 447-456.

Husnjak, K., S. Elsasser *et al.* (2008). Proteasome subunit Rpn13 is a novel ubiquitin receptor. *Nature* **453**: 481-488.

Ikeda, F. and I. Dikic (2008). Atypical ubiquitin chains: new molecular signals. 'Protein Modifications: Beyond the Usual Suspects' review series. *EMBO Rep* **9**: 536-542.

Imai, J., M. Maruya *et al.* (2003). The molecular chaperone Hsp90 plays a role in the assembly and maintenance of the 26S proteasome. *EMBO J* **22**: 3557-3567.

Iozef, R., S. Rahlfs *et al.* (2003). Glyoxalase I of the malarial parasite Plasmodium falciparum: evidence for subunit fusion. *FEBS Lett* **554**: 284-288.

Jensen, D. E., G. K. Belka *et al.* (1998). S-Nitrosoglutathione is a substrate for rat alcohol dehydrogenase class III isoenzyme. *Biochem J* **331 (Pt 2)**: 659-668.

Jia, L., C. Bonaventura *et al.* (1996). S-nitrosohaemoglobin: a dynamic activity of blood involved in vascular control. *Nature* **380**: 221-226.

Jortzik, E. and K. Becker (2012). Thioredoxin and glutathione systems in Plasmodium falciparum. *Int J Med Microbiol* **302**: 187-194.

Jortzik, E., L. Wang *et al.* (2012). Thiol-based posttranslational modifications in parasites. *Antioxid Redox Signal* **17**: 657-673.

Jung, T. and T. Grune (2013). The proteasome and the degradation of oxidized proteins: Part I-structure of proteasomes. *Redox Biol* **1**: 178-182.

Kalinowski, L., T. Matys *et al.* (2002). Angiotensin II AT1 receptor antagonists inhibit platelet adhesion and aggregation by nitric oxide release. *Hypertension* **40**: 521-527.

Kalyanaraman, B., V. Darley-Usmar *et al.* (2012). Measuring reactive oxygen and nitrogen species with

fluorescent probes: challenges and limitations. *Free Radic Biol Med* **52**: 1-6.

Kanzok, S. M., S. Rahlfs *et al.* (2002). Thioredoxin, thioredoxin reductase, and thioredoxin peroxidase of malaria parasite Plasmodium falciparum. *Methods Enzymol* **347**: 370-381.

Kanzok, S. M., R. H. Schirmer *et al.* (2000). The thioredoxin system of the malaria parasite Plasmodium falciparum. Glutathione reduction revisited. *J Biol Chem* **275**: 40180-40186.

Kappe, S. H., A. M. Vaughan *et al.* (2010). That was then but this is now: malaria research in the time of an eradication agenda. *Science* **328**: 862-866.

Kehr, S., E. Jortzik *et al.* (2011). Protein S-glutathionylation in malaria parasites. *Antioxid Redox Signal* **15**: 2855-2865.

Kehr, S., N. Sturm *et al.* (2010). Compartmentation of redox metabolism in malaria parasites. *PLoS Pathog* **6**: e1001242.

Kim, H. M., Y. Yu *et al.* (2011). Structure characterization of the 26S proteasome. *Biochim Biophys Acta* **1809**: 67-79.

Kisselev, A. F., T. N. Akopian *et al.* (1999). The sizes of peptides generated from protein by mammalian 26 and 20 S proteasomes. Implications for understanding the degradative mechanism and antigen presentation. *J Biol Chem* **274**: 3363-3371.

Klotz, F. W., L. F. Scheller *et al.* (1995). Co-localization of inducible-nitric oxide synthase and Plasmodium berghei in hepatocytes from rats immunized with irradiated sporozoites. *J Immunol* **154**: 3391-3395.

Knowles, R. G. and S. Moncada (1994). Nitric oxide synthases in mammals. *Biochem J* **298 (Pt 2)**: 249-258.

Komander, D. (2009). The emerging complexity of protein ubiquitination. *Biochem Soc Trans* **37**: 937-953.

Kornberg, M. D., N. Sen *et al.* (2010). GAPDH mediates nitrosylation of nuclear proteins. *Nat Cell Biol* **12**: 1094-1100.

Kreidenweiss, A., P. G. Kremsner *et al.* (2008). Comprehensive study of proteasome inhibitors against Plasmodium falciparum laboratory strains and field isolates from Gabon. *Malar J* **7**: 187.

Krnajski, Z., T. W. Gilberger *et al.* (2002). Thioredoxin reductase is essential for the survival of Plasmodium falciparum erythrocytic stages. *J Biol Chem* **277**: 25970-25975.

Krnajski, Z., T. W. Gilberger *et al.* (2001). The malaria parasite Plasmodium falciparum possesses a functional thioredoxin system. *Mol Biochem Parasitol* **112**: 219-228.

Laemmli, U. K. (1970). Cleavage of structural proteins during the assembly of the head of bacteriophage T4. *Nature* **227**: 680-685.

Lam, Y. W., Y. Yuan *et al.* (2010). Comprehensive identification and modified-site mapping of S-nitrosylated targets in prostate epithelial cells. *PLoS One* **5**: e9075.

Lambros, C. and J. P. Vanderberg (1979). Synchronization of Plasmodium falciparum erythrocytic stages in culture. *J Parasitol* **65**: 418-420.

Lander, G. C., E. Estrin *et al.* (2012). Complete subunit architecture of the proteasome regulatory particle. *Nature* **482**: 186-191.

Lee, B. H., M. J. Lee *et al.* (2010). Enhancement of proteasome activity by a small-molecule inhibitor of USP14. *Nature* **467**: 179-184.

Lee, M. J., B. H. Lee *et al.* (2011). Trimming of ubiquitin chains by proteasome-associated deubiquitinating enzymes. *Mol Cell Proteomics* **10**: R110 003871.

Leggett, D. S., J. Hanna *et al.* (2002). Multiple associated proteins regulate proteasome structure and function. *Mol Cell* **10**: 495-507.

Legorreta-Herrera, M., S. Rivas-Contreras *et al.* (2011). Nitric oxide is involved in the upregulation of IFN-gamma and IL-10 mRNA expression by CD8(+) T cells during the blood stages of P. chabaudi AS

infection in CBA/Ca mice. *Int J Biol Sci* **7**: 1401-1411.

Lehmann, A., K. Jechow *et al.* (2008). Blm10 binds to pre-activated proteasome core particles with open gate conformation. *EMBO Rep* **9**: 1237-1243.

Li, H., E. L. Ponder *et al.* (2012). Validation of the proteasome as a therapeutic target in Plasmodium using an epoxyketone inhibitor with parasite-specific toxicity. *Chem Biol* **19**: 1535-1545.

Lim, J., D. C. Gowda *et al.* (2005). Induction of nitric oxide synthase in Anopheles stephensi by Plasmodium falciparum: mechanism of signaling and the role of parasite glycosylphosphatidylinositols. *Infect Immun* **73**: 2778-2789.

Lima-Junior, J. C., R. N. Rodrigues-da-Silva *et al.* (2012). Cells and mediators of inflammation (C-reactive protein, nitric oxide, platelets and neutrophils) in the acute and convalescent phases of uncomplicated Plasmodium vivax and Plasmodium falciparum infection. *Mem Inst Oswaldo Cruz* **107**: 1035-1041.

Lindenthal, C., N. Weich *et al.* (2005). The proteasome inhibitor MLN-273 blocks exoerythrocytic and erythrocytic development of Plasmodium parasites. *Parasitology* **131**: 37-44.

Lindermayr, C., G. Saalbach *et al.* (2005). Proteomic identification of S-nitrosylated proteins in Arabidopsis. *Plant Physiol* **137**: 921-930.

Liu, L., A. Hausladen *et al.* (2001). A metabolic enzyme for S-nitrosothiol conserved from bacteria to humans. *Nature* **410**: 490-494.

Liu, L., Y. Yan *et al.* (2004). Essential roles of S-nitrosothiols in vascular homeostasis and endotoxic shock. *Cell* **116**: 617-628.

Liu, X., M. J. Miller *et al.* (1998). Diffusion-limited reaction of free nitric oxide with erythrocytes. *J Biol Chem* **273**: 18709-18713.

Loscalzo, J. (2013). The identification of nitric oxide as endothelium-derived relaxing factor. *Circ Res* **113**: 100-103.

Luckhart, S., Y. Vodovotz *et al.* (1998). The mosquito Anopheles stephensi limits malaria parasite development with inducible synthesis of nitric oxide. *Proc Natl Acad Sci U S A* **95**: 5700-5705.

Luders, J., J. Demand *et al.* (2000). The ubiquitin-related BAG-1 provides a link between the molecular chaperones Hsc70/Hsp70 and the proteasome. *J Biol Chem* **275**: 4613-4617.

Marois, E. (2011). The multifaceted mosquito anti-Plasmodium response. *Curr Opin Microbiol* **14**: 429-435.

Maron, B. A. and T. Michel (2012). Subcellular localization of oxidants and redox modulation of endothelial nitric oxide synthase. *Circ J* **76**: 2497-2512.

Marsh, N. and A. Marsh (2000). A short history of nitroglycerine and nitric oxide in pharmacology and physiology. *Clin Exp Pharmacol Physiol* **27**: 313-319.

McDonald, W. H., D. L. Tabb *et al.* (2004). MS1, MS2, and SQT-three unified, compact, and easily parsed file formats for the storage of shotgun proteomic spectra and identifications. *Rapid Commun Mass Spectrom* **18**: 2162-2168.

Menshikova, E. B., N. K. Zenkov *et al.* (2000). Nitric oxide and NO-synthases in mammals in different functional states. *Biochemistry (Mosc)* **65**: 409-426.

Miranda, M. and A. Sorkin (2007). Regulation of receptors and transporters by ubiquitination: new insights into surprisingly similar mechanisms. *Mol Interv* **7**: 157-167.

Mitchell, D. A. and M. A. Marletta (2005). Thioredoxin catalyzes the S-nitrosation of the caspase-3 active site cysteine. *Nat Chem Biol* **1**: 154-158.

Molina-Cruz, A., R. J. DeJong *et al.* (2008). Reactive oxygen species modulate Anopheles gambiae immunity against bacteria and Plasmodium. *J Biol Chem* **283**: 3217-3223.

Moncada, S., R. M. Palmer *et al.* (1991). Nitric oxide: physiology, pathophysiology, and pharmacology.

Pharmacol Rev **43**: 109-142.

Monostori, P., G. Wittmann *et al.* (2009). Determination of glutathione and glutathione disulfide in biological samples: an in-depth review. *J Chromatogr B Analyt Technol Biomed Life Sci* **877**: 3331-3346.

Mueller, T. D. and J. Feigon (2002). Solution structures of UBA domains reveal a conserved hydrophobic surface for protein-protein interactions. *J Mol Biol* **319**: 1243-1255.

Mueller, T. D. and J. Feigon (2003). Structural determinants for the binding of ubiquitin-like domains to the proteasome. *EMBO J* **22**: 4634-4645.

Muller, S. (2004). Redox and antioxidant systems of the malaria parasite Plasmodium falciparum. *Mol Microbiol* **53**: 1291-1305.

Muralidharan, V., A. Oksman *et al.* (2011). Asparagine repeat function in a Plasmodium falciparum protein assessed via a regulatable fluorescent affinity tag. *Proc Natl Acad Sci U S A* **108**: 4411-4416.

Murray, C. I., L. A. Kane *et al.* (2011). Site-mapping of in vitro S-nitrosation in cardiac mitochondria: implications for cardioprotection. *Mol Cell Proteomics* **10**: M110 004721.

Nahrevanian, H. (2006). Immune effector mechanisms of the nitric oxide pathway in malaria: cytotoxicity versus cytoprotection. *Braz J Infect Dis* **10**: 283-292.

Nahrevanian, H., J. Gholizadeh *et al.* (2006). Nitric oxide induction as a novel immunoepidemiological target in malaria-infected patients from endemic areas of the Islamic Republic of Iran. *Scand J Clin Lab Invest* **66**: 201-209.

Nakamura, T. and S. A. Lipton (2013). Emerging role of protein-protein transnitrosylation in cell signaling pathways. *Antioxid Redox Signal* **18**: 239-249.

Nakamura, T., L. Wang *et al.* (2010). Transnitrosylation of XIAP regulates caspase-dependent neuronal cell death. *Mol Cell* **39**: 184-195.

Nalepa, G., M. Rolfe *et al.* (2006). Drug discovery in the ubiquitin-proteasome system. *Nat Rev Drug Discov* **5**: 596-613.

Nickel, C., M. Trujillo *et al.* (2005). Plasmodium falciparum 2-Cys peroxiredoxin reacts with plasmoredoxin and peroxynitrite. *Biol Chem* **386**: 1129-1136.

Ostera, G., F. Tokumasu *et al.* (2008). Plasmodium falciparum: food vacuole localization of nitric oxide-derived species in intraerythrocytic stages of the malaria parasite. *Exp Parasitol* **120**: 29-38.

Ostera, G., F. Tokumasu *et al.* (2011). Plasmodium falciparum: nitric oxide modulates heme speciation in isolated food vacuoles. *Exp Parasitol* **127**: 1-8.

Peng, J., J. E. Elias *et al.* (2003). Evaluation of multidimensional chromatography coupled with tandem mass spectrometry (LC/LC-MS/MS) for large-scale protein analysis: the yeast proteome. *J Proteome Res* **2**: 43-50.

Perez-Mato, I., C. Castro *et al.* (1999). Methionine adenosyltransferase S-nitrosylation is regulated by the basic and acidic amino acids surrounding the target thiol. *J Biol Chem* **274**: 17075-17079.

Peters, J. M., W. W. Franke *et al.* (1994). Distinct 19 S and 20 S subcomplexes of the 26 S proteasome and their distribution in the nucleus and the cytoplasm. *J Biol Chem* **269**: 7709-7718.

Peterson, T. M., A. J. Gow *et al.* (2007). Nitric oxide metabolites induced in Anopheles stephensi control malaria parasite infection. *Free Radic Biol Med* **42**: 132-142.

Phyo, A. P., S. Nkhoma *et al.* (2012). Emergence of artemisinin-resistant malaria on the western border of Thailand: a longitudinal study. *Lancet* **379**: 1960-1966.

Pickart, C. M. (2001). Mechanisms underlying ubiquitination. *Annu Rev Biochem* **70**: 503-533.

Pickart, C. M. and M. J. Eddins (2004). Ubiquitin: structures, functions, mechanisms. *Biochim Biophys Acta* **1695**: 55-72.

Ponts, N., A. Saraf *et al.* (2011). Unraveling the ubiquitome of the human malaria parasite. *J Biol Chem* **286**: 40320-40330.

Ponts, N., J. Yang *et al.* (2008). Deciphering the ubiquitin-mediated pathway in apicomplexan parasites: a potential strategy to interfere with parasite virulence. *PLoS One* **3**: e2386.

Prudhomme, J., E. McDaniel *et al.* (2008). Marine actinomycetes: a new source of compounds against the human malaria parasite. *PLoS One* **3**: e2335.

Rabl, J., D. M. Smith *et al.* (2008). Mechanism of gate opening in the 20S proteasome by the proteasomal ATPases. *Mol Cell* **30**: 360-368.

Rabut, G. and M. Peter (2008). Function and regulation of protein neddylation. 'Protein modifications: beyond the usual suspects' review series. *EMBO Rep* **9**: 969-976.

Rahlfs, S., M. Fischer *et al.* (2001). Plasmodium falciparum possesses a classical glutaredoxin and a second, glutaredoxin-like protein with a PICOT homology domain. *J Biol Chem* **276**: 37133-37140.

Ralph, S. A. (2005). Strange organelles--Plasmodium mitochondria lack a pyruvate dehydrogenase complex. *Mol Microbiol* **55**: 1-4.

Ralser, M., M. M. Wamelink *et al.* (2007). Dynamic rerouting of the carbohydrate flux is key to counteracting oxidative stress. *J Biol* **6**: 10.

Ramiro, R. S., J. Alpedrinha *et al.* (2011). Sex and death: the effects of innate immune factors on the sexual reproduction of malaria parasites. *PLoS Pathog* **7**: e1001309.

Reyes-Turcu, F. E., K. H. Ventii *et al.* (2009). Regulation and cellular roles of ubiquitin-specific deubiquitinating enzymes. *Annu Rev Biochem* **78**: 363-397.

Reynolds, J. M., K. El Bissati *et al.* (2007). Antimalarial activity of the anticancer and proteasome inhibitor bortezomib and its analog ZL3B. *BMC Clin Pharmacol* **7**: 13.

Rivero, A. (2006). Nitric oxide: an antiparasitic molecule of invertebrates. *Trends Parasitol* **22**: 219-225.

Roberts, R. J. (1976). Restriction endonucleases. *CRC Crit Rev Biochem* **4**: 123-164.

Robien, M. A., J. Bosch *et al.* (2006). Crystal structure of glyceraldehyde-3-phosphate dehydrogenase from Plasmodium falciparum at 2.25 A resolution reveals intriguing extra electron density in the active site. *Proteins* **62**: 570-577.

Rockett, K. A., M. M. Awburn *et al.* (1991). Killing of Plasmodium falciparum in vitro by nitric oxide derivatives. *Infect Immun* **59**: 3280-3283.

Roth, E. J. (1990). Plasmodium falciparum carbohydrate metabolism: a connection between host cell and parasite. *Blood cells* **16**: 453-460.

Saeki, Y., E. A. Toh *et al.* (2009). Multiple proteasome-interacting proteins assist the assembly of the yeast 19S regulatory particle. *Cell* **137**: 900-913.

Sakata, E., S. Bohn *et al.* (2012). Localization of the proteasomal ubiquitin receptors Rpn10 and Rpn13 by electron cryomicroscopy. *Proc Natl Acad Sci U S A* **109**: 1479-1484.

Sarti, P., E. Forte *et al.* (2012). Cytochrome c oxidase and nitric oxide in action: molecular mechanisms and pathophysiological implications. *Biochim Biophys Acta* **1817**: 610-619.

Sauer, R. T. and T. A. Baker (2011). AAA+ proteases: ATP-fueled machines of protein destruction. *Annu Rev Biochem* **80**: 587-612.

Scanlon, T. C., B. Gottlieb *et al.* (2009). Isolation of human proteasomes and putative proteasome-interacting proteins using a novel affinity chromatography method. *Exp Cell Res* **315**: 176-189.

Schmidt, M., W. Haas *et al.* (2005). The HEAT repeat protein Blm10 regulates the yeast proteasome by capping the core particle. *Nat Struct Mol Biol* **12**: 294-303.

Schmidt, M., J. Hanna *et al.* (2005). Proteasome-associated proteins: regulation of a proteolytic machine. *Biol*

Chem **386**: 725-737.

Schreiner, P., X. Chen *et al.* (2008). Ubiquitin docking at the proteasome through a novel pleckstrin-homology domain interaction. *Nature* **453**: 548-552.

Sengupta, R., T. R. Billiar *et al.* (2010). Nitric oxide and thioredoxin type 1 modulate the activity of caspase 8 in HepG2 cells. *Biochem Biophys Res Commun* **391**: 1127-1130.

Sengupta, R. and A. Holmgren (2013). Thioredoxin and thioredoxin reductase in relation to reversible S-nitrosylation. *Antioxid Redox Signal* **18**: 259-269.

Sengupta, R., S. W. Ryter *et al.* (2007). Thioredoxin catalyzes the denitrosation of low-molecular mass and protein S-nitrosothiols. *Biochemistry* **46**: 8472-8483.

Sessler, N., K. Krug *et al.* (2012). Analysis of the Plasmodium falciparum proteasome using Blue Native PAGE and label-free quantitative mass spectrometry. *Amino Acids* **43**: 1119-1129.

Seth, D., A. Hausladen *et al.* (2012). Endogenous protein S-Nitrosylation in E. coli: regulation by OxyR. *Science* **336**: 470-473.

Sharon, M., T. Taverner *et al.* (2006). Structural organization of the 19S proteasome lid: insights from MS of intact complexes. *PLoS Biol* **4**: e267.

Shibatani, T. and W. F. Ward (1995). Sodium dodecyl sulfate (SDS) activation of the 20S proteasome in rat liver. *Arch Biochem Biophys* **321**: 160-166.

Sies, H. (1999). Glutathione and its role in cellular functions. *Free Radic Biol Med* **27**: 916-921.

Sobolewski, P., I. Gramaglia *et al.* (2005). Nitric oxide bioavailability in malaria. *Trends Parasitol* **21**: 415-422.

Sobolewski, P., I. Gramaglia *et al.* (2005). Hemoglobin serves to protect Plasmodium parasites from nitric oxide and reactive oxygen species. *J Investig Med* **53**: 246-252.

Sridhar, S., G. Bhat *et al.* (2013). Analysis of bortezomib inhibitor docked within the catalytic subunits of the 20S proteasome. *Springerplus* **2**: 566.

Stone, J. R. and M. A. Marletta (1994). Soluble guanylate cyclase from bovine lung: activation with nitric oxide and carbon monoxide and spectral characterization of the ferrous and ferric states. *Biochemistry* **33**: 5636-5640.

Stoyanovsky, D. A., Y. Y. Tyurina *et al.* (2005). Thioredoxin and lipoic acid catalyze the denitrosation of low molecular weight and protein S-nitrosothiols. *J Am Chem Soc* **127**: 15815-15823.

Sturm, N., E. Jortzik *et al.* (2009). Identification of proteins targeted by the thioredoxin superfamily in Plasmodium falciparum. *PLoS Pathog* **5**: e1000383.

Tabb, D. L., W. H. McDonald *et al.* (2002). DTASelect and Contrast: tools for assembling and comparing protein identifications from shotgun proteomics. *J Proteome Res* **1**: 21-26.

Tachado, S. D., P. Gerold *et al.* (1996). Glycosylphosphatidylinositol toxin of Plasmodium induces nitric oxide synthase expression in macrophages and vascular endothelial cells by a protein tyrosine kinase-dependent and protein kinase C-dependent signaling pathway. *J Immunol* **156**: 1897-1907.

Tai, H. C., H. Besche *et al.* (2010). Characterization of the Brain 26S Proteasome and its Interacting Proteins. *Front Mol Neurosci* **3**.

Tanahashi, N., Y. Murakami *et al.* (2000). Hybrid proteasomes. Induction by interferon-gamma and contribution to ATP-dependent proteolysis. *J Biol Chem* **275**: 14336-14345.

Taylor-Robinson, A. W. (1997). Antimalarial activity of nitric oxide: cytostasis and cytotoxicity towards Plasmodium falciparum. *Biochem Soc Trans* **25**: 262S.

Toledo, J. C., Jr. and O. Augusto (2012). Connecting the chemical and biological properties of nitric oxide. *Chem Res Toxicol* **25**: 975-989.

Tomko, R. J., Jr. and M. Hochstrasser (2013). Molecular architecture and assembly of the eukaryotic proteasome.

Annu Rev Biochem **82**: 415-445.

Towbin, H., T. Staehelin *et al.* (1992). Electrophoretic transfer of proteins from polyacrylamide gels to nitrocellulose sheets: procedure and some applications. 1979. *Biotechnology* **24**: 145-149.

Trager, W. and J. B. Jensen (1976). Human malaria parasites in continuous culture. *Science* **193**: 673-675.

Tsang, A. H., Y. I. Lee *et al.* (2009). S-nitrosylation of XIAP compromises neuronal survival in Parkinson's disease. *Proc Natl Acad Sci U S A* **106**: 4900-4905.

Tsihlis, N. D., C. S. Oustwani *et al.* (2011). Nitric oxide inhibits vascular smooth muscle cell proliferation and neointimal hyperplasia by increasing the ubiquitination and degradation of UbcH10. *Cell Biochem Biophys* **60**: 89-97.

Turturice, B. A., M. A. Lamm *et al.* (2013). Expression of cytosolic peroxiredoxins in Plasmodium berghei ookinetes is regulated by environmental factors in the mosquito bloodmeal. *PLoS Pathog* **9**: e1003136.

Tuteja, R. (2007). Malaria - an overview. *FEBS J* **274**: 4670-4679.

Valpuesta, J. M., J. Martin-Benito *et al.* (2002). Structure and function of a protein folding machine: the eukaryotic cytosolic chaperonin CCT. *FEBS Lett* **529**: 11-16.

van Schalkwyk, D. A., W. Priebe *et al.* (2008). The inhibitory effect of 2-halo derivatives of D-glucose on glycolysis and on the proliferation of the human malaria parasite Plasmodium falciparum. *J Pharmacol Exp Ther* **327**: 511-517.

Venturini, G., M. Colasanti *et al.* (2000). Nitric oxide inhibits falcipain, the Plasmodium falciparum trophozoite cysteine protease. *Biochem Biophys Res Commun* **267**: 190-193.

Verma, R., L. Aravind *et al.* (2002). Role of Rpn11 metalloprotease in deubiquitination and degradation by the 26S proteasome. *Science* **298**: 611-615.

Vincendeau, P., A. P. Gobert *et al.* (2003). Arginases in parasitic diseases. *Trends Parasitol* **19**: 9-12.

Vincent, S. R. (2010). Nitric oxide neurons and neurotransmission. *Prog Neurobiol* **90**: 246-255.

Wang, L., C. Delahunty *et al.* (2013). Protein S-nitrosylation in Plasmodium falciparum. *Antioxid Redox Signal*.

Wang, Q., P. Young *et al.* (2005). Structure of S5a bound to monoubiquitin provides a model for polyubiquitin recognition. *J Mol Biol* **348**: 727-739.

Wang, X., C. Guerrero *et al.* (2007). Proteomics of proteasome complexes and ubiquitinated proteins. *Expert Rev Proteomics* **4**: 649-665.

Wang, X. and L. Huang (2008). Identifying dynamic interactors of protein complexes by quantitative mass spectrometry. *Mol Cell Proteomics* **7**: 46-57.

Warnatsch, A., T. Bergann *et al.* (2013). Oxidation matters: the ubiquitin proteasome system connects innate immune mechanisms with MHC class I antigen presentation. *Mol Immunol* **55**: 106-109.

Washburn, M. P., D. Wolters *et al.* (2001). Large-scale analysis of the yeast proteome by multidimensional protein identification technology. *Nat Biotechnol* **19**: 242-247.

WHO (2010). World Malaria Report. 2010. Geneva, Switzerland, WHO Press: 259.

Wiederkehr, T., B. Bukau *et al.* (2002). Protein turnover: a CHIP programmed for proteolysis. *Curr Biol* **12**: R26-28.

Wilkinson, K. D. (1997). Regulation of ubiquitin-dependent processes by deubiquitinating enzymes. *FASEB J* **11**: 1245-1256.

Winget, J. M. and T. Mayor (2010). The diversity of ubiquitin recognition: hot spots and varied specificity. *Mol Cell* **38**: 627-635.

Wink, D. A., H. B. Hines *et al.* (2011). Nitric oxide and redox mechanisms in the immune response. *J Leukoc Biol* **89**: 873-891.

Wink, D. A. and J. B. Mitchell (1998). Chemical biology of nitric oxide: Insights into regulatory, cytotoxic, and

cytoprotective mechanisms of nitric oxide. *Free Radic Biol Med* **25**: 434-456.

Wolf, D. H. and A. Stolz (2012). The Cdc48 machine in endoplasmic reticulum associated protein degradation. *Biochim Biophys Acta* **1823**: 117-124.

Wu, C., T. Liu *et al.* (2010). Redox regulatory mechanism of transnitrosylation by thioredoxin. *Mol Cell Proteomics* **9**: 2262-2275.

Wu, C., A. M. Parrott *et al.* (2011). Thioredoxin 1-mediated post-translational modifications: reduction, transnitrosylation, denitrosylation, and related proteomics methodologies. *Antioxid Redox Signal* **15**: 2565-2604.

Xu, T., J. D. Venable *et al.* (2006). ProLuCID, a fast and sensitive tandem mass spectra-based protein identification program. *Mol Cell Proteomics* **5**: S174.

Yao, T. and R. E. Cohen (2002). A cryptic protease couples deubiquitination and degradation by the proteasome. *Nature* **419**: 403-407.

Yao, T., L. Song *et al.* (2006). Proteasome recruitment and activation of the Uch37 deubiquitinating enzyme by Adrm1. *Nat Cell Biol* **8**: 994-1002.

Young, P., Q. Deveraux *et al.* (1998). Characterization of two polyubiquitin binding sites in the 26 S protease subunit 5a. *J Biol Chem* **273**: 5461-5467.

Zhang, D., S. Raasi *et al.* (2008). Affinity makes the difference: nonselective interaction of the UBA domain of Ubiquilin-1 with monomeric ubiquitin and polyubiquitin chains. *J Mol Biol* **377**: 162-180.

Zhang, J., M. Krugliak *et al.* (1999). The fate of ferriprotorphyrin IX in malaria infected erythrocytes in conjunction with the mode of action of antimalarial drugs. *Mol Biochem Parasitol* **99**: 129-141.

Zhang, M., C. M. Pickart *et al.* (2003). Determinants of proteasome recognition of ornithine decarboxylase, a ubiquitin-independent substrate. *EMBO J* **22**: 1488-1496.

Zhang, N., Q. Wang *et al.* (2009). Structure of the s5a:k48-linked diubiquitin complex and its interactions with rpn13. *Mol Cell* **35**: 280-290.

Appendix Table 1. *S*-nitrosylated proteins identified in *P. falciparum* cell extracts

No.	[1]Protein name	PlasmoDB Accession No.	Mol. mass (kDa)	[2]Coverage %	[3]SNO site
Cellular redox homeostasis					
1	Peroxiredoxin 6 (Prx6)	PF08_0131	25.2	12.7 / 30.5 / 14.1	K.**C**CILPSVDNADLPK.L
2	Glutaredoxin 1	PFC0271c	12.4	21.6 / 36.9	
3	Glutathione peroxidase-like thioredoxin peroxidase	PFL0595c	24	18.5 / 12.7	
4	Glutathione reductase	PF14_0192	56.5	6.4 / 9.2 / 9.2	
5	Peroxiredoxin 1a (Prx1a)	PF14_0368	21.8	15.4 / 15.4	
6	Thioredoxin, putative	PF14_0545	11.7	37.5 / 37.5 / 37.5	
Cytoskeleton					
7	Actin I	PFL2215w	41.9	24.7 / 16.2 / 21.8	
8	Actin II	PF14_0124	42.6	7.2 / 7.2 / 7.2	
9	Alpha tubulin 1	PFI0180w	50.3	6.0 / 9.3 / 11.0	R.**C**VFVDLEPTVVDEVR.T
10	Profilin, putative	PFI1565w	19	31.0 / 35.7 / 39.8	
11	Tubulin beta chain	PF10_0084	49.8	20.2 / 14.4 / 17.5	
DNA and RNA metabolism and processing					
12	Adenosine deaminase, putative	PF10_0289	42.5	17.7 / 15.8 / 17.7	
13	AP endonuclease, putative	PFC0250c	72.4	5.4 / 4.5 / 5.2	
14	ATP-dependent DNA helicase, putative	PF13_0330	54.6	6.0 / 8.7	
15	ATP-dependent RNA helicase, putative	PFC0955w	86.6	5.0 / 2.9	
16	ATP-dependent RNA helicase, putative	PFI0860c	94.1	3.4 / 3.4	R.NTVSEE**C**TYSTNER.T
17	Carbamoyl phosphate synthetase	PF13_0044	273.4	2.1 / 1.6 / 1.9	K.VTINNSNNSISNNENVETNLN**C**VSER.A
18	Cytidine triphosphate synthetase	PF14_0100	98.5	6.8 / 5.1	
19	DEAD box helicase	PFB0445c	52.2	5.5 / 9.6	
20	DNA/RNA-binding protein Alba, putative	PF08_0074	27.3	16.9 / 32.7 / 22.2	R.**C**GSTVITDQYVSGQDNSEHVVQEK.T
21	DNA/RNA-binding protein Alba, putative	PF10_0063	12	43.0 / 20.6 / 43.0	
22	DNA/RNA-binding protein Alba, putative	MAL13P1.233	25	10.1 / 10.1	
23	GMP synthetase	PF10_0123	63.9	6.5 / 6.5 / 6.5	
24	Histone H2A variant, putative	PFC0920w	16.5	12.1 / 12.0	
25	Histone H3	PFF0510w	15.4	22.1 / 14.7 / 21.2	
26	Histone H4	PF11_0061	11.5	41.7 / 43.7 / 33.0	
27	Hypoxanthine phosphoribosyltransferase	PF10_0121	26.4	15.2 / 20.8	
28	Inosine-5'-monophosphate dehydrogenase	PFI1020c	56.2	6.7 / 6.1 / 10.6	
29	Lsm6 homolog, putative	PF13_0142	8.8	35.1 / 35.1 / 33.8	
30	MIF4G domain containing protein	PF11_0086	381.9	3.4 / 4.4 / 2.3	K.SIDALTENENNKNDAE**C**SDSTTVK.N
31	Minchromosome maintenance complex subunit	PF13_0291	105.7	4.7 / 4.5	
32	Minchromosome maintenance complex subunit, putative	PF07_0023	94.2	4.4 / 11.3 / 5.1	
33	Minchromosome maintenance complex subunit, putative	PFE1345c	109.8	7.5 / 10.0 / 7.2	
34	Minchromosome maintenance complex subunit, putative	PF13_0095	115.2	4.7 / 2.3 / 3.7	
35	Minchromosome maintenance complex subunit, putative	PFL0580w	85.9	6.1 / 4.0	
36	Nucleoside diphosphate kinase	PF13_0349	17	19.5 / 20.8	
37	Polyadenylate-binding protein, putative	PFL1170w	97.2	11.8 / 18.9 / 12.2	K.F**C**FINYADAESAK.N
38	Pre-mRNA splicing factor, putative	PF10_0217	62.1	4.5 / 4.1	
39	Proliferating cell nuclear antigen	PF13_0328	30.6	24.8 / 24.5 / 8.8	

No.	[1]Protein name	PlasmoDB Accession No.	Mol. mass (kDa)	[2]Coverage %	[3]SNO site
40	Purine nucleoside phosphorylase	PFE0660c	26.9	11.4 / 7.3 / 18	
41	Ribonucleoside-diphosphate reductase, large subunit	PF14_0352	96.9	4.8 / 3.5	
42	RNA-binding protein, putative	PF10_0068	29.5	19.1 / 19.1 / 23.6	
43	RNA-binding protein, putative	PFI1435w	33.6	14.5 / 14.5 / 14.5	
44	RNA-binding protein, putative	MAL8P1.40	32.4	16.1 / 14.3 / 9.8	
45	RNA-binding protein, putative	PFI1175c	23	12.4 / 21.3 / 14.4	
46	RNA-binding protein, putative	PF08_0086	117.1	4.2 / 5.3 / 2.7	
47	RNA-binding protein, putative	PF10_0028-a	29.8	18.7 / 7.7	
48	RNA-binding protein, putative	PF10_0028-b	30.1	18.5 / 7.7	
49	RNA-binding protein, putative	PFF0250w	85.6	10.6 / 4.5	
50	RNA-binding protein musashi, putative	PFI0820c	45.1	10.1 / 9.8	K.**C**NEAVASSPSTR.R
51	rRNA-associated RNA-binding protein, putative	PF13_0315	57.1	17.1 / 11.0 / 10.6	
52	SNF2 helicase, putative	PFF1185w	315.6	1.7 / 2.1 / 1.7	
53	Splicing factor, putative	MAL13P1.120	100.9	5.0 / 5.3	
Glycolysis					
54	6-Phosphofructokinase	PFI0755c	159.5	2.8 / 4.5 / 6.3	K.SLG**C**MSELQTSR.L
55	Enolase	PF10_0155	48.7	43.3 / 25.6 / 31.2	
56	Fructose-bisphosphate aldolase	PF14_0425	40.1	31.7 / 29.3 / 22.5	
57	Glucose-6-phosphate isomerase	PF14_0341	67.4	9.3 / 9.3 / 7.3	
58	Glyceraldehyde-3-phosphate dehydrogenase	PF14_0598	36.6	38.3 / 41.8 / 48.4	
59	Hexokinase	PFF1155w	55.3	8.5 / 7.1 / 15.6	
60	L-Lactate dehydrogenase	PF13_0141	34.1	27.2 / 34.2 / 32.3	
61	Phosphoglycerate kinase	PFI1105w	45.4	45.7 / 49.8 / 56.2	
62	Phosphoglycerate mutase, putative	PF11_0208	28.8	18.0 / 21.6 / 30.0	
63	Pyruvate kinase	PFF1300w	55.7	27.2 / 22.5 / 27.8	
64	Triosephosphate isomerase	PF14_0378	27.9	15.3 / 17.3 / 27.0	
Methionine and polyamine metabolism					
65	Adenosylhomocysteinase,S-adenosyl-L-homocysteine hydrolase	PFE1050w	53.8	14.8/ 14.0 / 20.7	
66	Ornithine aminotransferase	PFF0435w	46.1	32.1 / 23.4 / 29.5	
67	S-Adenosylmethionine decarboxylase/ornithine decarboxylase	PF10_0322	168.2	1.8 / 2.3	R.GTYEDTGMVN**C**VDVIYK.N
68	S-Adenosylmethionine synthetase	PFI1090w	44.8	26.6 / 27.4 / 24.9	K.VSIDEQSPDIAQ**C**VHENR.S
Mitosis					
69	Centrin-1	PFA0345w-a	16.4	32.6 / 32.6 / 32.6	
70	Centrin-1	PFA0345w-b	19.6	27.4 / 27.4 / 27.4	
71	Centrin-2	PF14_0443	19.3	43.5 / 24.4 / 20.2	
72	Centrin-3	PF10_0271	20.9	16.8 / 16.8	
Nucleosome assembly					
73	Chromatin assembly factor 1 protein WD40 domain, putative	PFA0520c	50.7	7.8 / 10.8 / 10.8	
74	Chromatin assembly protein (ASF1), putative	PFL1180w	31.5	9.5 / 12.1 / 8.4	
75	Chromodomain-helicase-DNA-binding protein 1 homolog, putative	PF10_0232	381.3	1.7 / 2.4 / 0.9	
76	Nucleosome assembly protein	PFI0930c	31.8	32.3 / 32.3 / 32.3	
77	Nucleosome assembly protein	PFL0185c	40.5	6.3 / 6.1	

No.	[1]Protein name	PlasmoDB Accession No.	Mol. mass (kDa)	[2]Coverage %	[3]SNO site
Pathogenesis / Evasion / Protein export / Antigen					
78	Antigen 332, DBL-like protein	PF11_0506	689.3	11.1 / 10.4 / 8.9	
79	Asparagine-rich antigen	PF08_0060	254.8	3.5 / 2.6 / 2.9	
80	Asparagine-rich antigen	PF11_0111	173.9	2.2 / 2.2 / 3.7	
81	Early transcribed membrane protein 5	PFE1590w	19	13.3 / 21.0 / 13.3	
82	High molecular weight rhoptry protein 2	PFI1445w	162.7	4.5 / 2.8	
83	High molecular weight rhoptry protein 3	PFI0265c	104.9	5.7 / 7.5 / 7.2	
84	Liver stage antigen 3	PFB0915w	175.7	3.3 / 2.4 / 2.4	
85	Macrophage migration inhibitory factor	PFL1420w	12.8	29.3 / 42.2 / 52.6	
86	Mature parasite-infected erythrocyte surface antigen	PFE0040c	168.3	19.3 / 16.9 / 15.6	
87	Merozoite capping protein 1	PF10_0268	43.9	10.4 / 24.9 / 18.1	
88	Merozoite surface protein 1	PFI1475w	195.7	14.1 / 12.7 / 10.9	
89	*Plasmodium*-exported protein (PHISTb)	PFL0050c	77.1	5.2 / 5.7 / 5.7	
90	*Plasmodium*-exported protein (PHISTb)	PFE1600w	60.2	4.9 / 4.9 / 4.9	
91	Rhoptry protein, putative	PF14_0637	169.3	4.7 / 3.8 / 4.4	
92	Rhoptry-associated membrane antigen	MAL7P1.208	103.6	2.0 / 3.5	
93	Rhoptry-associated protein 1	PF14_0102	90.1	8.2 / 5.8 / 4.2	
94	Surface protein, Pf113	PF14_0201	112.6	5.9 / 5.8	
95	Translocon component PTEX150	PF14_0344	112.4	8.2 / 5.9 / 5.9	
Pentose-phosphate shunt					
96	6-Phosphogluconate dehydrogenase, putative	PF14_0520	53	6.6 / 8.8 / 9.8	
97	Glucose-6-phosphate dehydrogenase-6-hosphogluconolactonase	PF14_0511	107	4.8 / 3.2 / 3.2	
98	Transketolase	PFF0530w	75.8	3.9 / 3.9	
Protein folding					
99	10 kD chaperonin	PFL0740c	11.2	52.4 / 52.4 / 32	
100	Activator of Hsp90 ATPase, putative	PFC0270w	41.6	6.6 / 6.0	
101	Co-chaperone GrpE, putative	PF11_0258	35	20.3 / 32.9 / 26.9	
102	Cochaperonin	PF13_0180	29.1	53.5 / 40.3 / 45.7	K.FSPFSNES**C**EFTYQNAK.Y
103	Cyclophilin, putative	PFE1430c	23.2	16.2 / 16.2	
104	DnaJ protein, putative	PF14_0700	52.5	28.2 / 31.1 / 30.8	R.NQEEGSTN**C**SNVVEEEMTLEK.C
105	DnaJ protein, putative	PF13_0036	38.9	10.6 / 12.4	
106	Endoplasmin homolog precursor, putative	PFL1070c	95	24.2 / 15.6 / 22.8	
107	FK506-binding protein (FKBP)-type peptidyl-propyl isomerase	PFL2275c	34.8	11.2 / 7.9	
108	Heat shock protein 40, putative	PFB0595w	37.4	11.3 / 7.3 / 18.3	
109	Heat shock protein 60	PF10_0153	62.6	23.8 / 34.3 / 27.4	
110	Heat shock protein 70	PFI0875w	72.4	49.5 / 46.9 / 50.0	
111	Heat shock protein 70	PF08_0054	73.9	33.4 / 33.4 / 41.2	
112	Heat shock protein 70	PF11_0351	73.3	33.3 / 33.3 / 34.7	
113	Heat shock protein 70, putative	MAL13P1.540	108.2	8.0 / 7.2 / 6.4	
114	Heat shock protein 90	PF07_0029	86.2	32.6 / 36.1 / 39.6	
115	Heat shock protein 90, putative	PF11_0188	108.5	7.3 / 6.6 / 4.5	
116	Heat shock protein 90, putative	PF14_0417	107	3.3 / 5.4	
117	Hsp70 interacting protein, putative	PFE1370w	51.1	8.7 / 12.4 / 15.5	R.D**C**TEALNLNIDSANAYK.V

No.	[1]Protein name	PlasmoDB Accession No.	Mol. mass (kDa)	[2]Coverage %	[3]SNO site
118	Hsp70/Hsp90 organizing protein, putative	PF14_0324	66.1	16.7 / 15.1 / 12.1	
119	Nascent polypeptide associated complex alpha chain, putative	PFF1050w	20.6	56.0 / 56.0 / 57.1	
120	Peptidyl-prolyl cis-trans isomerase	PFC0975c	19	11.1 / 19.3 / 19.9	K.RSVVITD**C**GEL.
121	Peptidyl-prolyl cis-trans isomerase,cyclophilin	PF11_0164	21.7	27.7 / 27.7 / 34.4	
122	Prefoldin subunit 2, putative	PF14_0167	16.7	38.8 / 46.9 / 55.8	
123	Prefoldin subunit, putative	PFE0595w	13.7	38.7 / 47.9 / 39.5	
124	Prefoldin subunit, putative	PFI0220w	15.3	22.5 / 32.6	
125	Protein disulfide isomerase	MAL8P1.17	55.5	27.3 / 23.8 / 27.3	
126	Small heat shock protein, putative	PF13_0021	25.2	23.2 / 23.7 / 14.2	
127	T-complex protein 1 epsilon subunit, putative	PFC0900w	59.2	8.4 / 10.1 / 6.2	
128	T-complex protein beta subunit, putative	PFC0285c	59.1	13.7 / 25.0 / 11.7	
129	TCP-1/cpn60 chaperonin family, putative	MAL13P1.283	58	14.4 / 12.5 / 13	
130	TCP-1/cpn60 chaperonin family, putative	PF11_0331	60.3	7.9 / 8.5	
131	TCP-1/cpn60 chaperonin family, putative	PFC0350c	59.6	4.6 / 6.9	
132	Tubulin-specific chaperone a, putative	PFA0460c	19.6	13.9 / 13.9	
Proteolysis / hemoglobin degradation					
133	Aminopeptidase P	PF14_0517	88.5	15.7 / 10.3 / 11.4	
134	Dipeptidyl aminopeptidase 1 (DPAP1)	PF11_0174	80.4	20.0 / 17.6 / 20.9	K.TSPNLTT**C**GSSQPNK.N
135	Cysteine proteinase falcipain 2a	PF11_0165	55.9	10.5 / 14.9 / 14.7	
136	Cysteine proteinase falcipain 2b	PF11_0161	55.8	10.6 / 14.9 / 14.7	K.LITLSEQELVD**C**SFK.N
137	Cysteine proteinase falcipain 3	PF11_0162	56.7	4.9 / 8.1	
138	Falcilysin	PF13_0322	138.9	5.8 / 4.0 / 5.2	
139	Falstatin	PFI0580c	47	8.0 / 8.0	
140	Insulinase, putative	PF11_0189	173.6	1.9 / 1.9	
141	M17 leucyl aminopeptidase	PF14_0439	67.8	9.8 / 12.2 / 10.2	
142	M1-family alanyl aminopeptidase	MAL13P1.56	126.1	12.4 / 9.9 / 12.1	
143	Plasmepsin II	PF14_0077	51.5	8.4 / 5.5	
144	Plasmepsin III,histo-aspartic protease	PF14_0078	51.7	10.4 / 4.7 / 8.0	
145	Plasmepsin IV	PF14_0075	51	13.6 / 11.1 / 7.6	
146	Serine repeat antigen 5	PFB0340c	111.8	14.3 / 18.3 / 17.5	
Protein transport					
147	Adapter-related protein, putative	PFI0200c	161.4	2.1 / 2.4	
148	Endoplasmic reticulum-resident calcium binding protein	PF11_0098	39.4	47.5 / 24.2 / 40.2	
149	GTP-binding nuclear protein ran/tc4	PF11_0183	24.9	33.2 / 33.2 / 44.4	
150	Karyopherin alpha	PF08_0087	61.2	9.7 / 7.9 / 5.5	
151	Karyopherin beta	PFE1195w	127.4	5.7 / 9.5 / 4.1	
152	Rab GTPase 18	PF08_0110	23.2	12.9 / 12.9	
153	Rab GTPase 7	PFI0155c	23.8	23.3 / 17.0	
154	Ran binding protein 1, putative	PFD0950w	33.2	22.9 / 32.5 / 28.2	K.VVANHYIYPNESY**C**K.L
Protein post-translational modification					
155	cAMP-dependent protein kinase regulatory subunit	PFL1110c	50.8	6.1 / 10.7 / 10.7	
156	Dolichyl-phosphate-mannose protein mannosyltransferase	PF10_0104	25.7	20.2 / 21.1	
157	Protein kinase, putative	PFI1280c	367	1.1 / 1.0	

No.	[1]Protein name	PlasmoDB Accession No.	Mol. mass (kDa)	[2]Coverage %	[3]SNO site
158	Protein phosphatase 2c	PF11_0396	105.4	25.1 / 18.0 / 18.0	
159	Serine/threonine protein kinase, FIKK family	MAL8P1.203	171.8	4.9 / 2.0 / 4.0	
160	Serine/threonine protein phosphatase	MAL13P1.274	76.9	4.4 / 4.4	
Signal transduction					
161	14-3-3 protein, putative	MAL8P1.69	30.2	48.9 / 34.7 / 50.8	K.EASN**C**AQEAYQK.A
162	Calmodulin	PF14_0323	16.9	27.5 / 48.3 / 44.3	
163	GTP binding protein, putative	MAL7P1.122	45.2	9.9 / 9.4 / 9.9	
164	Parasitophorous vacuolar protein 1	PF11_0302	52	12.2 / 17.0	
165	Phosphoinositide-binding protein, Putative	PF07_0017	118.8	8.8 / 8.7 / 3.8	
Transcription					
166	Basic transcription factor 3b, putative	PF14_0241	19.4	23.4 / 18.1	
167	High mobility group protein	MAL8P1.72	11.5	38.4 / 38.4 / 24.2	
168	Histone acetyltransferase GCN5	PF08_0034	170.9	2.3 / 2.9 / 1.8	
169	Minchromosome maintenance (MCM) complex subunit	PF14_0177	111.5	3.6 / 6.2 / 8.1	
170	Transcription factor with AP2 domain(s), putative	PFL1900w	299.4	4.6 / 3.3 / 5.2	K.NEEVNYIINEVDSSND**C**K.N
171	Transcription factor with AP2 domain(s), putative	PF10_0075	182.7	4.9 / 4.6 / 4.5	
172	Transcription factor with AP2 domain(s), putative	PFF0670w	485.6	2.5 / 1.3 / 1.4	
173	Transcriptional coactivator ADA2	PF10_0143	300.3	1.2 / 1.9	K.INENE**C**TSNDIEEDIK.S
174	Transcriptional regulator, putative	PFE0870w	132.7	4.1 / 4.1 / 4.1	
Translation					
175	40S ribosomal protein S12, putative	PFC0295c	15.4	43.3 / 21.3 / 29.1	K.LITTL**C**AEK.N
176	40S ribosomal protein S16, putative	PF08_0076	16.3	16.0 / 16.0	
177	40S ribosomal protein S21e, putative	PF11_0454	9.1	50.0 / 50.0 / 50.0	
178	40S ribosomal protein S2B, putative	PF10_0264	29.9	17.5 / 9.9 / 21.3	
179	40S ribosomal protein S8e, putative	PF14_0083	25.1	25.7 / 18.8 / 18.8	
180	60S acidic ribosomal protein P2, putative	PFC0400w	11.9	36.6 / 36.6 / 57.1	
181	60S ribosomal protein L12, putative	PFE0850c	18.1	20.6 / 28.5 / 26.1	
182	60S ribosomal protein L40/UBI, putative	PF13_0346	14.6	29.7 / 29.7 / 29.7	
183	60S ribosomal protein P0	PF11_0313	35	19.9 / 19.6 / 16.1	
184	Cysteinyl-tRNA synthetase, putative	PF10_0149	79.5	3.5 / 3.5	
185	Elongation factor 1 (EF-1), putative	PFC0870w	17.7	12.8 / 26.3	
186	Elongation factor 1-alpha	PF13_0305	49	31.2 / 35.9 / 28.4	
187	Elongation factor 1-beta	PFI0645w	32	16.7 / 27.5 / 22.8	
188	Elongation factor 1-gamma, putative	PF13_0214	47.8	5.8 / 6.3 / 9.0	
189	Elongation factor 2	PF14_0486	93.5	11.4 / 15.4 / 13.2	R.ETVTEESTIT**C**LGK.S
190	Eukaryotic initiation factor 5a, putative	PFL0210c	17.6	32.3 / 19.9 / 38.5	K.SVLVSVLSA**C**GQEK.I K.YEDI**C**PTSHNMDVPVVK.R
191	Eukaryotic translation initiation factor 2 gamma subunit putative	PF14_0104	51.2	4.9 / 4.9	
192	Eukaryotic translation initiation factor 3 subunit, putative	MAL7P1.81	37.3	7.6 / 7.6	
193	Eukaryotic translation initiation factor 3 subunit 7, putative	PF10_0077	63.1	6.4 / 6.4 / 6.4	
194	Eukaryotic translation initiation factor 3 subunit 8, putative	PFL0310c	116	5.1 / 3.9	
195	Eukaryotic translation initiation factor, putative	MAL8P1.83	31	16.9 / 19.2	
196	Glutamate-tRNA ligase, putative	PF13_0257	101.4	4.4 / 3.1 / 4.2	

No.	[1]Protein name	PlasmoDB Accession No.	Mol. mass (kDa)	[2]Coverage %	[3]SNO site
197	Glycine-tRNA ligase, putative	PF14_0198	104.3	3.1 / 2.8 / 4.4	
198	Helicase 45	PF14_0655	45.3	13.1 / 26.6 / 29.9	
199	Isoleucine-tRNA ligase, putative	PF13_0179	151.3	3.5 / 2.3 / 2.4	
200	Leucyl-tRNA synthase	PFF1095w	170.2	2.8 / 4.8 / 3.4	
201	Lysine-tRNA ligase, putative	PF13_0262	67.6	10.3 / 7.2 / 10.3	
202	Methionine-tRNA ligase, putative	PF10_0340	104.2	7.4 / 5.1 / 8.9	
203	Phenylalanyl-tRNA synthetase beta chain, putative	PF11_0051	72.5	7.7 / 4.2	
204	Seryl-tRNA synthetase, putative	PF07_0073	62.5	5.6 / 7.1	
205	Translation initiation factor IF-2, putative	PFF0345w	112.4	4.7 / 1.8 / 3.3	
206	tRNA binding protein, putative	PF14_0401	46.4	5.7 / 9.2	
Ubiquitin-dependent protein catabolic process					
207	26S proteasome AAA-ATPase subunit RPT3, putative	PFD0665c	44.7	10.7 / 7.9	
208	26S proteasome regulatory subunit 4, putative	PF10_0081	49.8	8.0 / 11.8	
209	26S proteasome regulatory subunit 6a, putative	PF11_0314	49.5	8.2 / 17.5	R.A**C**ASQTNATFLK.L
210	26S proteasome regulatory subunit, putative	PF14_0632	132.8	1.2 / 2.5	
211	Cell division cycle protein 48 homologue, putative	PFF0940c	92.4	24.9 / 20.0 / 23.2	K.TAGFSGADLAEL**C**QR.A
212	DNA repair protein RAD23, putative	PF10_0114	44.4	36.8 / 20.6 / 23.1	K.ESIDNI**C**AMGFEK.E
213	Polyubiquitin	PFL0585w	42.8	10.1 / 10.1 / 10.1	
214	Proteasome regulatory protein, putative	PFC0785c	26.5	15.6 / 22.2	
215	Proteasome regulatory subunit, putative	MAL13P1.343	35.2	8.0 / 11.3	
216	Proteasome subunit alpha type 2, putative	PFF0420c	26.5	20.4 / 20.4 / 15.7	
217	Proteasome subunit alpha type 5, putative	PF08_0109	55.1	8.7 / 5.8 / 5.8	
218	Proteasome subunit alpha type 5, putative	PF07_0112	28.4	19.9 / 15.2	
219	Proteasome subunit beta type 1, putative	PFE0915c	27.3	18.3 / 11.2 / 11.2	
220	Proteasome subunit, putative	MAL13P1.270	27.2	15.4 / 15.4 / 11.2	
221	Proteasome subunit alpha type 1, putative	PF14_0716	28.8	30.7 / 17.3 / 11.4	
222	Skp1 family protein, putative	MAL13P1.337	18.8	17.3 / 17.3 / 17.3	
223	Small ubiquitin-related modifier, putative	PFE0285c	11.1	21.0 / 19.0	
224	Ubiquitin carboxyl-terminal hydrolase a, putative	PFD0680c	98.5	3.2 / 3.2 / 5.2	
225	Ubiquitin carboxyl-terminal hydrolase isozyme L3	PF14_0576	26.9	10.8 / 10.8	
226	Ubiquitin-conjugating enzyme 13, putative	PFE1350c	17.4	25.0 / 25.0	
227	Ubiquitin-conjugating enzyme, putative	PF13_0301	22.9	6.4 / 13.9	
228	Ubiquitin regulatory protein, putative	MAL8P1.122	27.5	12.6 / 9.7	
229	Ubiquitin-specific protease, putative	PFI0225w	207.6	2.5 / 1.8 / 1.8	
Miscellaneous					
230	4-Methyl-5(B-hydroxyethyl)-thiazol monophosphate biosynthesis enzyme	PFF1335c	20.3	20.1 / 13.8 / 21.7	
231	Acyl-CoA synthetase	PFE1250w	76.9	5.9 / 5.2	
232	Adenylate kinase	PF10_0086	27.6	37.6 / 26.0 / 26.4	
233	ATP synthase beta chain, mitochondrial precursor, putative	PFL1725w	58.4	8.4 / 13.3 / 11.4	
234	Bifunctional dihydrofolate reductase-thymidylate synthase	PFD0830w	71.7	5.9 / 5.9	
235	Bromodomain protein, putative	PF10_0328	55.9	8.6 / 6.4	
236	Cg4 protein	PF07_0033	100	14.8 / 14.2 / 17.9	
237	Clustered-asparagine-rich protein	PFL1745c	51.5	4.9 / 4.5 / 9.7	
238	Coronin-binding protein, putative	PFF1110c	91.1	4.1 / 4.7	

No.	[1]Protein name	PlasmoDB Accession No.	Mol. mass (kDa)	[2]Coverage %	[3]SNO site
239	Cytoplasmic translation machinery-associated protein, putative	PFL2150c	39.7	8.1 / 10.7 / 14.9	
240	Cytosolic glyoxalase II	PFD0311w	30.5	10.6 / 10.6	
241	Dihydrolipoamide acyltransferase, putative	PFC0170c	51	10.3 / 15.0 / 17.0	
242	Ethanolamine kinase, putative	PF11_0257	49.9	7.8 / 9.0	
243	Gamma-glutamylcysteine synthetase	PFI0925w	124.5	3.3 / 2.8	
244	Glutamate dehydrogenase, putative	PF08_0132	160.4	2.1 / 3.1	
245	Glycerol-3-phosphate dehydrogenase, putative	PFL0780w	41.2	7.6 / 6.5	
246	Glycophorin binding protein	PF10_0159	95.8	2.3 / 4.0	
247	Haloacid dehalogenase-like hydrolase, putative	PF10_0325	32.8	9.4 / 12.5 / 9.4	
248	Mannose-6-phosphate isomerase, putative	MAL8P1.156	117.7	3.9 / 2.7	
249	MORN repeat protein, putative	PF10_0306	41.5	28.3 / 33.0 / 29.4	
250	MYND finger protein, putative	PFF0105w	29.4	8.7 / 14.3 / 31.3	K.YVLIS**C**DINNEIK.E R.I**C**STEIYGDAFLSK.T
251	Myo-inositol 1-phosphate synthase, putative	PFE0585c	69.1	9.8 / 10.6 / 15.6	
252	NADP-specific glutamate dehydrogenase	PF14_0164	52.5	11.9 / 18.9 / 9.4	
253	Nucleic acid binding protein, putative	PF11_0332	31.7	8.8 / 8.8	
254	Phosphatase, putative	PF14_0036	35.2	14.4 / 8.3	
255	Phosphatidylinositol-4-phosphate-5-kinase	PFA0515w	200	3.1 / 2.0 / 2.1	
256	Phosphoethanolamine N-methyltransferase	MAL13P1.214	31	51.1 / 42.5 / 38.3	
257	Pyrroline carboxylate reductase	MAL13P1.284	28.4	16.8 / 17.9 / 17.9	K.YTVMNAVEAA**C**EK.S
258	QF122 antigen	PF10_0115	131.6	3.3 / 5.4 / 5.3	
259	Receptor for activated c kinase	PF08_0019	35.7	18.9 / 19.2 / 18.9	
260	Replication factor A-related protein, putative	PFI0235w	56.2	9.3 / 7.2	
261	Serine hydroxymethyltransferase	PFL1720w	49.8	13.8 / 9.3 / 12.4	
262	SNO glutamine amidotransferase family protein	PFF1025c	33	16.6 / 9.3	
263	Translationally controlled tumor protein homolog, putative	PFE0545c	20	21.6 / 21.6 / 26.9	K.DVFTNDEV**C**SDSYVQQDPFEVPEFR.E
264	Vacuolar ATP synthase subunit a	PF13_0065	68.6	11.0 / 6.9 / 12.8	
265	Vacuolar ATP synthase subunit b	PFD0305c	55.8	11.7 / 19.2 / 14.6	
266	Vacuolar ATP synthase subunit g, putative	PF13_0130	14.2	20.3 / 29.3/ 20.3	
267	Zinc finger protein, putative	PF13_0313	70.3	7.3 / 4.9 / 4.6	

[1] Proteins identified with at least two peptides from at least two independent experiments were considered *S*-nitrosylated proteins and listed here. Proteins enriched in the avidin pull-down assay due to any reason except *S*-nitrosylation were excluded by the control samples that omitted ascorbate treatment.

[2] Each value represents the percentage of sequence coverage in one of the three independently conducted experiments. For more detail, please refer to the main text.

[3] *S*-nitrosylation (SNO) sites were assigned by the characteristic mass shift (+415.20 Da) of the peptides observed in the MS/MS data due to irreversible *S*-biotinylation of cysteine residues (formerly *S*-nitrosylated), indicated by the biotinylation reagent (EZ-Link Iodoacetyl-PEG2-Biotin) used in our biotin switch assay. The SNO-targeted cysteine residues are highlighted.

Appendix Table 2. *S*-nitrosylated hypothetical proteins identified in *P. falciparum* cell extracts

No.	[1]PlasmoDB Accession No.	Mol. mass (kDa)	[2]Coverage %	[3]SNO site
1	MAL8P1.95	36.3	15.2 / 15.2 / 22.5	
2	PF14_0257	33.0	32.7 / 34.2 / 41.6	
3	PF07_0087	29.3	12.7 / 18.4 / 18.4	
4	PFL0280c	39.0	7.2 / 17.1 / 12.9	
5	PF14_0390	26.3	19.4 / 19.4 / 19.4	
6	PFF0835w	53.0	8.1 / 8.3 / 12.1	
7	PF11_0218	184.9	9.3 / 9.2 / 9.6	
8	PF11_0069	30.7	21.4 / 25.2 / 21.4	
9	MAL13P1.237	42.2	18.5 / 17.2 / 18.5	
10	PF07_0042	350.7	0.9 / 3.7 / 2.3	
11	PFF0220w	334.4	3.5 / 2.2 / 3.4	
12	PF14_0329	28.9	15.9 / 21.0 / 16.7	
13	PFC0235w	135.7	10.4 / 8.9 / 6.5	
14	PF14_0046	34.7	22.2 / 16.5 / 23.5	
15	PFI1270w	24.7	12 / 16.1 / 16.1	
16	PFB0145c	237.7	1.3 / 2.3 / 1.3	
17	PFC0760c	403.0	0.9 / 2.0 / 1.4	
18	PFB0125c	158.8	4.6 / 5.1 / 3.3	
19	PF14_0487	176.2	1.8 / 6.1 / 4	
20	PF10_0361	192.7	1.8 / 4.2 / 3	
21	PF14_0228	183.6	3.0 / 3.9 / 4.0	K.NQTNDYSYAIAELD**C**R.Q
22	MAL13P1.336	78.6	7.2 / 7.2 / 5.1	
23	PF07_0016	218.4	1.8 / 1.8 / 1.8	
24	PF14_0558	174.1	5.8 / 2.7 / 3.9	
25	MAL13P1.295	235.1	2.8 / 1.6 / 1.6	
26	PF11_0055	49.3	7.3 / 9.7 / 9.7	
27	PF08_0081	76.9	5.5 / 3.8	
28	PF14_0586	37.0	15.2 / 9.3	
29	PFI0705w	28.4	11.2 / 12.4	
30	MAL7P1.204	196.6	4.8 / 2.2	
31	PF11_0413	52.6	10.3 / 6.5	
32	PF13_0099	23.2	18.0 / 21.5	
33	PFE1485w	225.5	2.3 / 2.4	
34	PFF0325c	280.4	1.5 / 2.7	
35	PF10_0166	36.4	9.7 / 9.7	
36	PF14_0546	76.0	5.5 / 7.0	
37	MAL7P1.98	17.8	24.8 / 24.8	
38	PFE0500c	297.6	1.9 / 1.7	
39	PF14_0649	295.8	1.7 / 1.3	
40	PFL0350c	311.4	1.5 / 1.2	
41	MAL7P1.77	60.6	8.4 / 12.1	
42	PF07_0056	159.5	2.1 / 3.2	
43	MAL7P1.202	145.5	2.0 / 3.3	
44	PF14_0138	29.5	9.9 / 9.9	
45	PFF0575c	374.9	0.8 / 1.2	
46	PFL1930w	691.4	0.5 / 1.2	
47	PF14_0783	12.6	33.9 / 33.9	K.DGNELTLLT**C**DNAEIK.C
48	PF13_0186	27.4	8.5 / 8.5	
49	PFL2355w	44.8	6.1 / 6.1	
50	PFL1815c	192.8	2.3 / 1.0	K.SNSE**C**VQGQNMNEQNNEMVYNK.Q
51	PF11_0206	208.6	2.3 / 2.3	
52	PF07_0101	260.8	1.2 / 1.4	K.Y**C**VEDITLYEVQK.E

[1] Only those proteins identified with at least two peptides from at least two independent experiments were considered *S*-nitrosylated proteins and listed here. Proteins enriched in the avidin pull-down due to any reason than *S*-nitrosylation were excluded by subtracting the proteins identified in the control samples that did not receive ascorbate treatment.

[2] Each value represents the percentage of sequence coverage in one of the three independently conducted experiments. For more detail, please refer to the main text.

[3] *S*-nitrosylation (SNO) sites were assigned by the characteristic mass shift (415.20 Da) of the peptides due to irreversible *S*-biotinylation of cysteine residues (formerly *S*-nitrosylated), indicated by the biotinylation reagent (EZ-Link Iodoacetyl-PEG2-Biotin) used in our biotin switch approach. The identified SNO-targeted cysteine residues are highlighted.